Encapsulation of Adsorptive Particles into CNT-Reinforced Alginate Gels for the Development of High-Performance Adsorbent for Cesium and Strontium Eliminations

Adavan Kiliyankil Vipin

Hokkaido University

2014

Encapsulation of Adsorptive Particles into CNT-Reinforced Alginate Gels for the Development of High-Performance Adsorbent for Cesium and Strontium Eliminations

「吸着性粒子をカーボンナノチューブ補強アルギン酸ゲルに内包するアプローチを用いたセシウムとストロンチウムを除去するための高性能吸着材の開発」

A Dissertation Submitted in Partial Fulfillment of the Requirements for the Degree of Doctor of Philosophy in the Field of Environmental Science

By

Adavan Kiliyankil Vipin

Division of Environmental Science Development

Graduate School of Environmental Science

Hokkaido University, Japan

2014

“This work is dedicated to my beloved family and supervisor”

ABSTRACT

Radioactive cesium and strontium are the inevitable medium lived fission products with half-lives of 30.17 and 28.8 years respectively. Until today, simultaneous removal of these extremely hazardous elements is an unsolved problem. For decades, scientists are familiar with various transition metal cyano ferrates as well as zeolites to decontaminate water from dangerous radioactive cesium and strontium. However, it is unfeasible to use such adsorptive material directly into water because their small particle size leads to further contamination. In addition, low permeability makes their application impractical in fixed bed columns for large-scale decontamination.

The caging of scavenger materials such as metal cyano ferrates and zeolites in nontoxic and inexpensive alginate vesicle will be a promising method for their safe and effective use. In order to enhance the stability and efficiency of encapsulated beads under extremely adverse conditions, highly dispersed multi walled carbon nanotubes (MWCNTs) should be a versatile supporter, because of their intense strength, high networking ability and huge surface area.

Adsorptive particle such as ferric hexacyanoferrate (prussian blue), sodium cobalt hexacyanoferrate and zeolite-A were successfully synthesized. After that, adsorptive particles were firmly encapsulated into CNT-reinforced alginate gels for the development of high-performance adsorbent for cesium and strontium

eliminations. The novel beads were characterized and performance evaluation on the aqueous elimination of cesium and strontium ions was conducted. The novel beads were highly stable and showed magnificent removal capability in all possible unfavorable conditions.

This dissertation consists of four chapters. In the first chapter, a brief introduction about environmental problems related to radioactive cesium and strontium was described. The significance of cesium and strontium removal from water was also pointed out. A comprehensive literature review also delineated the previous contributions to this field. The deep knowledge of literatures provided a theoretical framework towards the current problems that lead to a suitable original idea of encapsulation of adsorptive materials in alginate vesicle with MWCNTs.

The second chapter describes the materials and methodologies that were adopted to accomplish the problem solving research. The key adsorbing materials such as prussian blue, sodium cobalt hexacyanoferrate and zeolite-A were synthesized and purified systematically. The physical and chemical characterization of the prepared samples were scientifically completed using various techniques such as Scanning Electron Microscope (SEM), X-ray Diffraction (XRD) measurement, Fourier Transform Infrared Spectroscopy (FT-IR), Thermo Gravimetric analysis (TG-DTA), Energy Dispersive Spectroscopic analysis (EDS), etc. Then the three materials were encapsulated in micro-porous

beads using sodium alginate as the immobilizer and calcium ions (Ca^{2+}) as the cross-linker. In each case two types of beads were prepared; one was without MWCNTs and another with MWCNTs. The bead preparation was further optimized. The newly developed adsorbent beads could withstand in extreme pH, temperature and ionic strength. The developed beads were further examined by means of SEM and Brunauer–Emmett–Teller (BET) analysis to understand the morphological and porous peculiarities. A series of experiments were performed to analyze the practical applications of high performing adsorbent for the removal of cesium and strontium from aqueous solutions under batch and continuous flow (fixed bed column) conditions. Detailed kinetic, equilibrium and column breakthrough studies were performed. The research further extended to investigate the effect of pH and ionic competition on adsorption of cesium and strontium.

The major results obtained and the well discussions with valid points were described in chapter 3. Usually immobilization decrease the availability of adsorbent towards adsorbate, but MWCNTs enhanced the encapsulation efficiency along with making the adsorptive materials fully available for adsorption. Multipurpose MWCNTs made supporting physical networks over the caged crystals and that help them to remain more firmly inside the beads for risk-free direct application in water. The adsorption behavior and adsorption rate were carefully examined by means of different isothermal and kinetic models.

Mathematical fitting of experimental data on the adsorption isotherm model showed Langmuir isotherm greater than Freundlich isotherm. The maximum Cs^{+}/Sr^{2+} adsorption capacity of MWCNTs-modified prussian blue, sodium cobalt hexacyanoferrate and zeolite-A bead's were 143/55 mg/g, 133/72 mg/g and 113/107 mg/g, and that of without MWCNTs were 131/53 mg/g, 121/70 mg/g and 102/96 mg/g respectively. Similarly, in kinetic models study pseudo second order gave a better fitting than pseudo first order. The result showed that adsorption was monolayer site-to-site attachment and immediate. The investigation to the effect of pH and ionic competition on adsorption brought into a conclusion that the performance of beads was reliable within a broad range of pH as well as in high ionic competition. In addition, the fixed bed column adsorption analysis showed that the beads could be used for large-scale treatment decontamination.

In conclusion, the performance of this economic beads with respect to their stability, simplicity and removal capacity is innovative than currently available adsorbents. Their relevance ranges from low to high level of contaminant concentration. The novel beads will be much suitable for both household and industrial scale applications. Consequently, these newly developed adsorbents will be a potential solution for the existing radiation problem.

TABLE OF CONTENTS

LIST OF FIGURES

LIST OF TABLES

LIST OF ACRONYMS

Alg	Alginate
CoFC	Sodium cobalt hexacyanoferrate
EDS	Energy Dispersive Spectroscopic analysis
FT-IR	Fourier Transform Infrared Spectroscopy
MWCNTs	Multi Walled Carbon Nano Tubes
PB	Prussian blue
SEM	Scanning Electron microscope
TG-DTA	Thermo Gravimetric Analysis
XRD	X-Ray Diffraction

CHAPTER 1

GENERAL INTRODUCTION

Cesium-137 and strontium-90 are the principle medium lived fission products have half-lives of 30.17 and 28.8 years, respectively (Todd et al., 2004). Nuclear weapon testing, uncontrolled discharge of waste effluents from nuclear reactors and nuclear fuel reprocessing, and accidental release are the major routes by which radioactive cesium and strontium have been introducing into the environment (Avery, 1996). They are highly hazardous materials as they can contaminate our natural resources such as water, soil, and air. They also enter into the food chain through plants and ultimately incorporate into animals and human beings (Taj et al., 2011). Therefore, simultaneous removal of these dangerous radionuclides is highly desired.

Radioactive cesium-137 was produced when uranium and plutonium undergo fission, for example in nuclear reactors and nuclear weapons. Cesium-137 is one of the well-known fission products (Avery, 1995) that undergoes radioactive decay with the emission of beta particles and relatively strong gamma radiation. Cesium-137 decays to barium-137m, a short-lived decay product, which in turn decays to a nonradioactive form of barium (*Properties of Selected Radioisotopes*, 1968). Usually cesium-137 mimics biological potassium and tends to distribute along the body. People may ingest cesium-137 along with food and water, or may inhale it as dust (“Radiation Protection,” n.d.). If cesium-137 enters the body, it will distribute uniformly throughout the body's soft tissues. Slightly higher concentrations of the metal that accumulate in muscle, while slightly lower concentrations are deposit in bone and fat.

External exposure of cesium-137 may also occur that is exposure to its gamma radiation from outside (Yang et al., 2008). Like all radionuclides, exposure to radiation from cesium-137 results in increased risk of cancer. Exposure to waste materials, from contaminated sites, or from nuclear accidents can result in cancer risks much higher than typical environmental exposures (Faustino et al., 2008). If exposures are very high, serious burns, and even death, can result. Instances of such exposure are very rare. The magnitude of the health risk depends on exposure conditions. These include such factors as strength of the source, length of exposure, distance from the source, and whether there is shielding between you and the source.

Strontium has 16 known isotopes out of which four are stable such as Sr-84, -86, -87, and -88 and twelve other isotopes are radioactive. Strontium-90 is the most important radioactive isotope in the environment. Strontium-90 is a by-product of the fission of uranium and plutonium in nuclear reactors, and in nuclear weapons. Strontium-90 is found in waste from nuclear reactors also contaminate reactor parts and fluids ("Radiation Protection," n.d.). Strontium-90 is considered as one of the more hazardous components of nuclear wastes. The accident at the Chernobyl and Fukushima daichi nuclear power plant introduced a large amount of Sr-90 into the environment. In the decay of strontium-90, firstly it releases ionizing radiation and forms yttrium-90 (Y-90), which again decays to form stable zirconium. The half-life of Sr-90 is 29.1 years, and that of Yttrium-90 is 64 hours. Sr-90 emits moderate energy beta particles, while Y-90

emits very strong (energetic) beta particles (*Properties of Selected Radioisotopes*, 1968).

Strontium-90 forms many chemical compounds, such as halides, oxides, and sulfides, and spread easily through the environment. People inhale trace amount of strontium-90 as a contaminant in dust. However, the primary pathway of intake is swallowing with food or water. About 70-80% of Strontium -90 passes through the body and the remaining 20-30% absorbed and deposited in the bone. About 1% distributes among the blood volume, extracellular fluid, soft tissue, and surface of the bone. Strontium-90 is chemically similar to calcium, and tends to deposit in bone and blood-forming tissue (bone marrow). Thus, strontium-90 is referred to as a "bone seeker" (“Radiation Protection,” n.d.). Internal exposure of strontium-90 links to bone cancer, cancer of the soft tissue near the bone, and leukemia. The risk depends on the concentration of strontium-90 in the environment, and on the exposure conditions.

Therefore, simultaneous removal of dangerous cesium and strontium radionuclides is highly desired. There are large numbers of technologies have been studied and many of them are capable of separating cesium and/or strontium under certain conditions only (Todd et al., 2004). However, there are only a handful of technologies that have been developed to the stage where they are ready for testing in prototypic equipment and processes. The separation methods can be broadly classified into physical, chemical and biological

methods, out of which physical methods such as membrane filtration have poor removal efficiency and selectivity. Whereas biological methods such as microbial treatment and phyto-remediation are time consuming as well as bring into being large volumes of secondary waste. Chemical method is considered to the best for the removal of radioactive cesium and strontium removal from water. Chemical separation techniques fall into two main categories, which are solvent extraction and ion exchange (Todd et al., 2004). Out of these techniques, solvent extraction method will be applicable only for the treatment of higher concentration of contaminants. In solvent extraction, chemicals are adding directly into the contaminated sample in order to fix the pollutants. In that case large volume of secondary chemical waste will generate and seek for further treatment procedure. So we can conclude that ion exchange is the most simple, economic and effective technique (*Application of Ion Exchange Processes for the Treatment of Radioactive Waste and Management of Spent Ion Exchangers*, 2002; El-Kamash, 2008).

Large numbers of organic and inorganic ion ecxchangers are available such as phlogopite mica, titanates and silicotitanates, amonium molybdophosphate, titanium and zirconium phosphate, antimony pentoxide, zirconium monohydrogen phosphate, polyantimonic acid, macrocyclic polyether, metal cyanoferrate, zeolite etc. Several polymers, clay minerals, dead biomass, and metal oxides have been already reported (Gupta and Dubey, 2005). While considering the adsorption capacity and selectivity metal hexacyanoferrates and

zeolite are the most effective scavenger for the removal of cesium and strontium from water (Denton et al., 2009; Naushad, 2009).

Sparingly soluble metal ferrocyanide, are known as an excellent scavenger of cesium, often used for the removal of radioactive cesium from nuclear waste solutions (Ishihara et al., 2011). Over the past four decades a wide variety of hexacyanoferrate(II) complexes of alkali and transition metal were prepared (Lehto et al., 1987). From the insights of their structure and ion exchange properties, most of them are highly selective ion exchanger for cesium (Nilchi et al., 2003) out of them prussian blue often used for the removal of radioactive cesium from the gastrointestinal tract of animals by oral treatment (Taj et al., 2011). Prussian blue is a complex composed of Fe_4 $[Fe(CN)_6]_3$. X H_2O (X=14-16) with a cubic face centered structure. Its crystalline structure was established on the basis of its powder diffraction pattern (Keggin and Miles, 1936). Prussian blue is a mixed valence species with a basic cubic structure consisting of alternating high spin iron (III) ligated octahedrally by six nitrogen atoms and low spin iron (II) ligated by six carbon atoms of cyanide in a face centered cubic lattice to form ferricferrocyanide (Crumbliss et al., 1984; Karyakin, 2001). Prussian blue is classified as both soluble and insoluble, depending on the absence or presence of a monovalent ion in the lattice. Thus, Fe_4 $[Fe\ (CN)\ _6]_3$ is known as insoluble where as KFe_3 $[Fe\ (CN)_6]_3$ is soluble prussian blue (Buser et al., 1977). Sodium cobalt hexacyanoferrate is one of the novel analogue of prussian blue materials known to be highly selective for cesium adsorption from

aqueous waste (Mardan et al., 1999). Compare with prussian blue sodium cobalt hexacyanoferrate is more insoluble and containing many ion exchangeable sodium ions in the crystal lattice and surface. Therefore, along with cesium adsorption a little amount of strontium uptake is also achievable. Sodium ions in the crystal will replace with cesium ions whereas sodium ions in the surface will get replace with strontium ions. The mechanism of cesium binding on metal hexacyanoferrate crystals is still a controversial point. Cesium is one of the largest monovalent alkali metal ions, possessing low charge density, and capable of ionic binding with anions. The binding force may be chemical ion exchange; ion trapping as well as physical adsorption may occur (Faustino et al., 2008; Taj et al., 2011). The metal binding to insoluble prussian blue mainly due to ion exchange between hydrogen ion presents in the crystal lattice or simple ion trapping. Metal hexacyanoferrate shows a good tendency to enclose alkali metal ions during the preparation stage itself. In this experiment $Na_4Fe\ (CN)_6$ was an ingredient for the production of metal hexacyanoferrate, leading to the generation of metal hexacyanoferrate with sodium ions incorporated into the crystal lattice. Cesium and other monovalent ions can readily penetrate to the crystal lattice and easily displace sodium ions from the lattice. The schematic representation of cesium uptake by prussian blue (soluble and insoluble) and sodium cobalt hexacyanoferrate are depicted in Figure 1-1 and Figure 1-2 respectively (Shokouhimehr et al., 2010).

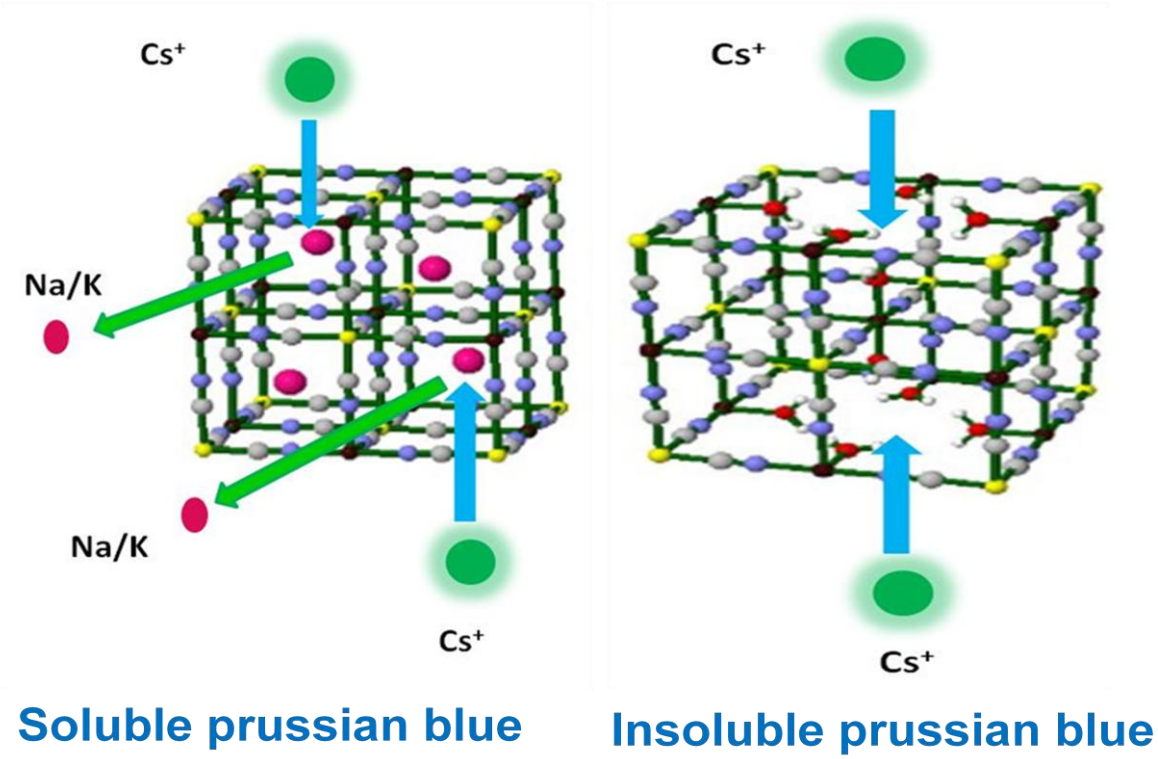

Figure 1-1 Schematic representation of cesium uptake by soluble and insoluble PB

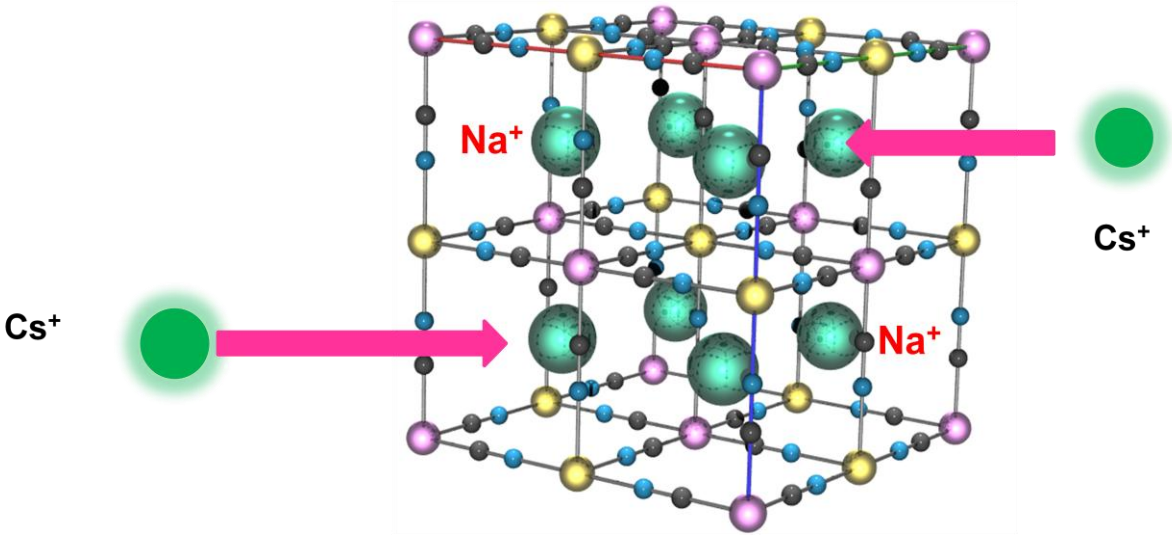

Figure 1-2 Schematic representation of cesium uptake by CoFC

In radioactive liquid treatment zeolite is a unique inorganic ion exchanger, which is widely used for the treatment of liquid nuclear waste (El-Kamash, 2008; Foo and Hameed, 2011). The cationic radioisotopes such as cesium and strontium can easily adsorb onto zeolite by replacing sodium ions from the crystals. Zeolite is hydrated aluminosilicates (Figure 1-3) of the alkaline and alkaline earth metals (Round et al., 1997). About forty natural zeolites have been identified during the past 200 years. More than 150 zeolites have been synthesized; the most common are zeolite A, X, Y and ZMS-5. Out of which zeolite A are most widely using for the treatment of radioactive waste. SiO_4 and AlO_4 are the primary building units of the framework (Ismail et al., 2010). The presence of aluminium results in a negatively charged framework, which compensated by protons or cations, mostly sodium ion as loosely bound counter ion. These sodium ions can be readily displaced by other ions (Figure 1-4) for which a particular framework has much greater affinity, thus giving zeolites significant ion exchange properties.

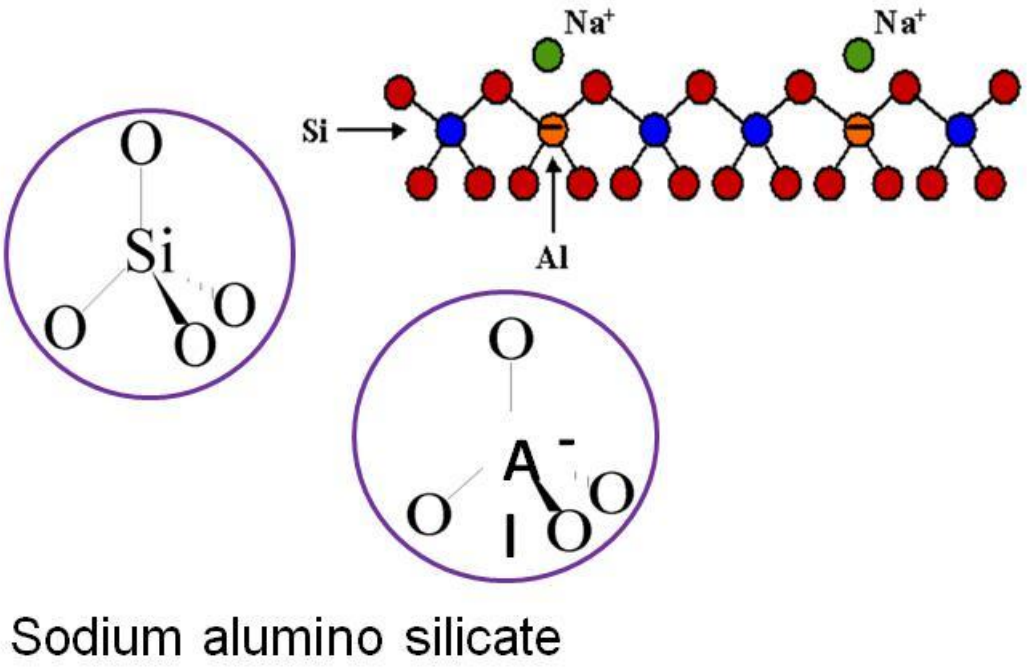

Figure 1-3 SiO_4 and AlO_4 as the primary building units for the zeolite framework

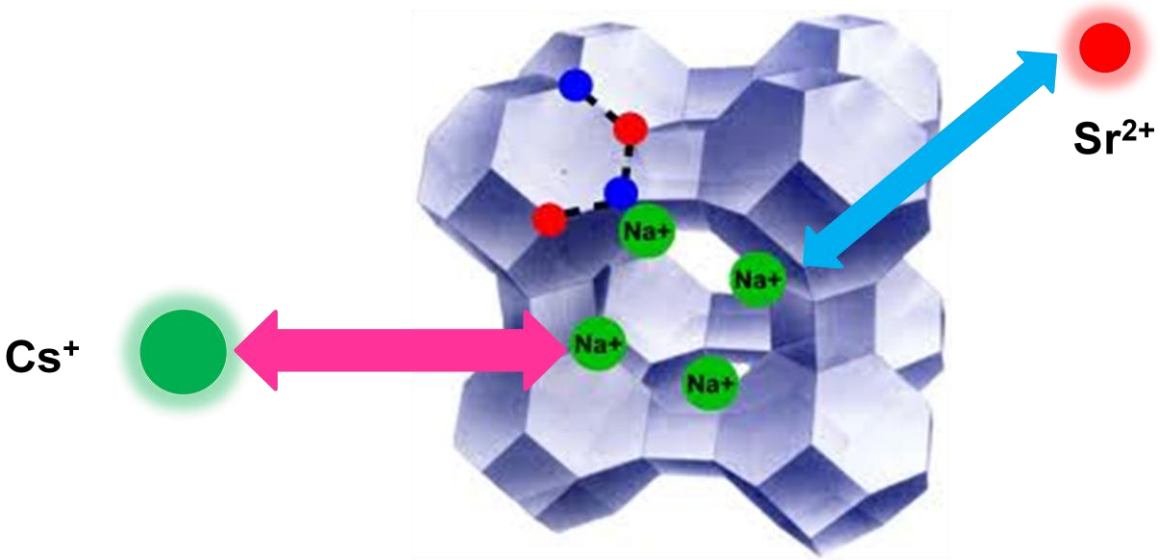

Figure 1-4 Schematic representation of cesium and strontium uptake by zeolite-A

However, it is unfeasible to use Ferric hexacyanoferrate (Prussian blue), sodium cobalt hexacyanoferrate and zeolite-A materials directly into water because of the small particle sizes, the recovery of adsorbent after taking contaminants become another problem. Also low permeability made their application in fixed-bed columns impractical. Therefore a powerful immobilizer is required for the safe use of those materials. For that purpose alginate was selected as a promising and versatile immobilizer.

Alginate is a heteropolysaccharide, a linear anionic copolymer of 1, 4-linked β-D mannuronic and α-L-guluronic acid residues, each containing one carboxylate group per monomeric unit. Alginate is nontoxic, has high viscosity, a molecular weight ranging from several thousands to a hundred thousand and is widely distributed in organisms such as seaweeds and bacteria (Lin et al., 2005; Papageorgiou et al., 2008, 2006)]. The chemical structure of alginate polymer is articulated in Figure 1-5 (Smidsrød and Skjåk-Braek, 1990).

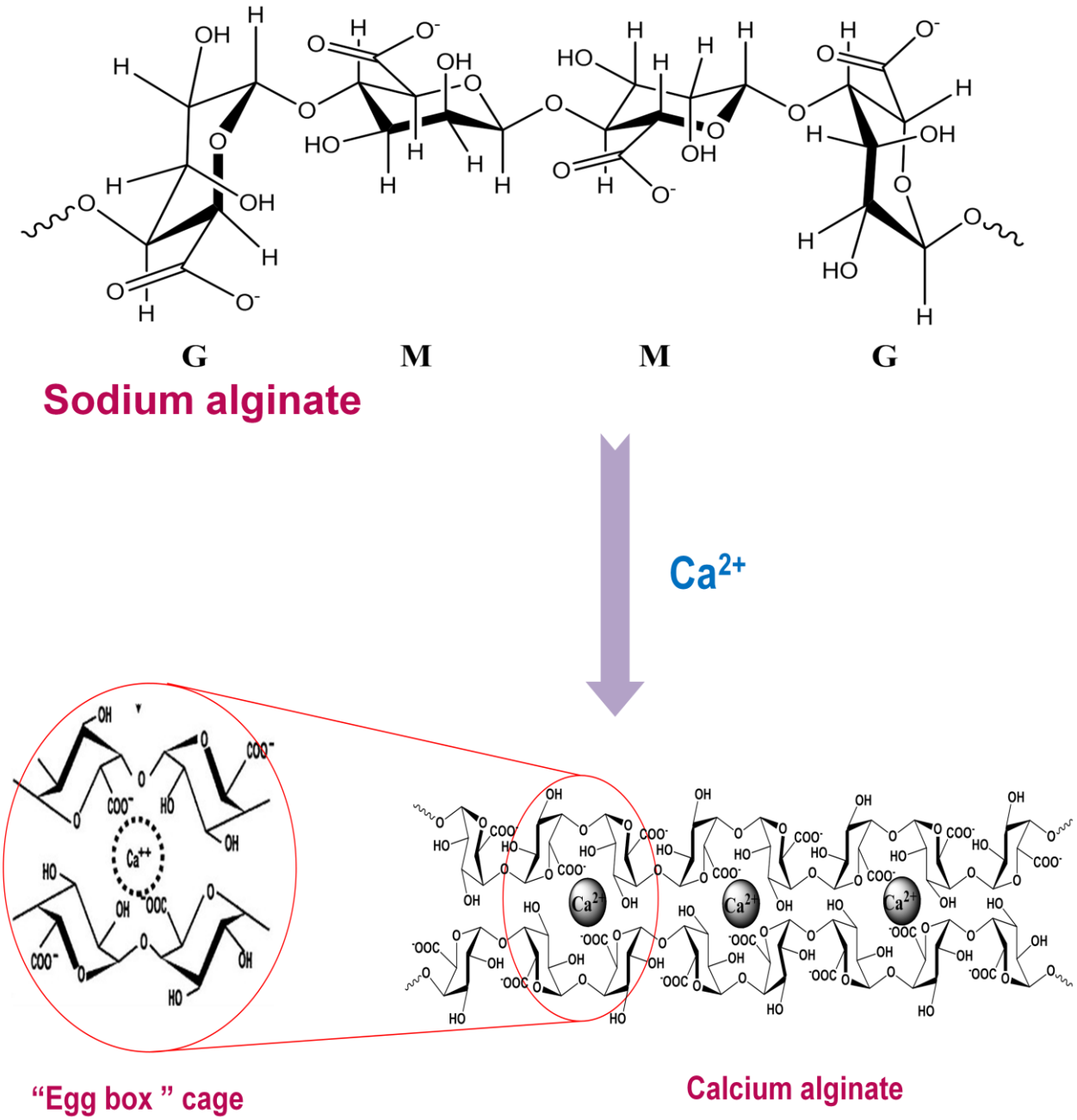

Figure 1-5 Alginate gelation: water-soluble sodium alginate forms water insoluble calcium alginate gel

Since the 1970s, alginate has been used as an immobilising agent because of its capability to form stable biodegradable gels in the presence of divalent cations (Fundueanu et al., 1999; Rousseau et al., 2004). Simultaneous binding of divalent cations such as Ca^{2+} or Ba^{2+} to different chains of α-L-guluronate units results in gelation. Cross-linking of the chains forms a structure resembling an "egg box". The gelation process is almost instantaneous and irreversible. The gelling properties of alginate are affected by monomeric composition, block structure, molecular size, concentration of polymer and calcium ion concentration (Blandino et al., 1999).

In order to make the practical application of our adsorbent in real radioactive waste solution further stabilization is needed. For that, the highly dispersed multi walled carbon nanotubes (MWCNT) is a promising material. MWCNT a multipurpose material were used to create a strong physical network over adsorptive crystals in order to make them more stable in calcium alginate vesicle. Also the CNT helped increase the effective surface area of the composite material that improved sorption which directed to a meaningful removal capability (Hu et al., 2012).

Ideally, graphite is the starting material for the production of carbon nanotubes. Exfoliated graphite sheets are called graphene. The one dimensional carbon nanotubes are made from two dimensional graphene sheets by rolling them into tubes. Depending on the number of graphene sheets rolled, the carbon nanotubes are of different types such as single walled (SWCNT), double walled

(DWCNT) and multiwalled tubes (MWCNT) (Figure 1-6).

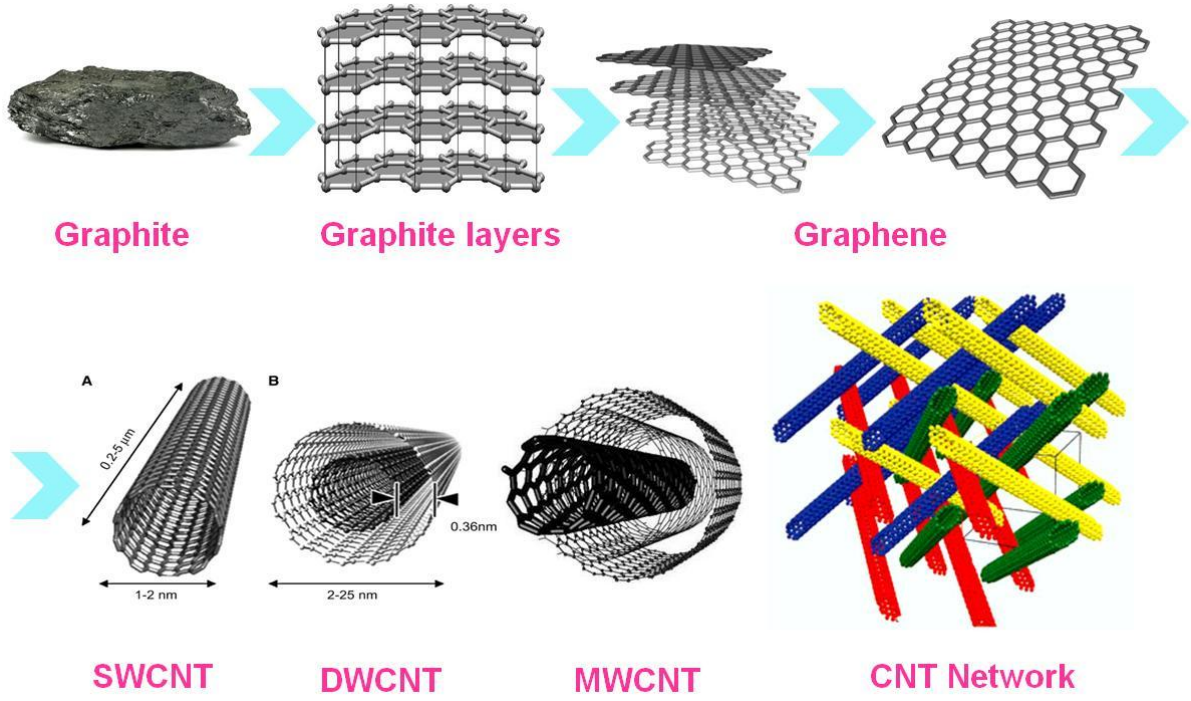

Figure 1-6 Schematic representation of CNT production from graphite, types of CNTS and CNT physical network formation

The present work deals with the development of adsorptive particle/calcium alginate beads modified with the dispersed carbon nanotubes. A set of experiments were done to evaluate the practical application of developed adsorbent for the removal of cesium and strontium from aqueous solutions under batch and continuous flow conditions in a fixed bed column. Later on, the kinetic, equilibrium and breakthrough studies were conducted. The research was further extended on the effect of pH and ionic competition on adsorption.

CHAPTER 2

DEVELOPMENT OF NOVEL BEADS BY ENCAPSULATING ADSORPTIVE PARTICLES INTO MWCNTS-REINFORCED ALGINATE GEL

2.1. Chemicals and reagents

Sodium alginate 500-600 cP, calcium chloride anhydrous, cobalt nitrate hexahydrate, sodium ferrocyanide decahydrate, ferric chloride, sodium alumina silicate, sodium metasilicate, cesium chloride, strontium chloride, magnesium chloride, sodium chloride, potassium chloride, aluminium chloride, hydrochloric acid and sodium hydroxide purchased from Wako Chemicals, Japan.

2.2. Preparation of prussian blue (PB)

To a solution of sodium ferrocyanide decahydrate (0.96 M in deionised water 500 mL) was slowly added ferric chloride hexahydrate (0.72 M, in deionised water 500 mL) with constant mechanical stirring (Hu et al., 2012). The solution was mixed for overnight. The colloidal product was a mixture of soluble and insoluble PB, with high level of sodium chloride. The PB was separated via centrifugation at 10,000 rpm and the separated sample was washed three times with deionised water allowed to dry at 80 ºC for 12 h in an oven. This dried PB sample was characterized. Scanning Electron Microscopy (SEM) measurements was performed on the PB crystalline product by using JEOL scanning electron microscope, Japan. Thermo gravimetric analysis (TGA) was done on samples after their initial drying at 80 ºC for 12 h. Thermal decomposition in the air was conducted over the temperature range of 30-1000 ºC using SII EXSTAR 6000 TG/DTA analyzer. The FT-IR spectrum was acquired with a JASCO FT/IR-460 *plus* in the range of 4000-400 cm^{-1} by

preparing the pellets with KBr. The X-ray diffraction (XRD) measurement was conducted with the help of a Rigaku RINT Ultima diffraction apparatus having Cu-Kα radiation and an X-ray power of 40Kv/20mA at a scan rate of 40/min. Energy Dispersive Spectroscopy (EDS) provided elemental analysis, performed with the HR-TEM, HD-2000 apparatus from Hitachi Co.

2.3. Preparation of sodium cobalt hexacyanoferrate (CoFC)

To a solution of sodium ferrocyanide decahydrate (0.6 M in deionised water 500 mL) cobaltnitrate hexahydrate (0.6 M, in deionised water 500 mL) was added slowly with mechanical stirring (Lehto et al., 1987). The solution was mixed overnight. The colloidal product was separated via centrifugation at 10,000 rpm and the sample was washed three times in deionised water. Finally, the CoFC was allowed to drying at 80 ºC for 12 h in an oven. Further chemical and physical characterisation of pure, dried CoFC was completed. Scanning Electron Microscopy (SEM) measurements was performed on the CoFC crystalline product by using JEOL Scanning Electron microscope, Japan. Thermo gravimetric analysis (TGA) was done on samples after their initial drying at 80 ºC for 12 h. Thermal decomposition in the air was conducted over the temperature range of 30-1000 ºC using SII EXSTAR 6000 TG/DTA analyzer. The FT-IR spectrum was acquired with a JASCO FT/IR-460 *plus* in the range of 4000-400 cm^{-1} by preparing the pellets with KBr. The X-ray diffraction (XRD) measurement was conducted with the help of a Rigaku RINT Ultima diffraction apparatus having Cu-Kα radiation and an X-ray power of 40Kv/20mA at a scan

rate of 40/min. Energy Dispersive Spectroscopy (EDS) provided elemental analysis. These studies were performed with the HR-TEM, HD-2000 apparatus from Hitachi Co.

2.4. Preparation of Zeolite A

0.723g of sodium hydroxide pellets dissolved in 80ml of deionised water. The sodium hydroxide solution was divided into two equal parts of 40ml in polypropylene bottles. Then, 8.258g sodium aluminate added into one-half and mixed gently in capped bottle until clear. To the second half added 15.48g of sodium metasilicate and mixed gently in capped bottle until the solution became clear. Poured silicate solution into aluminate solution quickly (Thompson and Franklin, 2001). The formed thick gel mixed very well until homogenized. The synthesised zeolite was washed several times with deionised water until the pH become neutral. The washed crystals were dried and characterized. The SEM analysis was done to know the morphology of prepared zeolite crystals. The X-ray diffraction (XRD) measurement was conducted using Rigaku RINT Ultima diffraction apparatus having Cu-Kα radiation and an X-ray power of 40Kv/20mA at a scan rate of 40/min.

2.5. Development of novel beads

Preparation of sodium alginate solution was simple; approximately 15 g of sodium alginate weighed out and shaken well with one litre of deionised water for one day. Calcium alginate beads were prepared by slowly dropping down

1.5% (w/v) aqueous solution of sodium alginate into a beaker containing 5% (w/v) calcium chloride solution under magnetic stirring. The beads were kept stirring in the same solution about 2 hours for maturation. Successively, beads were collected, and washed three times with deionised water and stored in 1 % (w/v) calcium chloride solution (Veglio' et al., 2002). Large-scale bead production was possible with the help of a small pump and flow controller (Figure 2-1).

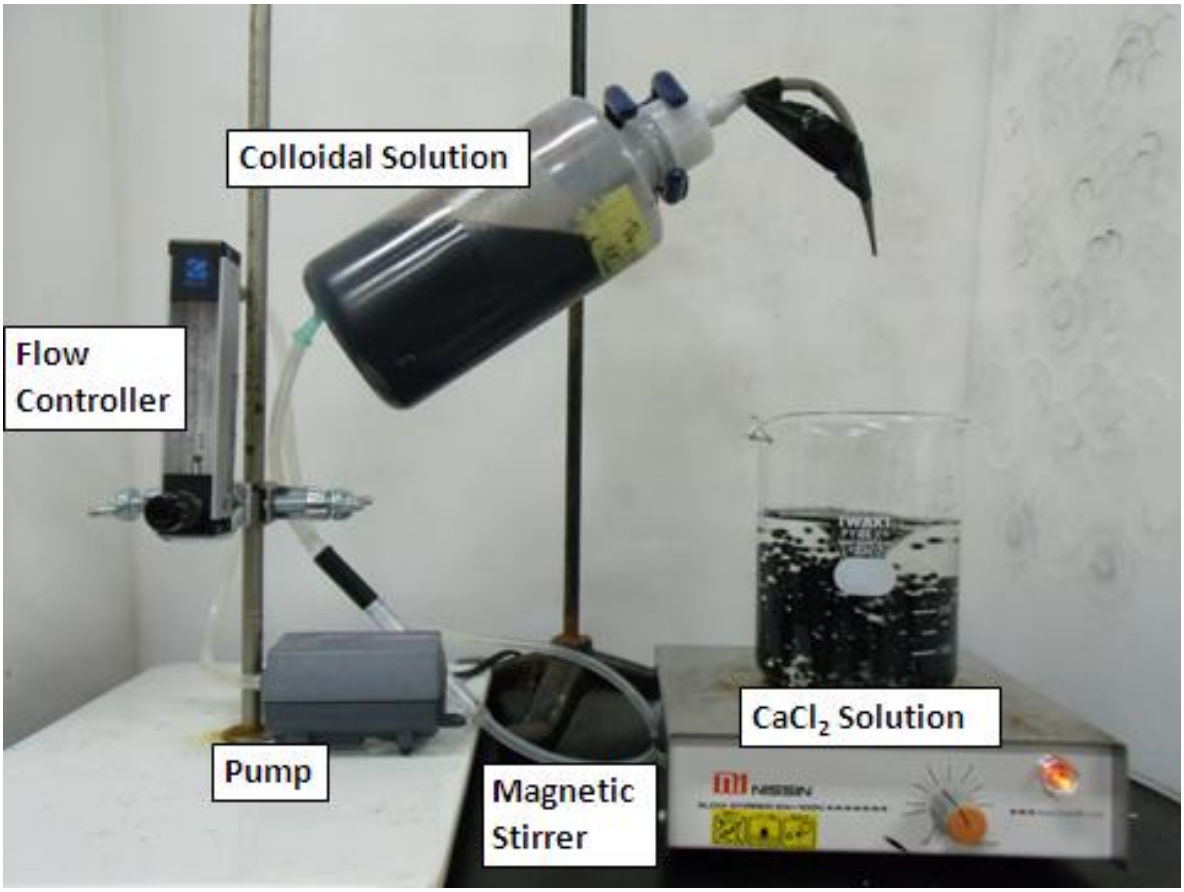

Figure 2-1 Photograph of bead preparation process.

Same methodology can be used for making all other beads with different colloidal solution. Calcium alginate encapsulated carbon nanotubes beads were prepared by using a colloidal solution composed of 1.5% sodium alginate and 1% highly dispersed MWCNTs (Figure 2-2). In order to make calcium alginate encapsulated PB beads, a colloidal solution having 1.5% sodium alginate and 2.5% PB was used. Calcium alginate-encapsulated PB beads reinforced with carbon nanotubes were prepared by dropping a solution composed of 1.5% sodium alginate, 2.5% PB and 1% MWCNTs into 5% calcium chloride solution. Similarly, to make calcium alginate encapsulated CoFC beads, a colloidal solution having 1.5% sodium alginate and 2.5% CoFC was required. For calcium alginate-encapsulated CoFC beads reinforced with carbon nanotubes; a solution composed of 1.5% sodium alginate, 2.5% CoFC and 1% MWCNTs into 5% calcium chloride solution was used. Zeolite encapsulated calcium alginate beads were made by using a colloidal solution having 1.5% sodium alginate and 2.5% zeolite-A. MWCNTs-reinforced calcium alginate zeolite-A beads were synthesized by dropping down solution made up of 1.5% sodium alginate, 2.5% CoFC and 1% MWCNTs into 5% calcium chloride solution. SEM and BET studies performed on the synthesized beads, which were freeze-dried for maintain the exact structure.

Control studies verified that the stability of the beads depended upon the concentration of sodium alginate and MWCNTs; the optimum sodium alginate

concentration was 3% w/v and that of MWCNTs was 4% w/v.

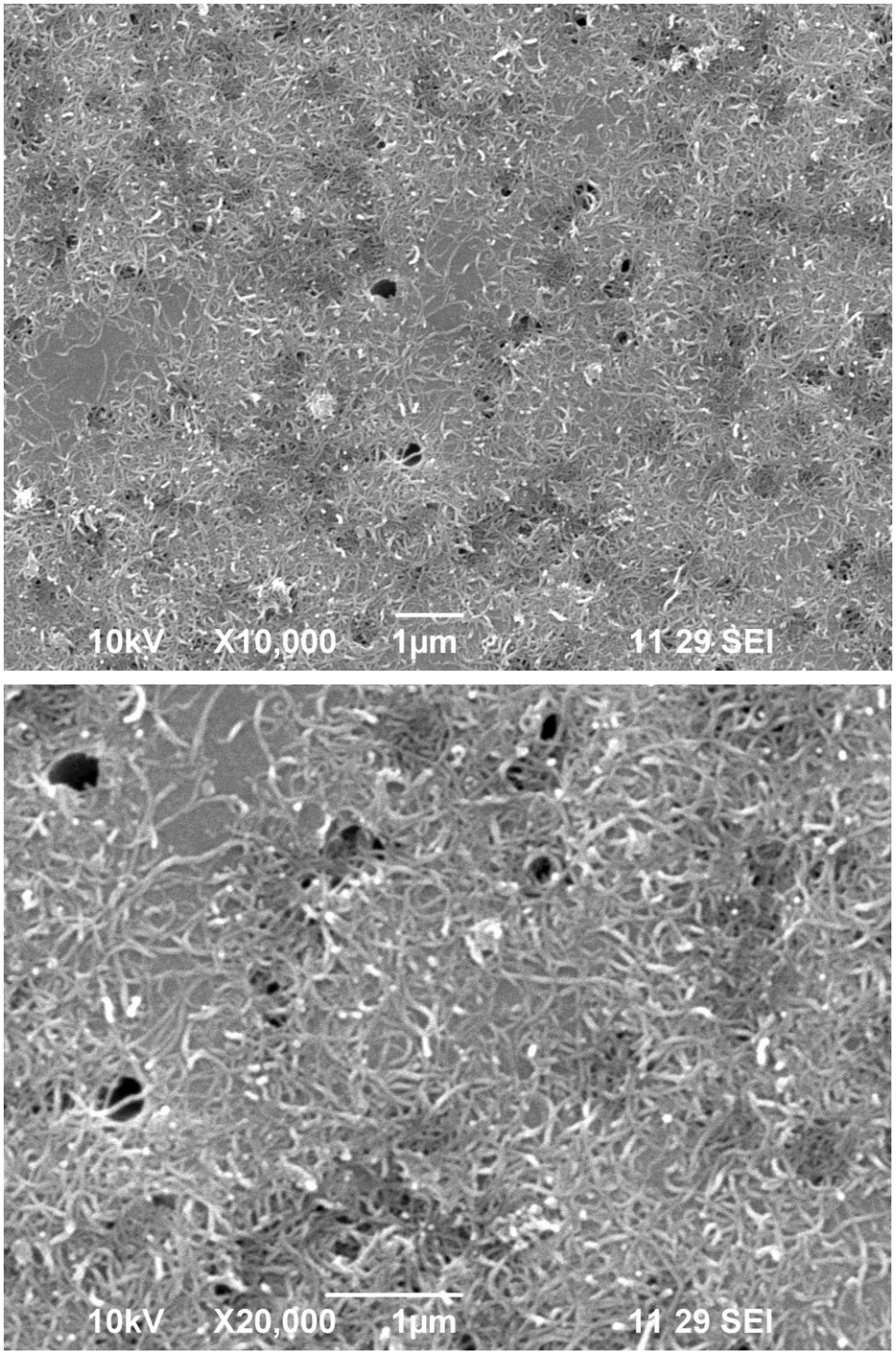

Figure 2-2 SEM images of dispersed MWCNTs covered over micro porous filter paper.

2.6. Adsorption batch studies

Collected beads were washed three times with the deionised water and air dried for 20 min at 80ºC. Beads of a known weight were added into adsorbate solutions at different concentrations in a sealable plastic tube. The solutions were shaken on a vortex shaker at 300 rpm at room temperature. The samples were collected at different time intervals and a residual ion left in solution was determined by Inductively Coupled Plasma-Atomic Emission Spectrometer (ICP-AES-9000, Shimadzu). The studies included the determination of important adsorption parameter such as adsorption capacity (q), these parameter can be calculated by using equation (1) (Sun et al., 2012; Yakout and Elsherif, 2010).

$$q = \frac{V\,(C_0 - C_e)}{m} \qquad (1)$$

Where C_0 and C_e are the initial and final concentrations (mg/L) of adsorbate ions in the aqueous solution, respectively, V is the volume of the solution (L), and m is the weight of adsorbent (g).

2.7. Adsorption kinetic models

In solid/solution adsorption processes, kinetic studies permit us to evaluate uptake rate performance and mechanism. Various widely using adsorption kinetic models are available to analyze sorption kinetics. In this study two models, the pseudo first order and pseudo second order models were considered (Azizian, 2004; Maliyekkal et al., 2009; Rudzinski and Plazinski, 2006) .

2.7.1. Pseudo first order model

In order to describe solid/liquid phase adsorption, we may invoke the pseudo first order rate equation, expressed as equation (2) (Augustine et al., 2007; Ho and Mckay, 2002; Qiu et al., 2009)

$$\frac{dq_t}{dt} = k_1(q_e - q_t) \qquad (2)$$

Where q_e and q_t are the sorption capacities (mg/g) at equilibrium and at time t, respectively, and k_1 is the pseudo first order rate constant (L/min). Upon integration and applying boundary conditions t=0 to t=t and q_t=0 to q_t=q_t, a simplified linear form of the rate equation can be obtained as below.

$$\ln(q_e - q_t) = \ln q_e - k_1 t \qquad (3)$$

A plot of ln(q_e-q_t) versus t will give a straight line, from the slope intercept we can calculate the value of k_1 and q_e. The pseudo first order model parameters k_1 and q_e were calculated. The correlation coefficient (R^2) determines the applicability of a model (goodness of fit) on experimental data.

2.7.2. Pseudo second order model

In 1995, Ho put forward a pseudo second order rate equation described by equation (4).

$$\frac{dq_t}{dt} = k_2(q_e - q_t)^2 \qquad (4)$$

Where q_e and q_t are the sorption capacities (mg/g) at equilibrium and at time t, respectively, and k_2 is the pseudo second order rate constant (g/mg.min). On integration and applying boundary conditions t=0 to t=t and q_t=0 to q_t=q_t, a

simplified linear form of the rate equation can be obtained as equation (5).

$$\frac{t}{q_t} = \frac{1}{h} + \frac{t}{q_e} \qquad (5)$$

Here h is the initial sorption rate (mg/g.min) as q_t/t tends toward zero hence,

$$h = k_2 q_e^{\,2} \qquad (6)$$

A plot of t/qt versus t gives a linear relationship from which q_e, k_2, and h can be obtained from slope and intercept of the plot.

For predicting the optimum kinetics and to determine parameters involved in them, non-linear method was found to be better compared to linear method. Therefore, for the present study, I followed nonlinear regression analysis. The correlation coefficient (R^2) determines the applicability of a model (goodness of fit) on experimental data (Kumar, 2006).

2.8. Equilibrium isotherm models

For the adsorption of a metal ion to an adsorbent, equilibrium describes the state of dynamic balance between the concentration of free metal ion in the bulk solution and the amount of metal ion bound to the adsorbent matrix. Equilibrium adsorption (the ratio of the amount of metal ion adsorbed to the amount remaining in the solution) studies are very important for sorption analysis. These studies permit us to determine the adsorption isotherm, which gives the empirical relationship between the amount of material adsorbed by a unit weight of adsorbent and the amount of adsorbate remaining in the bulk medium when the two phases have reached equilibrium at a constant

temperature (Abd El-Latif and Elkady, 2010; Farah et al., 2012; Foo and Hameed, 2010). Knowledge of the equilibrium isotherm provides information regarding the sorption mechanism, surface properties, and the affinity of the sorbent. In this study, the relationship between adsorbed ions and its residual concentration in aqueous solution at equilibrium was analysed by the help of Langmuir and the Freundlich isotherm models.

2.8.1. Langmuir isotherm

The Langmuir isotherm is the most widely used isotherm relating gas-solid phase adsorption (Ho et al., 2002). This empirical model assumes homogeneous monolayer adsorption on well defined sites, which are identical and equivalent. Therefore, equilibrium describes the point beyond which no further adsorption take place. Each of the definite localized sites holds one molecule and possesses equal enthalpy and sorption energy. Lateral interaction between adsorbed molecules and transmigration of the adsorbate in the plane of the surface are absent. The non linear form of Langmuir isotherm is represented by equation (7) (Abd El-Latif and Elkady, 2010; Foo and Hameed, 2010).

$$q_e = \frac{q_m K C_e}{1 + K C_e} \qquad (7)$$

Where q_e is the amount of ligand (adsorbate) adsorbed (mg/g) at equilibrium, C_e is the equilibrium concentration of the adsorbate ions (mg/L), q_m and K are Langmuir constants related to maximum adsorption capacity (mg/g) and energy of adsorption (L/mg), respectively.

The linear form of the Langmuir isotherm is represented by equation (8).

$$\frac{C_e}{q_e} = \frac{1}{q_m K} + \frac{C_e}{q_m} \qquad (8)$$

A plot of C_e/q_e versus C_e should be a straight line with slope $1/q_m$ and intercept $1/q_mK$. The applicability of a model (goodness of fit) on experimental data can be easily evaluated from the correlation coefficient (R^2) value. The Langmuir parameters of q_m and K were calculated from the slope and intercept values.

The essential characteristics of Langmuir isotherm can be explained by a dimensionless separation factor R_L, equation (9) which indicates the isotherm shape and predicts whether an adsorption is favorable or not (Günay et al., 2007).

$$R_L = \frac{1}{1+KC_0} \qquad (9)$$

Where C_0 is the initial concentration (mg/L) of the adsorbate. A lower R_L value reflects that the adsorption is favorable. In details adsorption will be either unfavorable ($R_L > 1$), linear ($R_L = 1$), favourable ($0 < R_L < 1$) or irreversible (R_L=0). In this study, the separation factor R_L was between zero and one in each case indicating the favourable adsorption.

2.8.2. Freundlich isotherm

The Freundlich isotherm is one of the earliest known isotherm models (Ho et al., 2002) which describes non-ideal and reversible adsorption. This empirical adsorption isotherm is widely used to explain multilayer adsorption on a heterogeneous surface with no uniform distribution of adsorption heat and affinity (Foo and Hameed, 2010).

The nonlinear Freundlich isotherm is represented by equation (10).

$$q_e = K_f C_e^{\,1/n_f} \qquad (10)$$

where q_e is the equilibrium solid phase concentration (mg/g), K_f and n_f are the isotherm parameters of adsorption capacity (mg/g) and adsorption intensity, respectively; C_e is the equilibrium liquid phase concentration (mg/L) (Günay et al., 2007).

The linear form of Freundlich isotherm can be represented as given below.

$$\ln q_e = \ln K_f + \frac{1}{n_f} \ln C_e \qquad (11)$$

When $\ln q_e$ is plotted against $\ln C_e$ a straight line with slope $1/n_f$ and intercept $\ln K_f$ will obtain. The value $1/n_f$ is the heterogeneous factor, describing a surface that becomes more heterogeneous as the value gets closer to zero; value < 1 indicates a chemisorption process whereas $1/n_f > 1$ is an indication of cooperative adsorption. The Freundlich parameters such as K_f and n_f were calculated from the slope and intercept values.

2.9. Effect of pH on adsorption

An environmental factor that affects every adsorption experiment is hydrogen ion concentration. The influence of hydrogen ion concentration is high in the case of ion exchange processes, especially for monovalent ion adsorption because of ionic competition. At low pH, ion exchange sites are mainly protonated, making them less available for ion exchange. When pH values increase, the sites become available for ion exchange, leading to higher adsorption (Yakout and Elsherif, 2010). The pH has a unique ability to change the whole reaction chemistry and adsorption behaviour. In this study, the effect of pH was estimated in terms of adsorption capacity between pH 2 to 10.

2.10. Effect of ionic competition on adsorption

The adsorption of a metal ion generally depends on the competition with other ions, which are present in solution. In this study, we considered the competition of sodium, potassium, calcium and magnesium ions with the adsorption of cesium and strontium ions. In the control groups, concentrations of cesium and strontium, ions were 0.75 mM and 1.1 mM respectively.

2.11. Fixed bed column adsorption

A series of continuous column analyses was conducted to investigate the practical applicability of the newly prepared adsorbent. A fixed bed system was prepared with a chromatographic glass column of length 30 cm and internal diameter 1.5 cm. The column contained 40 mL of beads. Cesium and strontium

solutions were passed through the column using a small pump and flow controller (Figure 2-3). The column study was specifically focused on the practical feasibility of large-scale treatment of cesium and strontium contaminated water (Al-Degs et al., 2009; Vijaya and Krishnaiah, 2010).

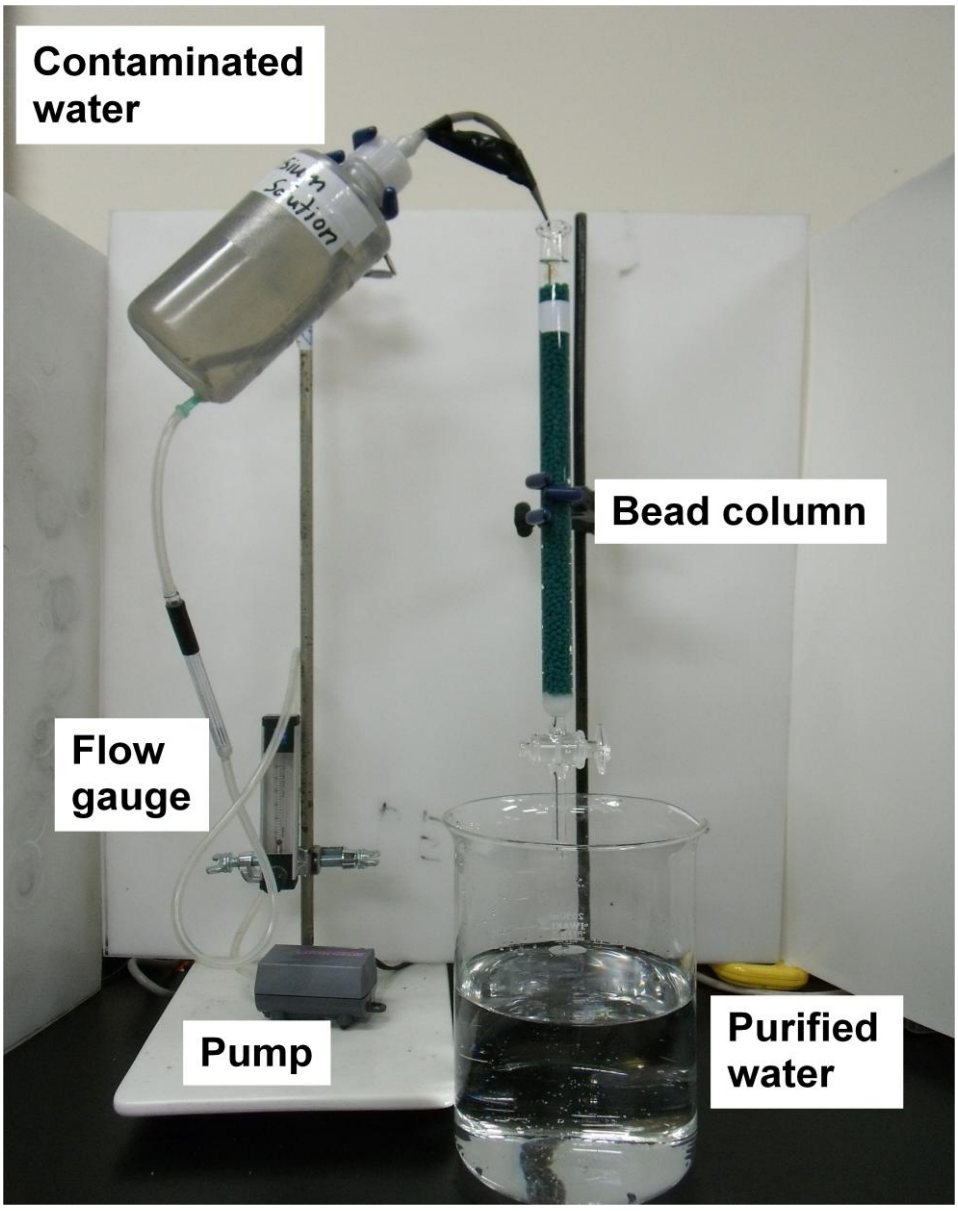

Figure 2-3 Photograph of fixed bed column apparatus

Chapter 3

PEFORMANCE EVALUATION ON THE AQUEOUS ELIMINATION OF CESIUM AND STRONTIUM IONS USING SYNTHESISED BEADS

3.1. Physical characterisation of PB and CoFC

3.1.1. SEM characterisation

The SEM images of prussian blue (Figure 3-1) and sodium cobalt hexacyanoferrate (Figure 3-2) showed the morphological idea of fine nanometre sized crystals. The nanosized crystals are clustered together to form a lump of material. Size of sodium cobalt hexacynoferrate crystals was comparatively larger than prussian blue. Single primary crystals of each of them were only several manometers in size. Whereas, the single primary crystals are clustered together to form big secondary particle have several micrometer in size. The synthesized micrometer sized prussian blue and sodium cobalt hexacyanoferrate were suitable for encapsulation into alginate vesicle. Because if the size is too small encapsulation faces leakage problem, whereas if the size is too big effective encapsulation will not be possible more over deformation in the morphology will happen.

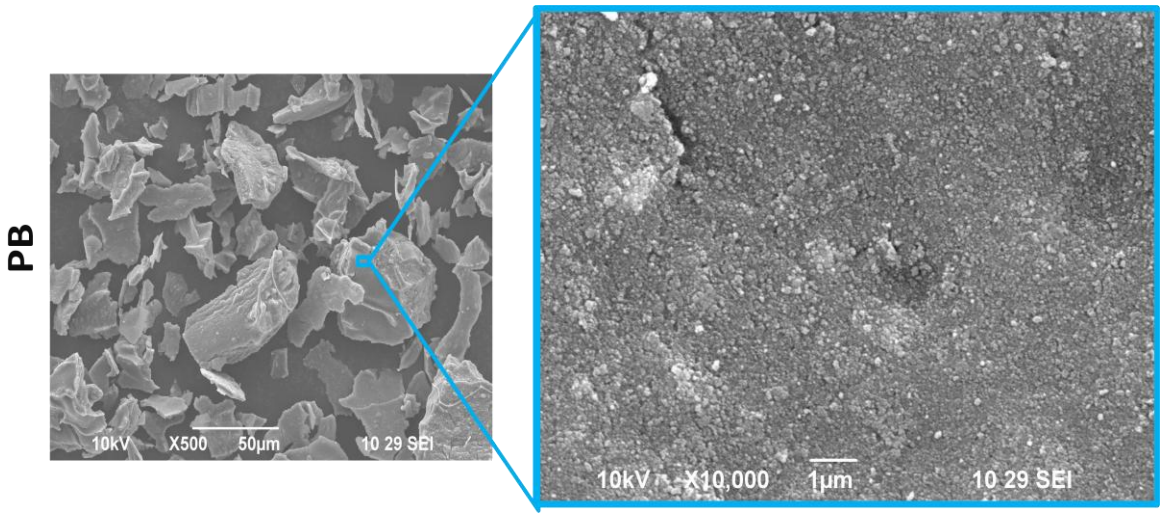

Figure 3-1 SEM images of PB crystals

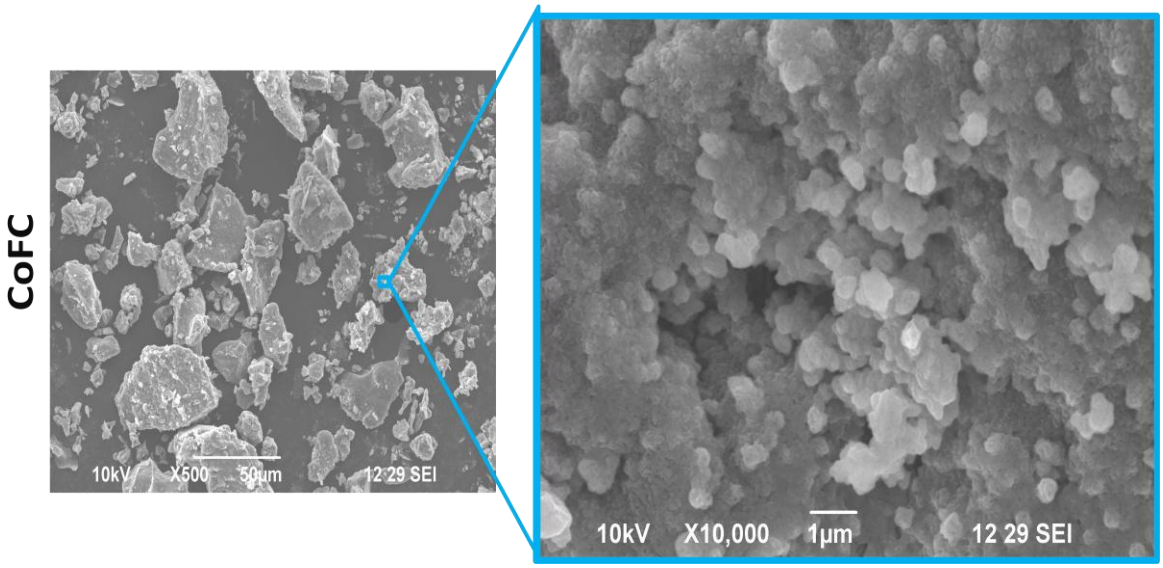

Figure 3-2 SEM images of CoFC crystals

3.1.2. TG characterisation

As an iron cyano complex, prussian blue has several water molecules incorporated in its crystal structure. The water molecules are of two types, zeolitic (physically adsorbed) and coordinating (chemically adsorbed). The number of zeolitic water depends on the drying condition while the number of coordinating water is usually six. The present sample of prussian blue contained 14 water molecules at 30 ºC, out of which eight were zeolitic and six were coordinating. The zeolitic water molecules release first on heating and then the coordinating ones at higher temperatures. In general, when insoluble prussian blue is heated, one endothermic effect corresponds to the release of water molecules occur. Afterward, thermal decomposition of the rest of the molecule occurs at higher temperatures

The thermogram indicated four decomposition steps: I (30-250 ºC), II (250-350 ºC), III (350-550 ºC) and IV (550-1000 ºC) (Aparicio et al., 2011). Thermo Gravimetric analysis curve for the decomposition of Prussian blue is revealed in Figure 3-3.

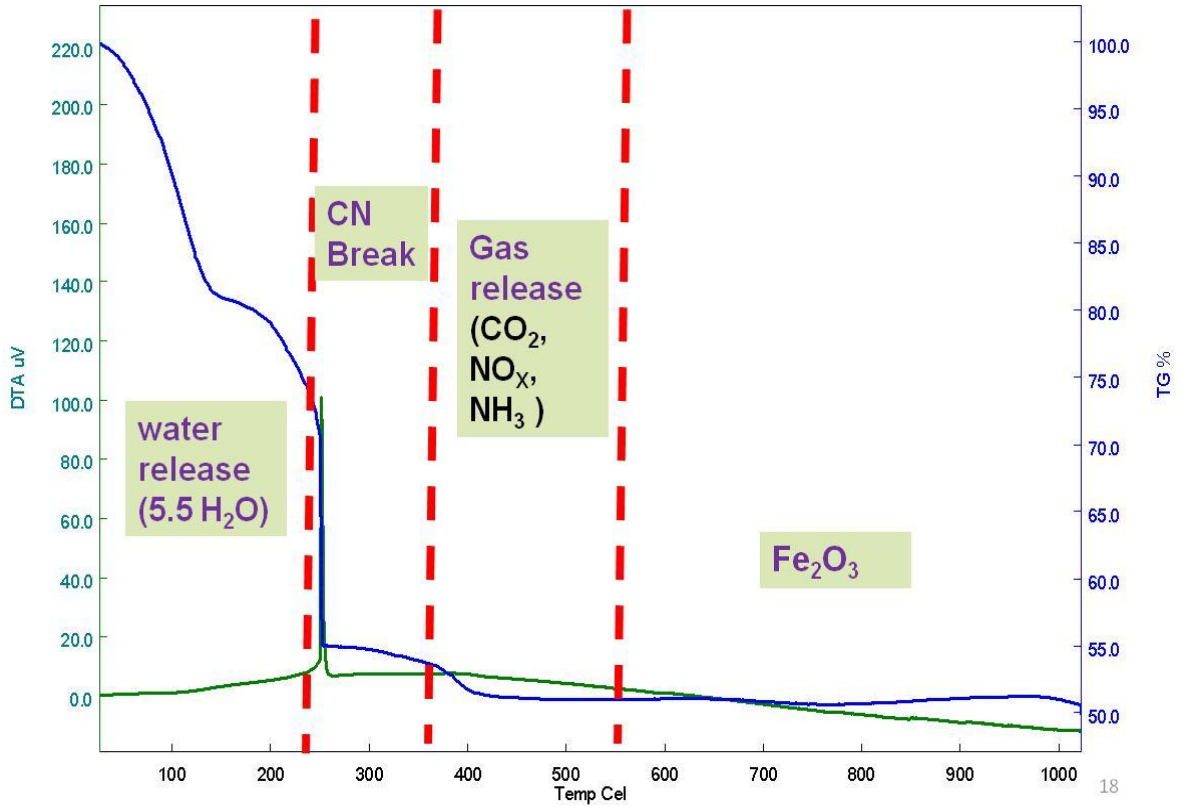

Figure 3-3 TGA thermogram of PB.

Since the samples had been dried at 80 ºC prior to analysis, the weight loss in step I is due to release of the 5.5 crystalline water molecules (coordinating), per one molecule of prussian blue. The mass decrease is consistent with the loss of 6 waters. However, this water loss does not affect the crystal structure. Step II is the most crucial step because it describes the initial steps of the decomposition of the cyano group (Lehto et al., 1990; Mimura et al., 1997). The decomposition is exothermic in nature and formed several intermediate products. In Step III, the decomposition of the intermediate products occurred. The weight loss was due to evolution of gaseous compounds of carbon and nitrogen such as CO_2, NO_x and NH_3 (Jukka et al., 1995). The solid product formed in this step was Fe_2O_3. Above 550 ºC is the final stage of the decomposition, which yields

Fe_2O_3 as the final product.

When CoFC is heated, one endothermic effect corresponds to a release of water molecules observed. Afterward, thermal decomposition of the rest of the molecule occurs at higher temperatures. The thermogram indicated four decomposition steps: I (30-250 ºC), II (250-450 ºC), III (450-650 ºC) and IV (650-1000 ºC) (Kunrath et al., 1978). Thermo gravimetric analysis curve for the decomposition of CoFC is shown in Figure 3-4.

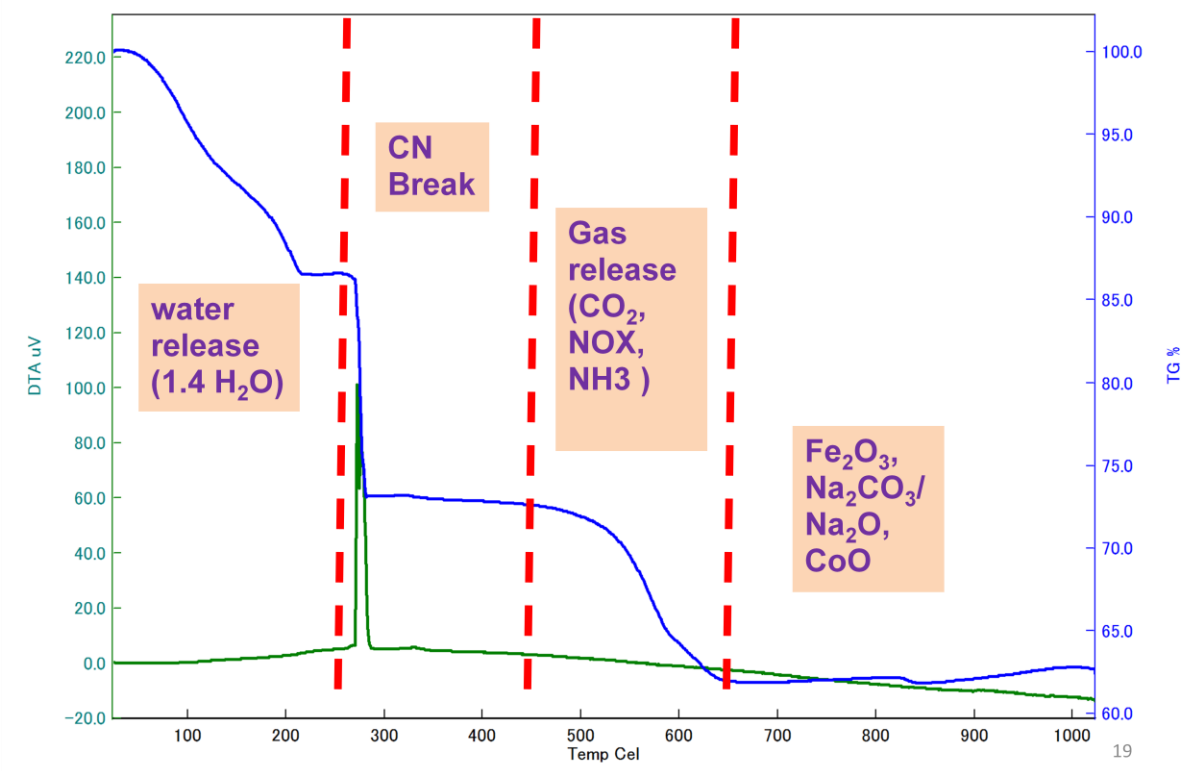

Figure 3-4 TGA thermogram of CoFC

The samples were dried at 80 ºC prior to analysis, the weight loss in step I was due to the release of 1.4 crystalline water molecules (coordinating), per one molecule of CoFC. However, this water loss did not affect the crystal structure. Step II is the most crucial step because it describes the initial steps of the decomposition of the cyano group (Jukka et al., 1995; Lehto et al., 1990). The decomposition is exothermic in nature and formed several intermediate products mainly $Na_3Fe(CN)_6$ and/or $Na_3Co(CN)_6$, Na_2CO_3, Fe_2O_3, Co_3O_4 and $CoFe_2O_4$. In Step III, the decomposition of the intermediate products occurred. The weight loss was probably due to the evolution of gaseous compounds of carbon and nitrogen such as CO_2, NOx and NH_3. The solid products formed in this step were Na_2CO_3, Fe_2O_3, Co_3O_4 and $CoFe_2O_4$. Above 650 ºC, the final stage of the decomposition was reached, which yields Na_2CO_3/Na_2O, Fe_2O_3 and CoO as the final products (Lehto et al., 1990).

The detailed thermo gravimetric analysis revealed that the synthesized sample were true prussian blue and cobalt hexacyanoferrate.

3.1.3. FT-IR characterisation

In the FT-IR spectrum of prussian blue (Figure 3-5), the sharp peak at 2071.02 cm^{-1} is characteristic of the Fe-CN bond, corresponding to the stretching vibration of Fe-CN. The peaks at 3357.86 cm^{-1} and 1602.17 cm^{-1} were characteristic of O-H stretching and H-O-H bending modes, respectively, of the interstitial water molecules. Peaks at 594.93 cm^{-1} and 501.4 cm^{-1} were associated with the metal- carbon –nitrogen bending modes (Farah et al., 2012;

Kulesza et al., 1996; Liu et al., 2011; Ruiz-Bermejo et al., 2009).

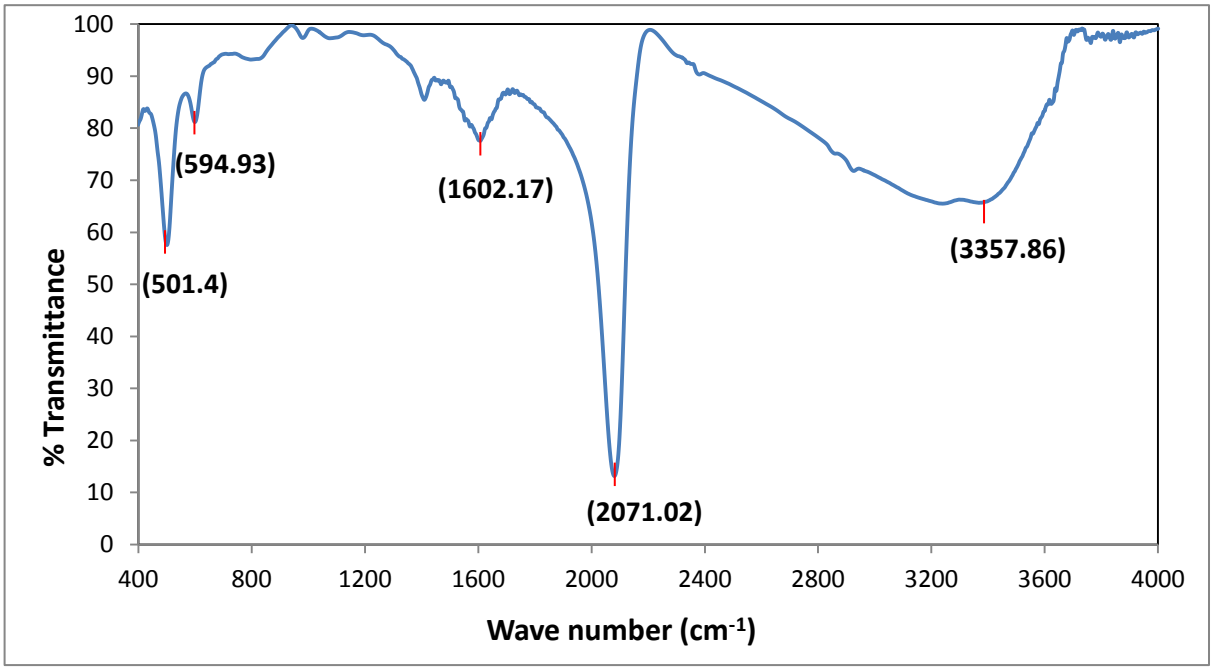

Figure 3-5 FT-IR spectrum of PB.

In the FT-IR spectrum of CoFC (Figure 3-6), the sharp peak at 2079.85 cm^{-1} is characteristic of the Fe-CN bond, corresponding to the stretching vibration of Fe-CN. The peaks at 3339.13 cm^{-1} and at 1612.16 cm^{-1} were characteristic of O-H stretching and H-O-H bending modes, respectively, of the interstitial water molecules. Peaks at 588.25 cm^{-1} and 457 cm^{-1} were associated with the metal-carbon-nitrogen bending modes (Chen, 1998; Gao et al., 1991; Ismail et al., 1998; Mimura et al., 1997; Moon et al., 2004).

FT-IR spectrum of synthesized samples was exactly matching with reported data, thus the samples were identified as pure prussian blue and cobalt hexacyanoferrate.

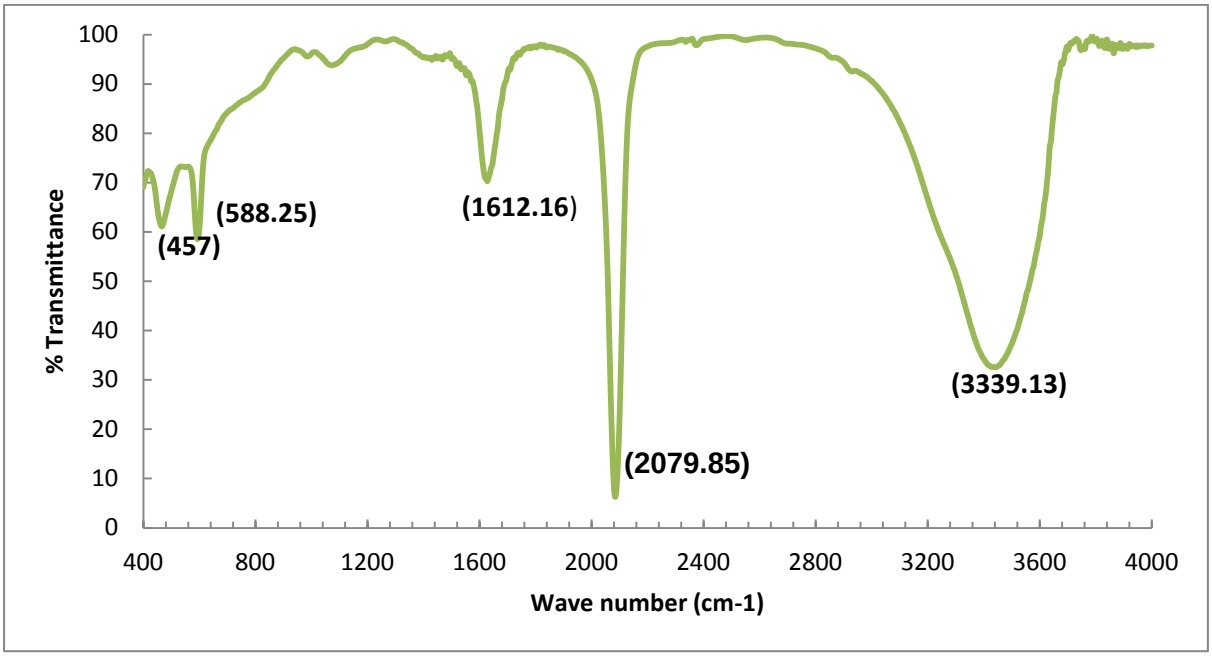

Figure 3-6 FT-IR spectrum of CoFC

3.1.4. XRD characterisation

The XRD pattern of prussian blue (Figure 3-7) showed characteristic diffraction peaks at 17.52, 24.78, 35.3, 39.52, 43.6, 50.72, 53.8 and 57.3º corresponding to the 200, 220, 400, 420, 422, 440, 600 and 620 crystal planes, respectively. This pattern is consistent with prussian blue having a face centered cubic structure with space group Fm3m (Farah et al., 2012; Li et al., 2004; Liu et al., 2011; Mimura et al., 1997).

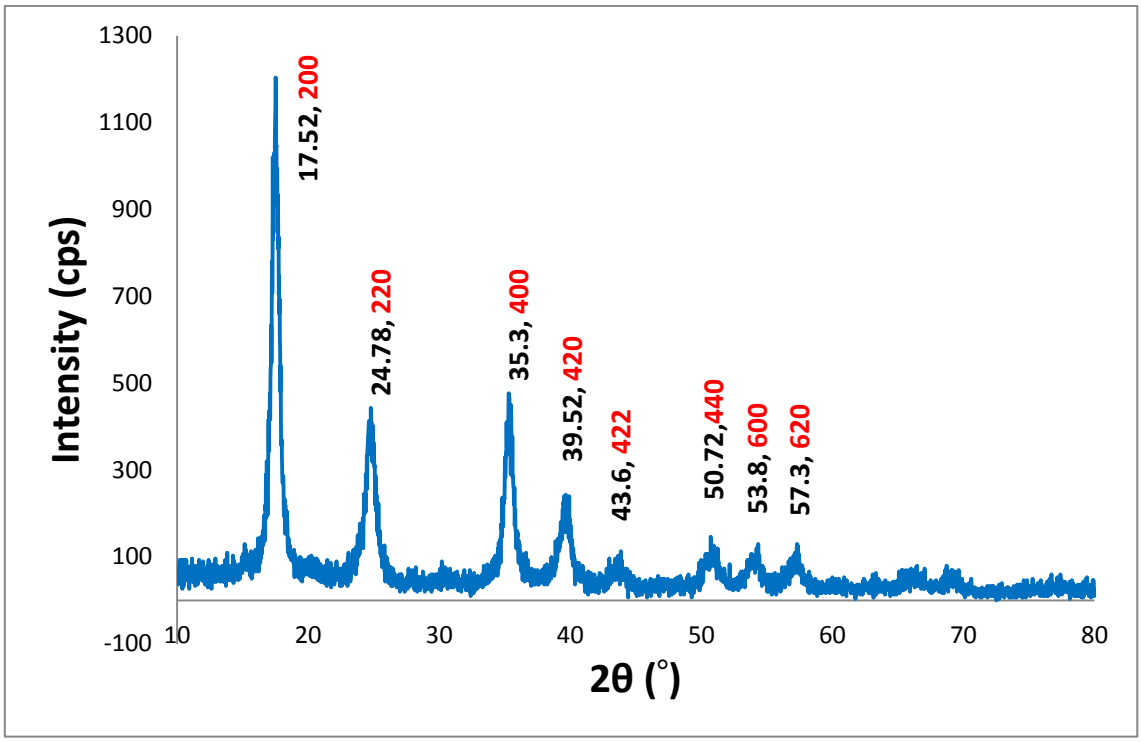

Figure 3-7 XRD spectrum of PB.

The XRD pattern of CoFC (Figure 3-8) showed characteristic diffraction peaks at 17.16, 24.42, 34.66, 39.14, 42.32, 50.32, 53.26 and 56.42º corresponding to the 200, 220, 400, 420, 422, 440, 600 and 620 crystal planes, respectively. This pattern confirmed that CoFC having a face centered cubic structure with space group Fm3m (Farah et al., 2012; Mimura et al., 1997).

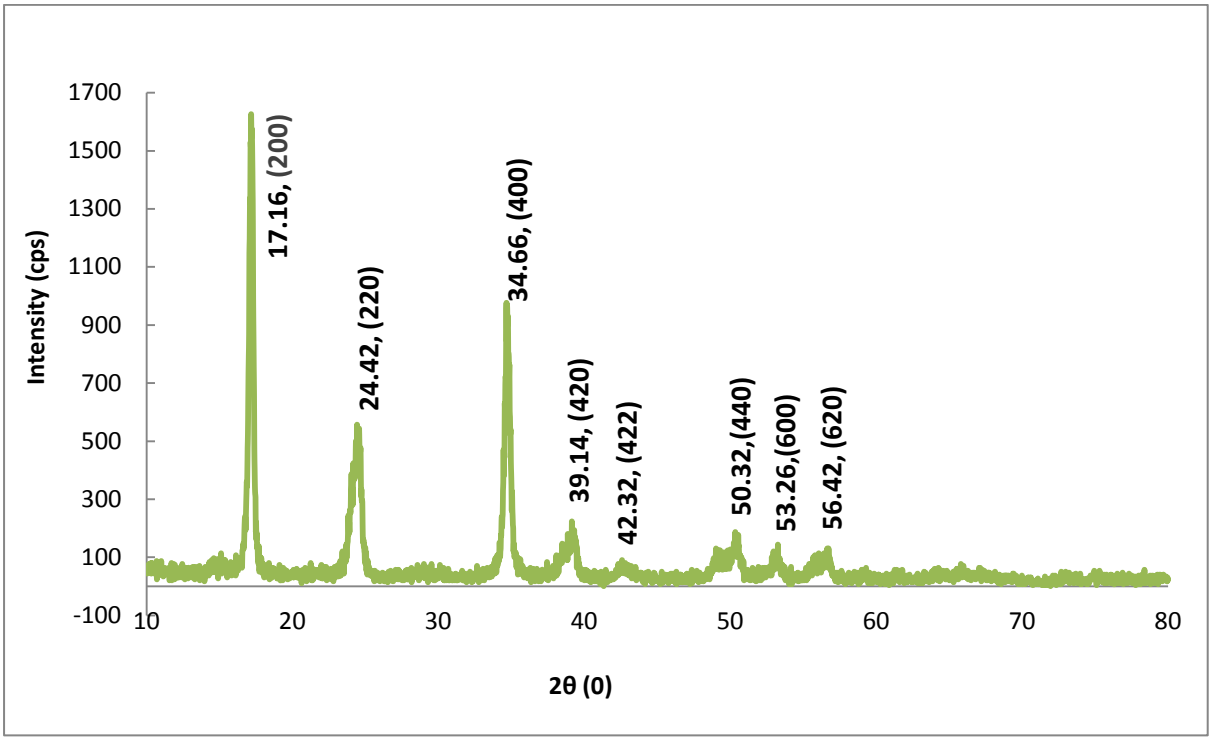

Figure 3-8 XRD pattern of CoFC

3.1.5. EDS Analysis

Energy Dispersive Spectroscopic analysis is an effective method in order to understand the surface elemental distribution of a material. The specific elemental distribution of synthesized prussian blue and sodium cobalt hexacyanoferate showed in figure 3-9. From the EDS analysis confirmed that the surface of the PB crystals contain no or any sodium ions, whereas 1.1% sodium ion was distributed on the surface of CoFC crystals.

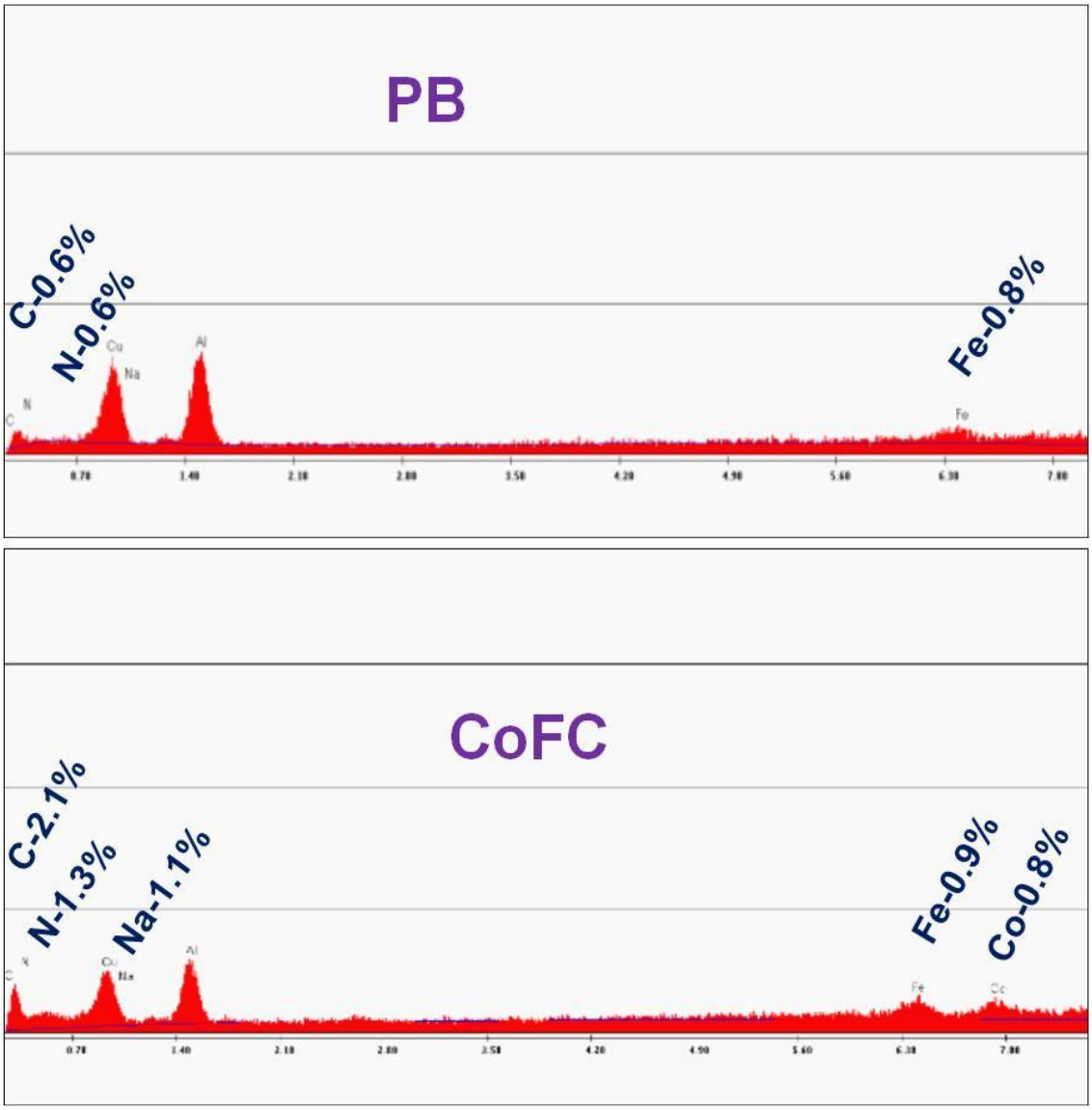

Figure 3-9 Energy Dispersive Spectrum of PB and CoFC crystals

3.2. Physical characterisation of Zeolite

3.2.1. SEM characterisation

The SEM images of zeolite is showed in Figure 3-10. The morphology of fine nanometre sized crystals is clearly visible in the SEM images. The morphology of prepared zeolite has unique cubic structure. Size of the single zeolite crystals ranges from two to four micrometer. Size of zeolite was comparatively bigger than prussian blue and sodium cobalt hexacyanoferrate.

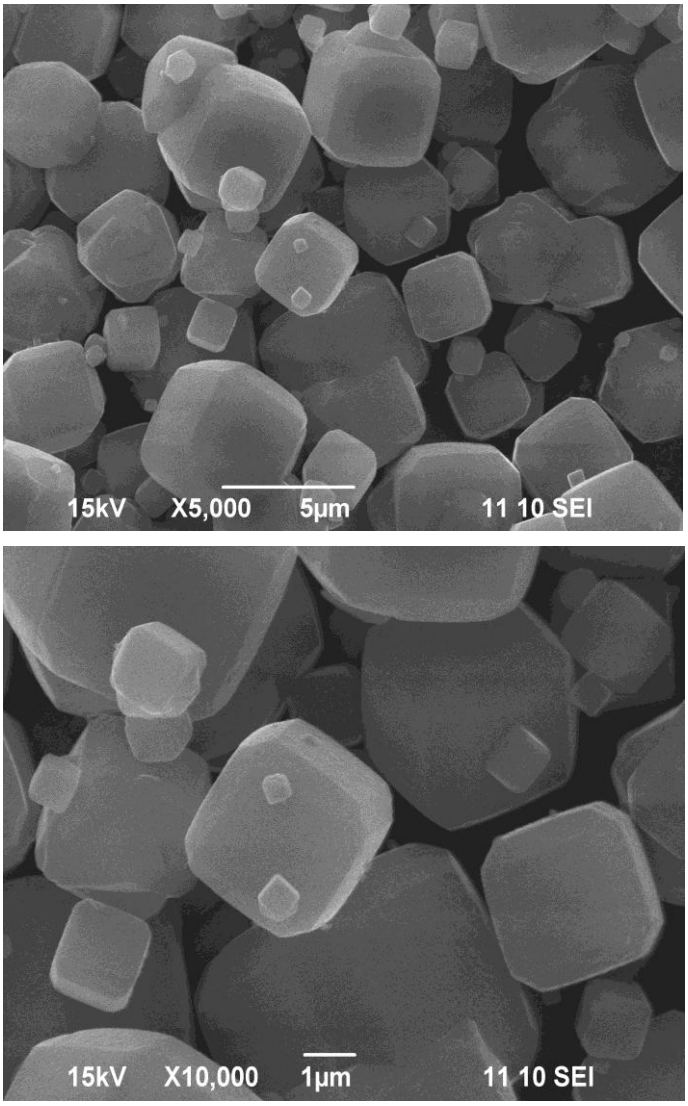

Figure 3-10 SEM images of zeolite crystals

3.2.2. XRD characterisation

The XRD pattern of zeolite (Figure 3-11) showed characteristic diffraction peaks at 2θ value 7.2, 10.3, 12.6, 21.8, 24, 26.2, 27.2, 30, 30.9, 31.1, 32.6, 33.4, and 34.3 degrees corresponding to the 100, 110, 111, 210, 220, 300, 311, 320, 321, 410, 411, 420 and 421 crystal planes, respectively. This typical pattern confirm that the synthesized zeolite was A type (Ismail et al., 2010).

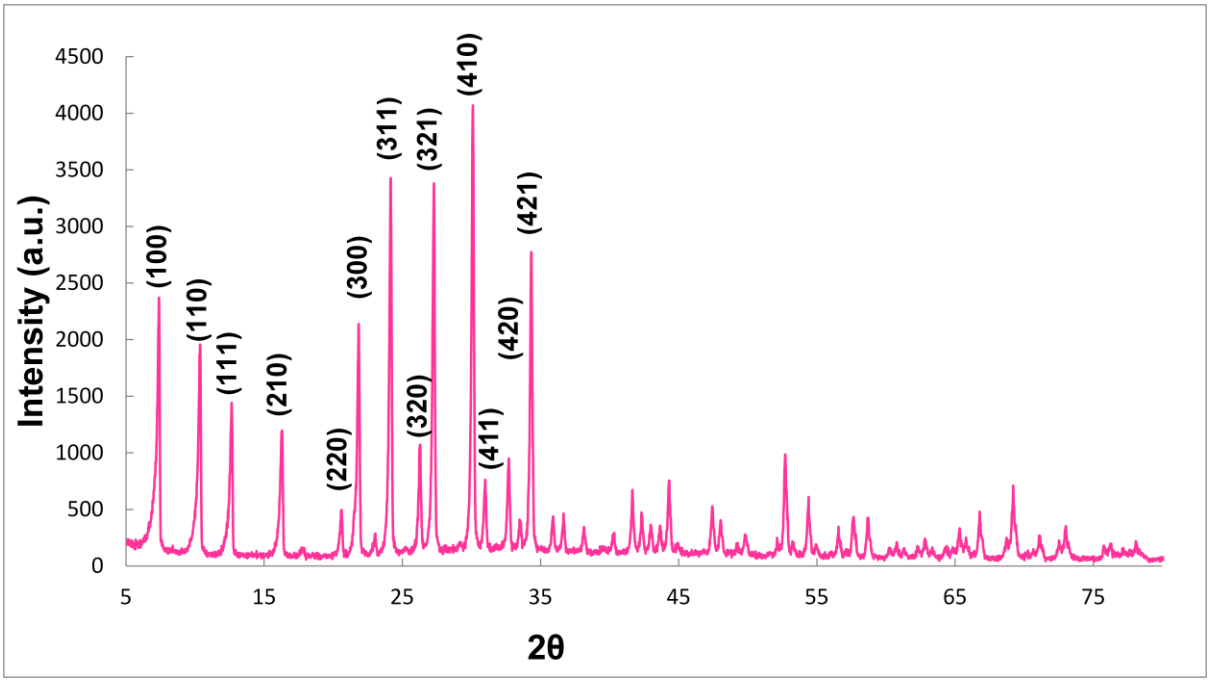

Figure 3-11 XRD spectrum of zeolite A

3.3. Morphological characterisation of developed beads

The photographs of all prepared beads after freeze-drying are given in figure 3-12. Eight different types of beads were shown. The images showed that all the beads have almost same size and morphology. The colour of adsopritve materials was masked by black colour.of MWCNTs while reinforcing, which demostrating that the dispersion of MWCNTs in the beads was high.The beads were stable, strong and easy to handle.

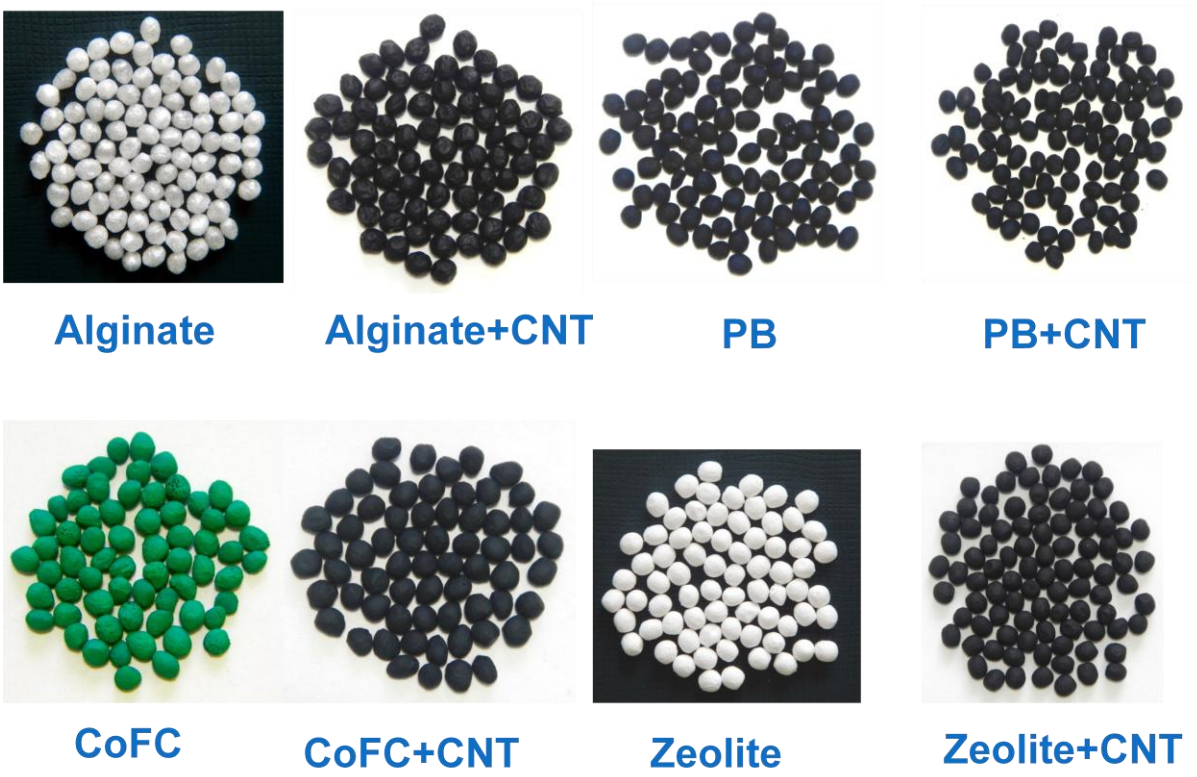

Figure 3-12 Photographs of different types of developed beads.

3.3.1. PB encapsulated beads

The images (Figure 3-13) of freeze dried beads of prussian blue encapsulated in alginate with and without MWCNTs reinforcements showed that both types of the full sized beads were remarkably similar in size, ranging from 2.3-2.5 mm in diameter (Figure 3-13A vs 3-13E). Images of the vertical cross section of the beads (Figure 3-13B and 3-13G) showed that the beads contained several porous channels. In horizontal cross section, the shape and structure of the channels were more visible, substantiating the similar structures of the two types of beads (Figure 3-13C and 3-13F). In highly magnified images of both types of beads, they appear highly cross-linked and with immense porosity. The capacity of calcium alginate to support and stabilize the encapsulated Prussian blue beads is evident. During bead formation, numerous prussian blue crystals aggregated together and became encapsulated in the network of calcium alginate (Figure 3-13D). Reinforcement by MWCNTs held the Prussian blue more strongly inside the beads by forming a physical network over Prussian blue crystals figure, as illustrated by Figure 3-13H.

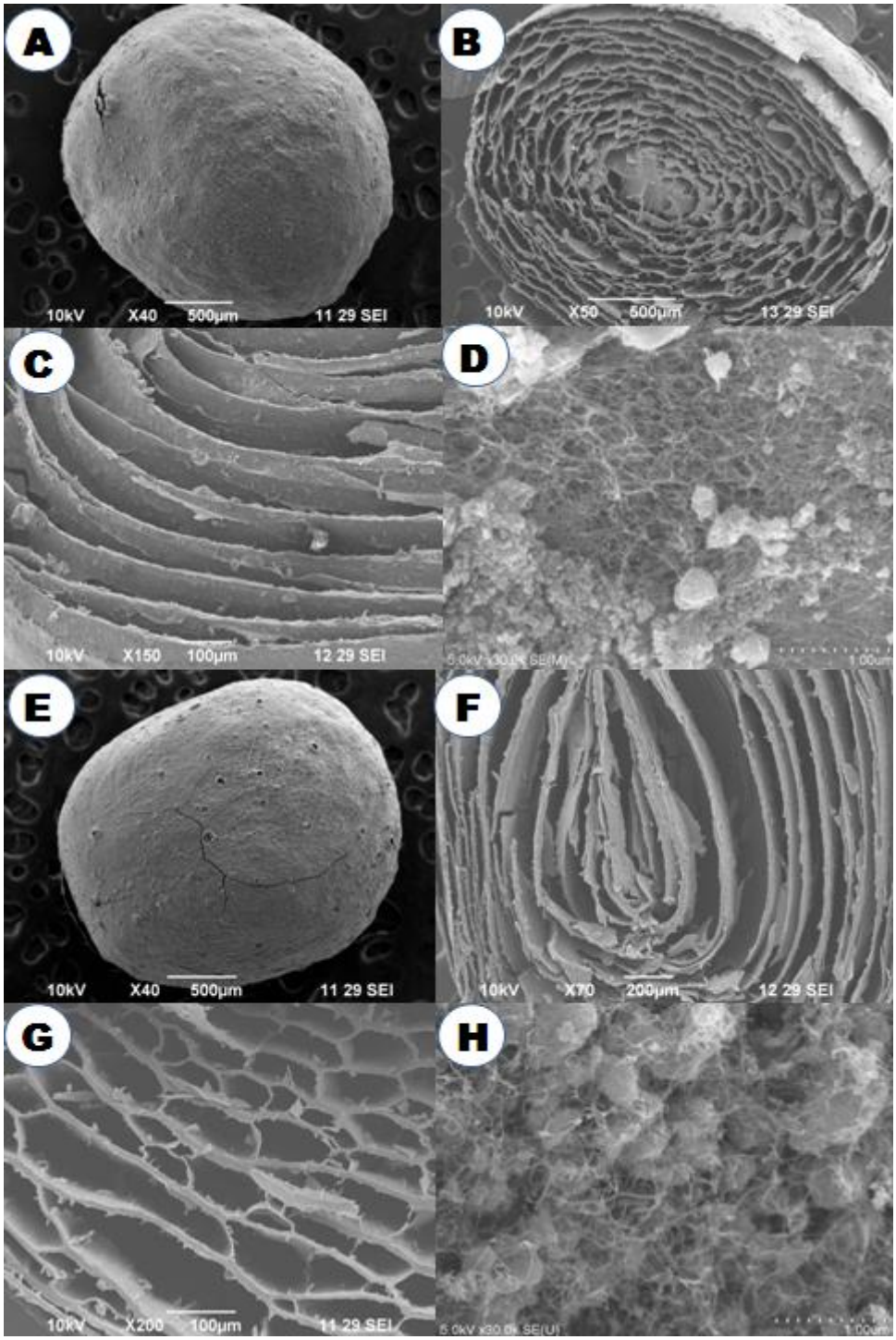

Figure 3-13 SEM images of beads. Prussian blue encapsulated bead without CNTs: (A) whole sized, (B) vertical cross section, (C) horizontal cross section and (D) Highly magnified images. Prussian blue encapsulated bead with MWCNTs: (E) whole sized, (F) vertical cross-section, (G) horizontal cross section and (H) highly magnified images.

3.3.2. CoFC encapsulated beads

The SEM images (Figure 3-14) of freeze dried beads of CoFC encapsulated in alginate with and without MWCNTs reinforcement showed that both types of the full sized beads were remarkably similar in size, ranging from 2.3 to 2.5 mm in diameter (Figure 3-14A vs 3-14 E). Images of the vertical cross section of the beads (Figure 3-14B and 3-14 F) showed that the beads contained several porous channels. In the horizontal cross section, the shape and structure of the channels were more visible, substantiating the similar structures of the two types of beads (Figure 3-14C and 3-14 G). In highly magnified images of both types of beads, they appeared highly cross-linked and with immense porosity. The capacity of calcium alginate to support and stabilize the encapsulated CoFC beads is evident. During bead formation, numerous CoFC crystals aggregated together and became encapsulated in the network of calcium alginate Figure 3-14D. Reinforcement by MWCNTs held the CoFC more strongly inside the beads by forming a physical network over CoFC crystals figure, as illustrated by Figure 3-14H. Moreover, MWCNTs help to enclose more CoFC inside each bead, which will enhance the adsorption efficiency.

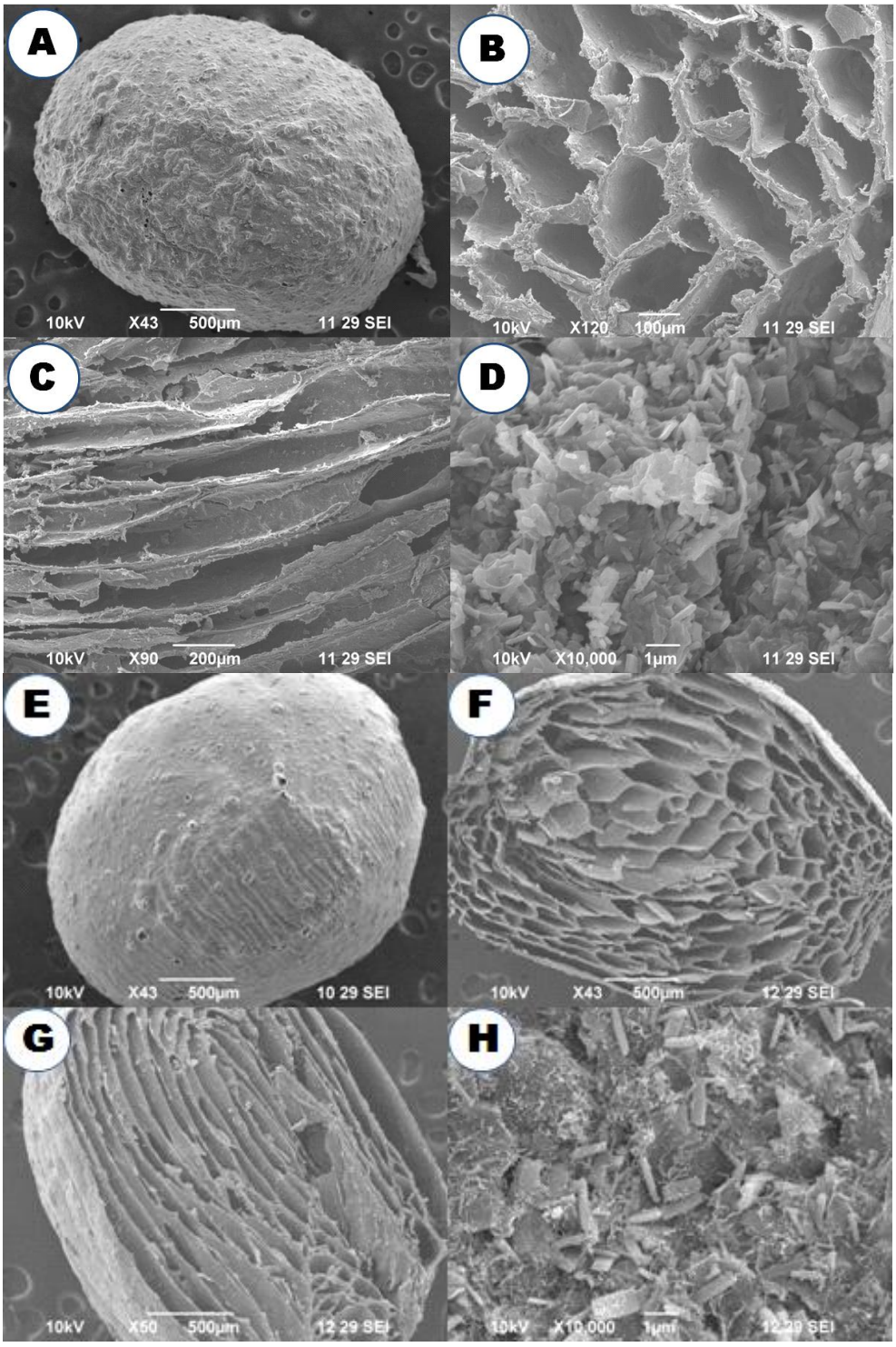

Figure 3-14. SEM images of beads. Sodium cobalt hexacyanoferrate encapsulated bead without CNT: (A) whole sized, (B) vertical cross section, (C) horizontal cross section and (D) highly magnified images. Sodium cobalt hexacyanoferrate encapsulated bead with MWCNTs: (E) whole sized, (F) vertical cross-section, (G) horizontal cross section and (H) highly magnified images.

3.3.3. Zeolite encapsulated beads

Figure 3-15 gives the morphological information of zeolite encapsulated alginate beads modified with MWCNTs. Figure 3-15A is the whole sized beads having the diameter 2-2.5 mm. The image of vertical crosection at low magnification is depicted in Figure 3-15B. The unique MWCNTs network over zeolite is clearly visible in Figure 3-15C.

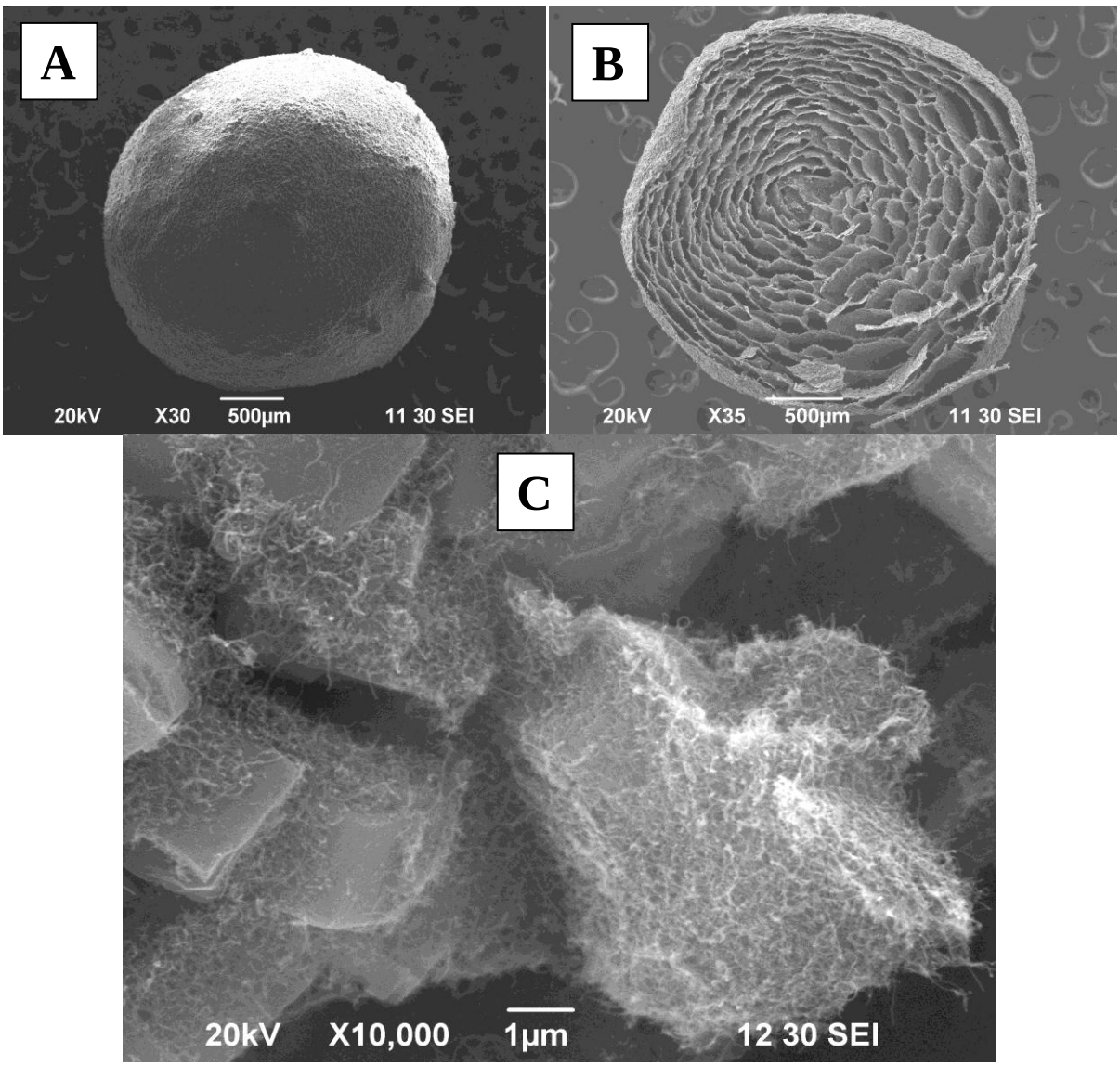

Figure 3-15 SEM images of zeolite encapsulated bead with MWCNTs: (A) whole sized, (B) vertical cross section, (C) highly magnified image

3.3.4. MWCNTs network formation

Figure 3-16 gave a clear proof about MWCNTs network formation. While cutting the beads, the wall got disturbed and lot of MWCNTs lost from the surface (Figure 3-16A). However, when we observed the undisturbed portion in Figure 3-16B we could see MWCNTs network along with alginate vesicle. A layer of physically cross-linked MWCNTs was formed that will hold adsorptive material more strongly inside the alginate matrix. So the leaching of adsorptive material from the beads is completely blocked.

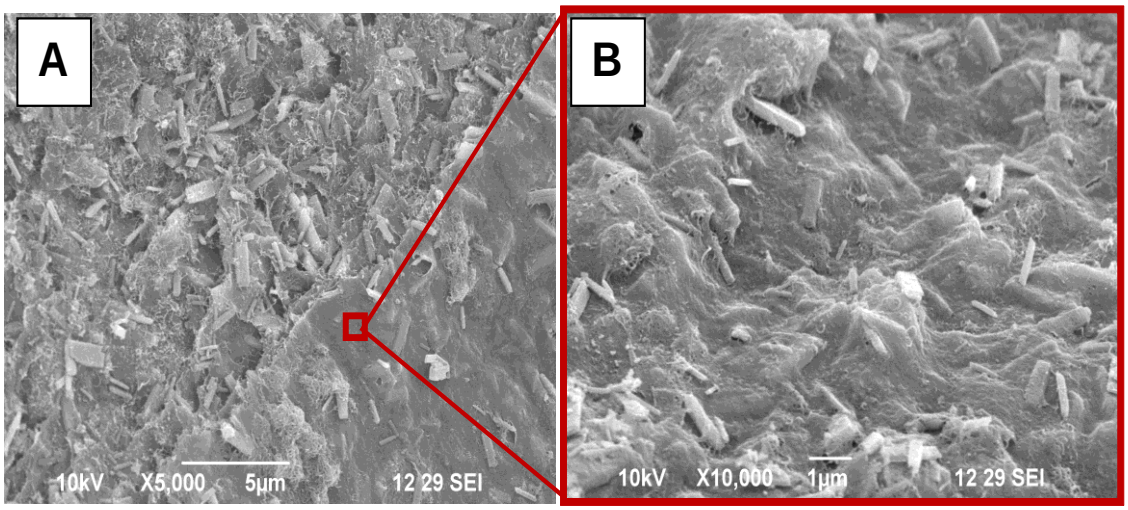

Figure 3-16 Carbon nanotubes physical network formation. A) Cut wall of beads B) Undisturbed area with carbon nanotube network.

3.4. BET analysis of beads.

Surface area and porosity are important characteristics, which affect the quality and utility of materials in adsorption. In addition, they are helpful in understanding the structure, formation and applications of materials. For this reason, it is important to determine and control them accurately. The most widely used technique for estimating surface area is the BET method (Brunauer, Emmett and Teller, 1938). The important BET parameters of developed beads are given in Table 1. We could understand that MWCNTs succeeded to enhance the beads surface area and effective pore volume. Pore size was between 2 to 46 nm in diameter, which means that pores were mesoporous. The surface area of beads was depending on the encapsulated adsorptive particle. Prussian blue crystals were relatively small so the surface area of PB encapsulated beads with and without MWCNTs showed highest surface area value. Because of zeolite's unique porous structure, zeolite beads showed higher surface area than CoFC beads even though single crystals of zeolite were bigger than CoFC. At high surface area alginate matrix gets more chance to contact with more divalent ions that make the beads stronger. From the SEM and BET studies, we could confirm the importance of MWCNTs.

Table 1. BET parameters of beads

Beads/Parameters	**Surface Area m^2g^{-1}**	**Monolayer Volume (V_m) m^3g^{-1}**	**Pore size nm**
Alg	32.6	7.4847	46.44
Alg+CNT	33.1	7.6	18.12
Alg +PB	184.3	42.35	2.49
Alg+PB+CNT	256	58.8	7.09
Alg+CoFC	37.9	8.70	25.86
Alg+CoFC+CNT	44.5	10.217	38
Alg +Zeolite	64.6	20.2	5.6
Alg +zeolite+CNT	82.4	32.36	4.89

3.5. Effect of MWCNTs on the morphology of beads.

MWCNTs have its own contribution to the encapsulation efficiency and morphological stability of beads. In 3wt% alginate, maximum encapsulation of adsorptive particle was only 10wt% (Figure 3-17A). When the amount of adsorptive particle was further increased, the deformation in the morphology of beads was observed. Figure 3-17B was the beads from colloidal solution containing 15wt% zeolite without MWCNTs. The formed beads were bigger than normal size. Moreover, most of the beads were with a long tale because of high viscosity of colloidal solution. The morphological deformation could fix by the addition of MWCNTs (Figure 3-17C). Up to 25wt% adsorptive particle encapsulation into 3wt% alginate solution was possible by the help of MWCNTs. The main reason for this advantage was the unique networking properties of MWCNTs. MWCNTs forms a strong physical network over crystals, which hold each crystal closer in the matrix.

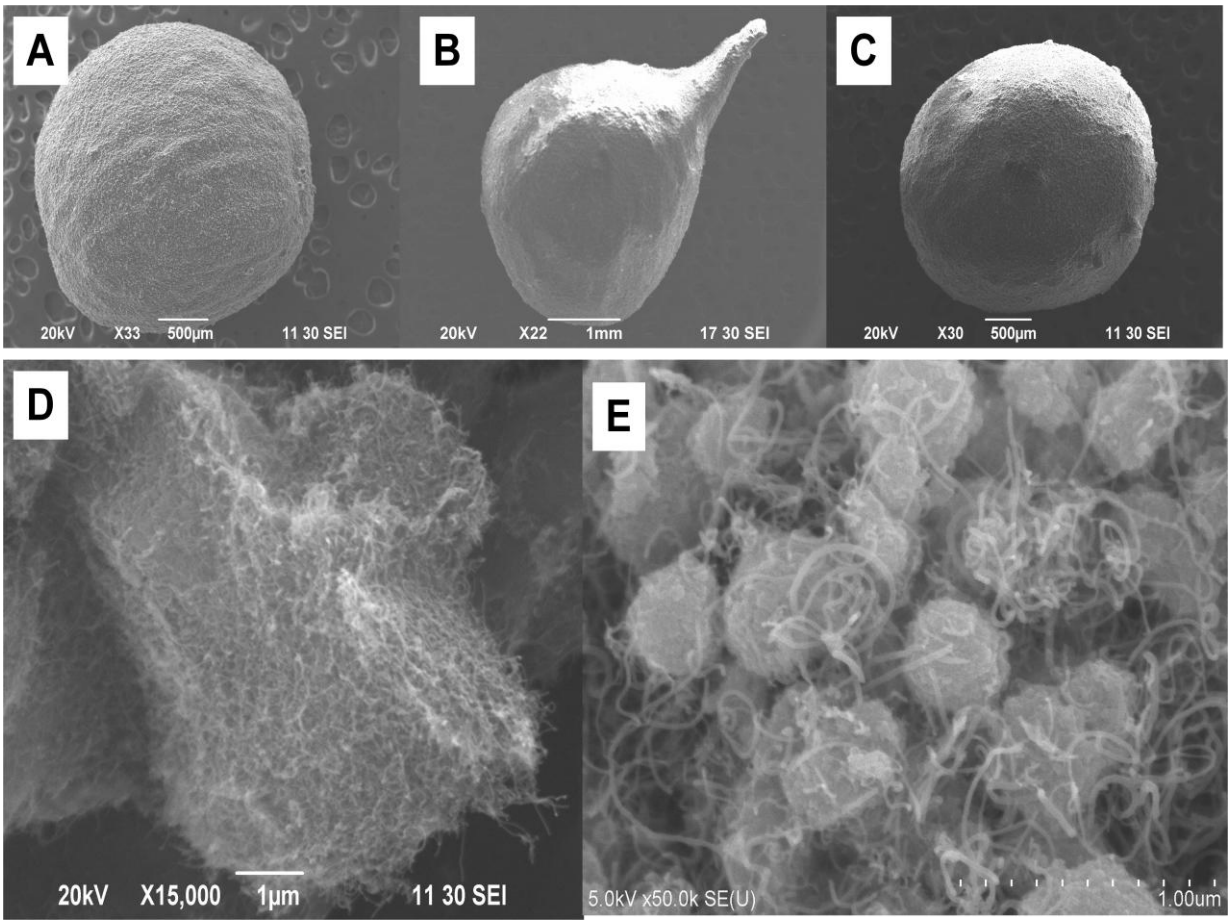

Figure 3-17 A. Beads from colloidal solution containing 10wt% zeolite (without MWCNTs). **B.** Beads from colloidal solution containing 15wt% zeolite (without MWCNTs). **C.** Beads from colloidal solution containing 15wt% zeolite (with MWCNTs).**D.** MWCNTs wrapping over zeolite crystals. **E.** CNT networks (high magnification).

3.6. Comparative study on cesium and strontium adsorption

The principle aim of the study was simultaneous removal of cesium and strontium from aqueous medium. For that purpose, three adsorptive materials were used for encapsulation. As the primary stage of experiment, I conducted a comparative study on the adsorption capability of prepared beads.

Forty beads were added to 40 mL, 200 ppm cesium solution and allowed to shake at 300 rpm. The adsorption efficiency of the different types of beads with respect to time is shown in Figure 3-18. Pure alginate beads showed very low adsorption efficiency, with values below 7%. Thus, specific adsorption by the alginate matrix was negligible. Prussian blue encapsulated alginate beads showed a distinct improvement in cesium uptake, removing ~85% of cesium from the solution. The presence of carbon nanotubes in the prussian blue encapsulated alginate beads had no deleterious effect on cesium uptake. Indeed, the CNTs gave an improvement (90% removal) to adsorption of cesium from the solution. The effectiveness of both types of beads was dependent on encapsulation efficiency of prussian blue. This slight increase in adsorption conferred by MWCNTs may reflect a greater physical network composed of nanotubes that can entrap cesium inside the beads.

In the case of strontium, initial concentration was 100 ppm and the number beads used was twenty. Adsorption efficiency was measured at different time interval. Adsorption of strontium primarily depends on the availability of alginate matrix. In that case, encapsulation decreases effective availability of

sites for adsorption. From the removal capacity data easily understood that pure alginate beads showed higher adsorption capacity than alginate based MWCNTs beads (Figure 3-19). Prussian blue encapsulated alginate beads showed less adsorption capacity than pure alginate beads. The presence of carbon nanotubes in the prussian blue encapsulated alginate beads again decreasing the strontium uptake. Thus, we can conclude that prussian blue encapsulated alginate beads are excellent adsorbent for cesium uptake, but the strontium adsorption was not promising.

In order to solve this problem we selected stable analogue of prussian blue, sodium cobalt hexacyanoferrate. However, in our study, we found that CoFC encapsulated beads showed high sorption efficiency towards strontium (Figure 3-19). The results indicating that a collective adsorption by both alginate and CoFC was happened. Because the presence of sodium ions on the surface of the CoFC crystals. More over carbon nanotubes in the CoFC encapsulated alginate beads increasing the strontium uptake by enhancing the encapsulation.

Both calcium alginate and calcium alginate encapsulated MWCNTs beads have negligible adsorption ability towards cesium uptake. CoFC was the vital material for the adsorption of cesium ions, therefore, CoFC encapsulated alginate beads as well as Carbon nanotubes reinforced CoFC encapsulated alginate beads were very central. The effectiveness of both types of beads was depending on encapsulation efficiency. Figure 3-19 gives a clear indication that reinforced beads have higher adsorption capacity than normal CoFC

encapsulated beads. This increase may be due to the participation of carbon nanotubes, via physical entrapment by forming a physical network inside the beads. Cesium removal using CoFC encapsulated beads were relatively lesser than PB encapsulated beads. Whereas, CoFC encapsulated bead's strontium removal was much higher than PB encapsulated beads. However, strontium removal by PB encapsulated beads was not so higher than pure alginate beads.

In order to improve strontium removal zeolite-A was considered in this study. The enhanced encapsulation of zeolite was possible by the help of MWCNTs. Zeolite encapsulated bead's cesium removal was relatively lesser than CoFC and PB encapsulated beads, whereas strontium removal was much higher than all other beads. From the results, we could understand that the MWCNTs not only reinforcing the beads stability but also enhancing the adsorption rate in some extent.

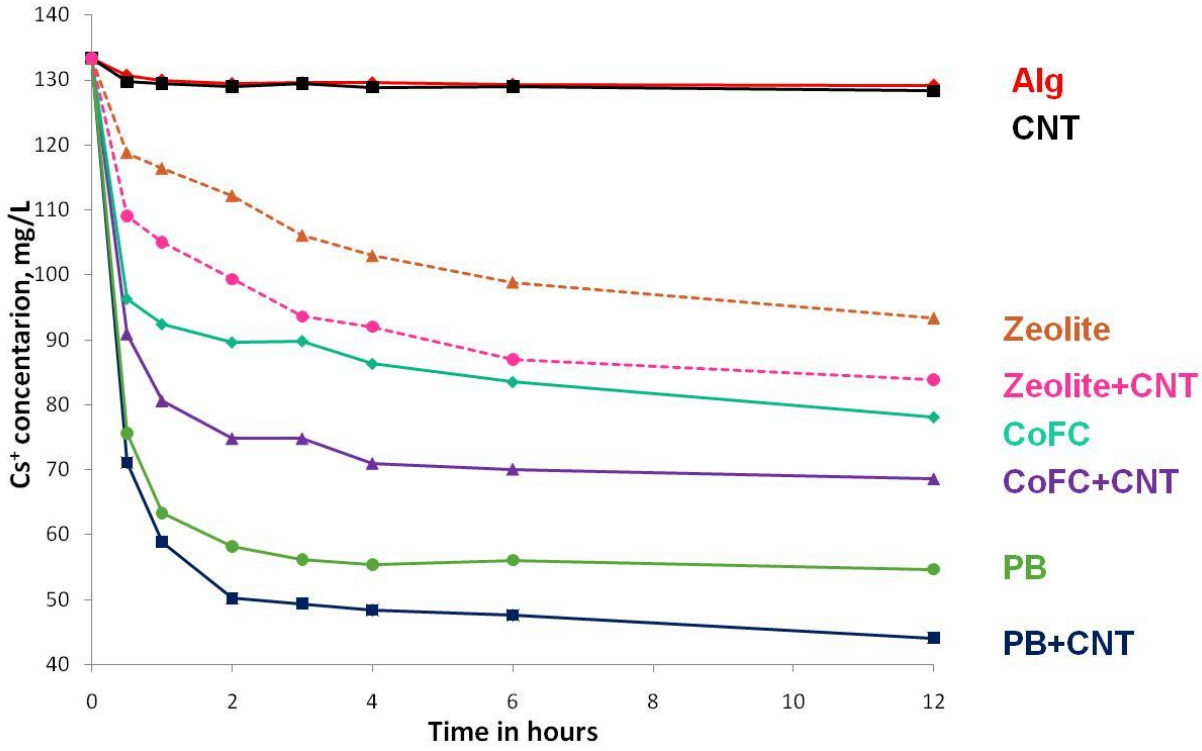

Figure 3-18 A comparative study on cesium removal by different beads

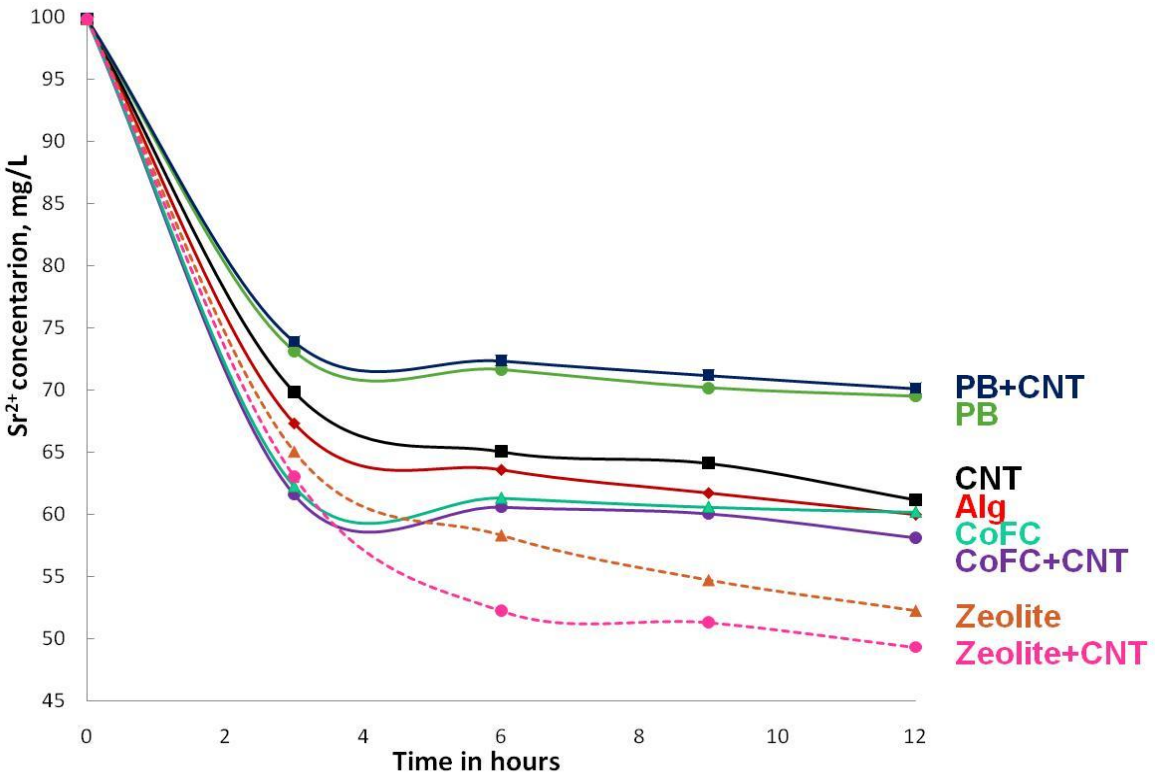

Figure 3-19 A comparative study on strontium removal by different beads

3.7. Adsorption kinetic study

To understand the adsorption behavior and rate kinetic models are very necessary. Large numbers of kinetic models are available, out of which pseudo first order and pseudo second order models are most widely using for adsorption experiments. Therefore, in the study two adsorption isotherm model were took into consideration, they were pseudo first order and pseudo second order models.

For both cesium and strontium adsorption, the pseudo second order correlation values for all beads were higher than pseudo first order models, Indicating that Adsorption following the pseudo second order models for all beads. When an experimental data fit with pseudo second order models, certain assumption on adsorption behavior and mechanism is possible.

Major assumptions obtained from the pseudo second order models was that the rate-limiting step might be chemical adsorption involving sharing or exchange of electrons. The main advantages of pseudo second order model are no need to know adsorption equilibrium capacity, adsorption rate and adsorption capacity can be easily obtain (Kumar, 2006; Qiu et al., 2009). From pseudo second order model adsorption rate in the case of both cesium and strontium adsorption by different beads were calculated and articulated in Figure 3-20 and Figure 3-21 respectively. The various adsorption kinetic parameters and non-linear curve fitting plots are given in the Appendix I and Appendix II respectively. Compare with strontium, cesium adsorption was fast. In the case of cesium adsoption, both metal hexacyanoferrate beads showed higher rate than

zeolite beads and reached its equilibrium at faster rate. The results brought into a conclusion that the cesium binding ability on metal hexacyanoferrates was strong. However, in the case of strontium adsorption, all the beads have almost same rate. More precisely zeolite beads are comparatively better performance than metal hexacyanoferrate beads. The effect of MWCNTs on the adsorption rate was also noticeable. MWCNTs helped to increase the adsoption rate by increasing the surface area of the beads. Higher the surface area the adsorbate can easily make contact with the adsorptive particle, thus the adsorption rate also increase. The MWCNTs helped to disperse the adsorptive particle into the beads rather than making them into big cluster. MWCNTs Also provide more active pathway for contaminate ions to reach into target adsorbing sites very easily.

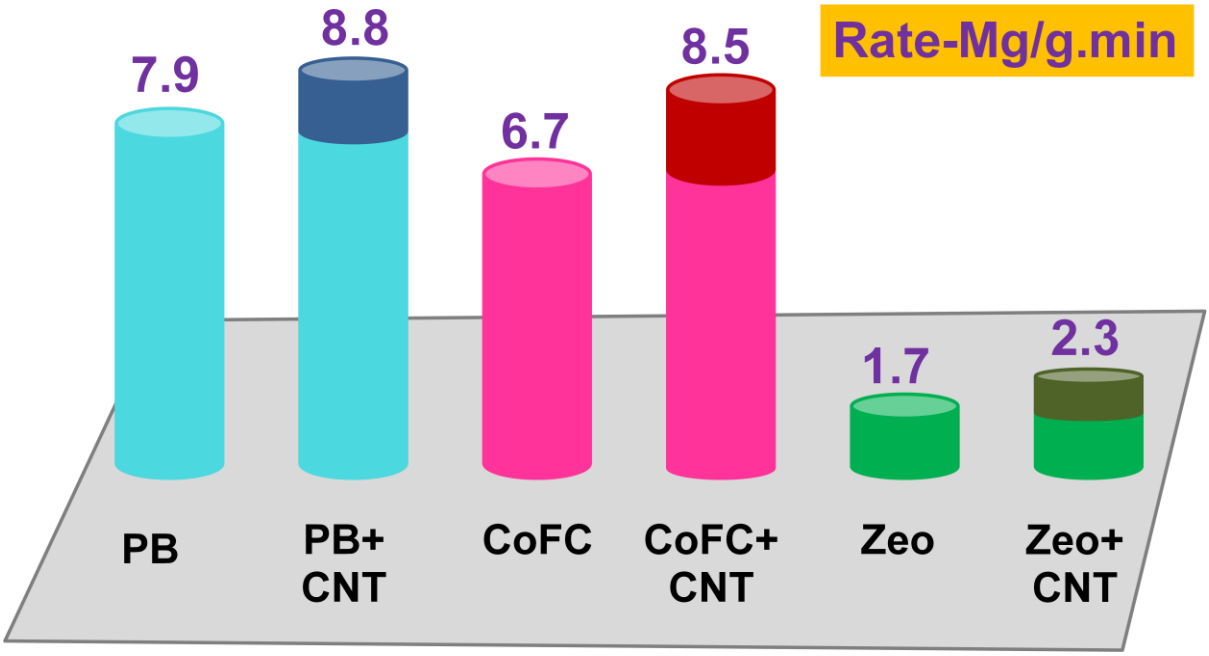

Figure 3-20 Cesium adsorption rate of each adsorbent bead

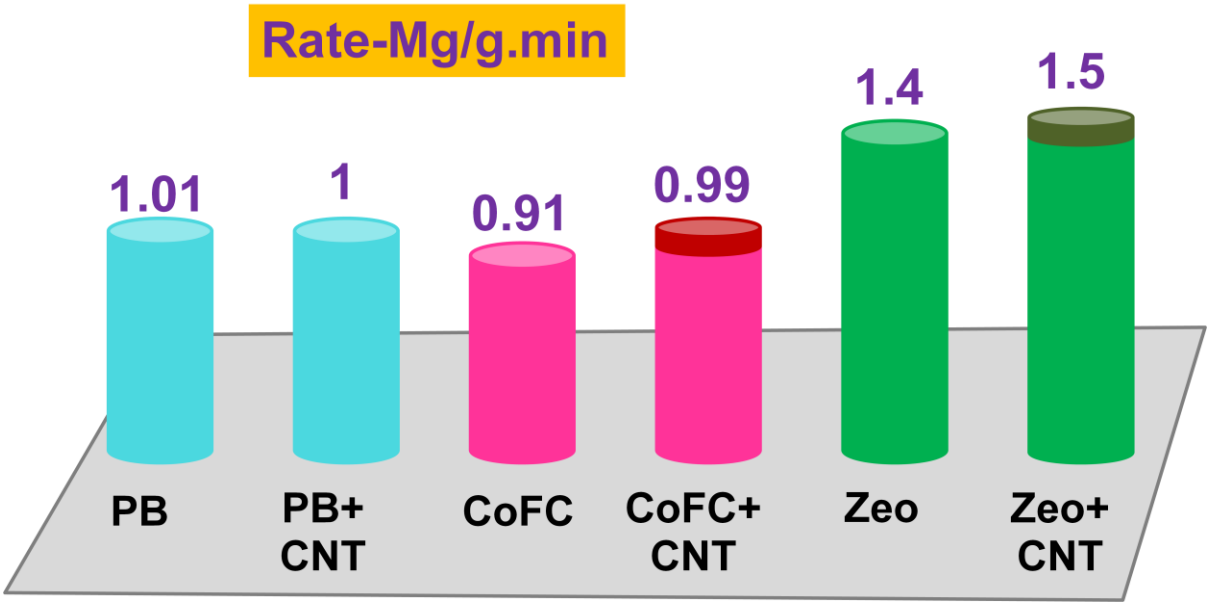

Figure 3-21 Strontium adsorption rate of each adsorbent bead

3.8. Adsorption isotherm study

In order to understand the adsorption behavior and mechanism isotherm models are very useful. Large numbers of isotherm models are available, out of which Langmuir and Freundlich models are most widely using for adsorption experiments. In the study two adsorption isotherm models were took into consideration, they were Langmuir and Freundlich model. In the case of both cesium and strontium adsorption the Langmuir correlation values of all adsorptive particles encapsulated beads without and with MWCNTs was higher than Freundlich. The higher correlation values indicating a very good mathematical fit with Langmuir model. Adsorption follows the Langmuir model. The various adsorption isotherm parameters and linear fitting plots are given in the Appendix I and Appendix II respectively.

When an experimental data fit with Langmuir model, certain assumption on adsorption behavior and mechanism is possible. Major assumptions obtained from the Langmuir model were as follows. The surface containing the adsorbing sites was perfectly flat plane with no corrugations that is the surface was homogeneous, all adsorbent sites were equivalent, and each site can hold only one molecule of same type, there were no interactions between adsorbate molecules on adjacent sites. Most importantly, the adsorption was monolayer chemisorptions involving ion exchange (Abd El-Latif and Elkady, 2010; Foo and Hameed, 2010; Ho et al., 2002). The Langmuir parameters of q_m (maximum monolayer adsorption capacity) and K were calculated from the slope and

intercept values. In this study, the separation factor R_L was between zero and one in each case indicating the favourable adsorption. The maximum adsorption capacity in the case of both cesium and strontium adsorption by different types beads were articulated in Figure 3-22 and Figure 3-23 respectively.

The maximum monolayer adsorption capacity of cesium by prussian blue encapsulated beads with CNTs slightly exceeded the value (~8% higher) than encapsulated beads that were not reinforced by CNTs. The maximum monolayer adsorption capacity of CoFC encapsulated beads with CNT exceeded by ~8.5% than CoFC encapsulated beads without CNTs. Similarly, in the case of zeolite beads the enhancement of cesium adsorption while modifying with CNT was ~10%.

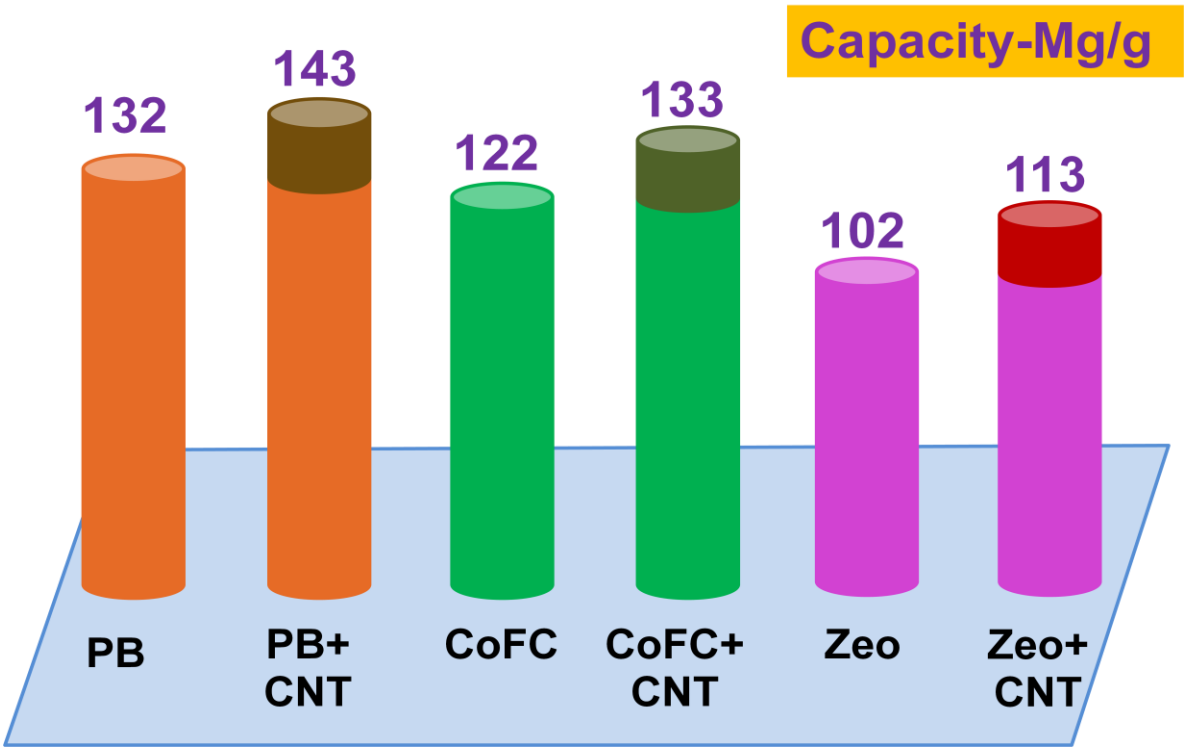

Figure 3-22 Maximum cesium adsorption capacity of each adsorbent bead

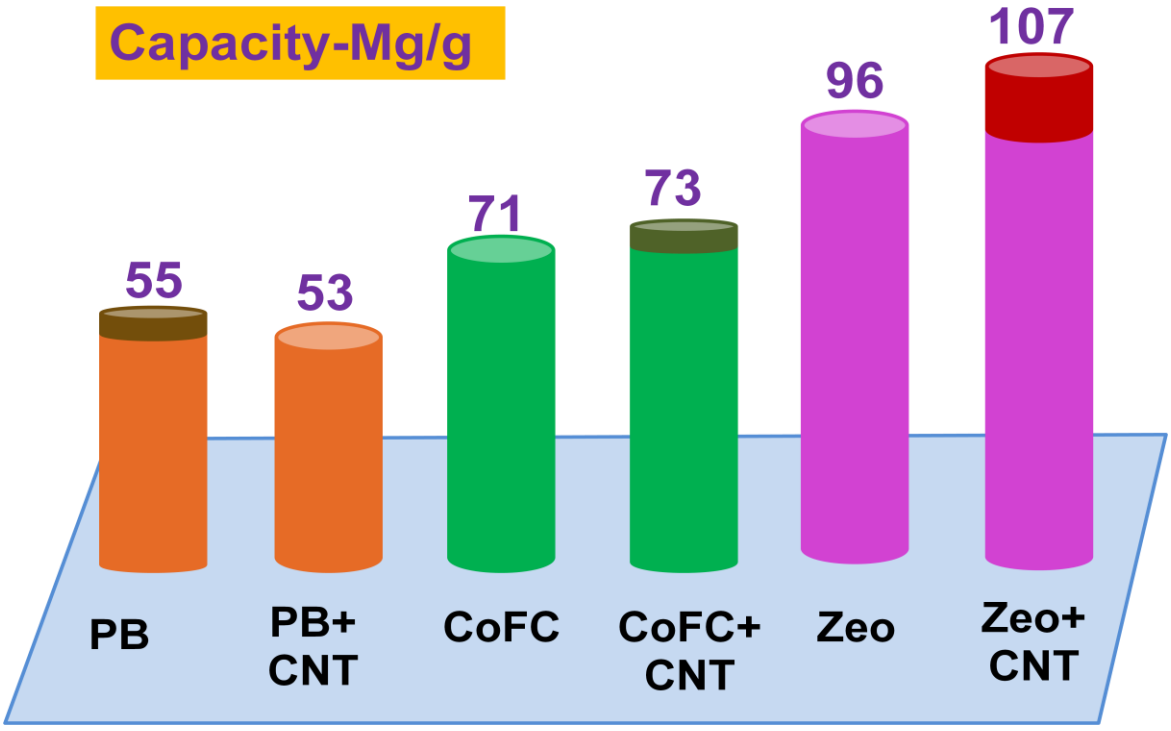

Figure 3-23 Maximum strontium adsorption capacity of each adsorbent bead

The presence of reinforcing MWCNTs had no adverse effect on cesium uptake. Indeed, the MWCNTs gave a small enhancement to adsorption of free cesium from the solution. The effectiveness of both types of beads was dependent on encapsulation of adsorptive particle; MWCNTs have great ability to increase the encapsulation. This slight boost in adsorption conferred by MWCNTs may reflect a larger physical network that can entrap cesium inside the beads. In short MWCNTs modified Prussian blue, sodium cobalt hexacyanoferrate and zeolite-A bead´s Cs^+ maximum adsorption capacity were 143 mg/g, 133 mg/g and 113 mg/g, and that of without MWCNTs were 131 mg/g, 121 mg/g and 102 mg/g respectively. For cesium removal prussian blue encapsulated beads showed highest among all other beads.

3.9. Adsorption mechanism

Prussian blue structure provides sufficient crystallographic position for approximately 14-16 water molecules. The pH of prussian blue usually varies between 2 to 3, indicating the presence of H^+ (as H_3O^+). In addition, the use of ferric chloride leads to the contamination of the crystal by chloride and these negative charges are sometimes compensated by binding H^+ (as H_3O^+). The mechanism of cesium binding on metal hexacyanoferrate is still not known clearly a. Cesium is one of the largest monovalent alkali metal ions, possessing low charge density, and capable of ionic binding with anions. The binding force may be chemical ion exchange; ion trapping as well as physical adsorption (Faustino et al., 2008; Taj et al., 2011). The metal binding to insoluble prussian

blue was mainly due to ion exchange between hydrogen ion presents in the crystal lattice or simple ion trapping by taking the advantages of cesium size. Metal hexacyanoferrate shows a good tendency to enclose alkali metal ions during the preparation stage itself, leading to the generation of sodium ions incorporated into the crystal lattice. Cesium and other monovalent ions can readily penetrate to the metal hexacyanoferrate crystal lattice and easily displace sodium ions from the lattice. The schematic representation of cesium uptake by prussian blue (soluble and insoluble) and sodium cobalt hexacyanoferrate are depicted in Figure 1-1 and Figure 1-2 respectively (Shokouhimehr et al., 2010).

The uptake of cesium and strontium ions by zeolite is also ion exchange (Figure 1-3 & Figure 1-4). Aluminium, silicon and oxygen are arranged in a regular structure of SiO_4- and AlO_4- tetrahedral units that form a framework with small pores also called tunnels or cavities about 0.1-2 nm diameter (Ismail et al., 2010; Osmanlioglu, 2006). A second consequence of the framework being built from negatively charged units is that it possesses a net negative charge that must be balanced by the presence of positively charged ions. Mostly zeolite have sodium ion as a loosely bound counter ion (El-Kamash, 2008). These can be readily displaced by cesium or strontium ions. It should be noted that the ion exchange and the pore size are partially linked. When the zeolite is in the sodium form (it has positively charged sodium ions balancing the negative charge on the aluminosilicate framework), the sodium ions are associated with the tetrahedral aluminium or silicon atoms at the entrance and because of their

finite size, and they effectively reduce the diameter of the pore opening slightly. If the sodium ions are replace by potassium ions then the opening of the pore is effectively reduced even further. This behaviour permits a degree of control over the size of material that can enter the pores.

These assumptions were clearly justified from the isotherm studies with the Langmuir model which suggested a monolayer type adsorption. A physical adsorption onto the crystal lattice followed by strong electrostatic forces could lead to chemical adsorption as calculated from the isotherm models. Due to the micro porosity of the beads, water can easily enter into the core of beads containing adsorptive clusters. In this study, the majority of the cesium was adsorbed by adsorptive particle and the remaining part was trapped in the cross-linked alginate structure. The MWCNTs physical network further enhanced the process by means of weak van der Waals forces of attraction (Lehto et al., 1987; Mardan et al., 1999; Moon et al., 2004; Nilchi et al., 2003).

In the composite beads, alginate matrix was the key scavenger of strontium ions. Therefore, adsorption mainly depends on the available alginate content of the beads. The adsorption mechanism of divalent ions on alginate vesicle was well known to scientists for many years. Alginate beads contain carboxylic and hydroxyl functional groups from mannuronic and guluronic acids. Those sites are protonated or deprotonated, depending on the pH of the aqueous medium. The carboxylic –COOH group or the lone pair of electrons present in oxygen might be involved in the binding of strontium. The adsorption of strontium onto

alginate matrix occurs by cation exchange (Figure 1-5), primarily to carboxyl group, and hydroxyl group plays a secondary role. Hydroxyl group plays a key role not only in ion exchange but also in determining the affinity of the complex towards different metal ions (Papageorgiou et al., 2008, 2006). PB has have no or any ability to absorb strontium ions so while encapsulating PB in alginate matrix the effective availability of alginate for strontium adsorption was decreased . More over while using MWCNTs effective encapsulation of PB in the beads increased which further decreases the uptake of strontium adsorption. However, in the case of CoFC beads the contribution of CoFC needs to be concerned. Because of small ionic radii of strontium ion than the available window of CoFC, the uptake should be lower. However, exchange at the surface of the crystals as hydrated ions is possible (Lehto et al., 1992). Our isotherm study verified monolayer chemisorptions, because the experimental data fit well with Langmuir isotherm model (Papageorgiou et al., 2008, 2006). As a conclusion MWCNT modified Prussian blue, sodium cobalt hexacyanoferrate and zeolite-A bead´s Sr2+ maximum adsorption capacity were 55 mg/g, 72 mg/g and 107 mg/g, and that of without MWCNT were 53 mg/g, 70 mg/g and 96 mg/g respectively.

3.10. pH effect on adsorption

An environmental factor that can affect every adsorption experiment is hydrogen ion concentration. The pH has a unique ability to change the whole reaction chemistry and adsorption behaviour. The influence of hydrogen ion concentration is high in the case of ion exchange processes, especially for monovalent ions because of high ionic competition. In this study, the effect of pH was estimated in terms of adsorption capacity. Series of experiment conducted with varying the pH from 2 to 12. Cesium adsorption variation with pH by PB and CoFC beads are given in Figure 3-24. Similarly, that of strontium adsorption is depicted in Figure 3-25. Adsorption capacity value reached a steady maximum at pH 4 in each beads, there after adsorption capacity stood steady until pH 10. Thus, the adsorption is feasible across a wide range of pH values.

At low pH, ion exchange sites are mainly protonated, making them inaccessible for ion exchange. When pH values increase, the sites become available for ion exchange, which leads to higher adsorption. The beads were not stable above pH 10 because at higher pH calcium alginate get decompose. This may be because water insoluble calcium alginate converts into water-soluble salt of alginate such as sodium alginate etc. Similarly, at lower pH calcium in the calcium alginate will replace with hydrogen ions to form weak alginic acid. Alginic acid is also water insoluble but comparatively weaker than calcium alginate. In short, by considering the adsorption capacity and beads

stability, the most suitable range of pH was 4 to 10. These wide ranges of pH tolerance make the beads more suitable for the practical applications.

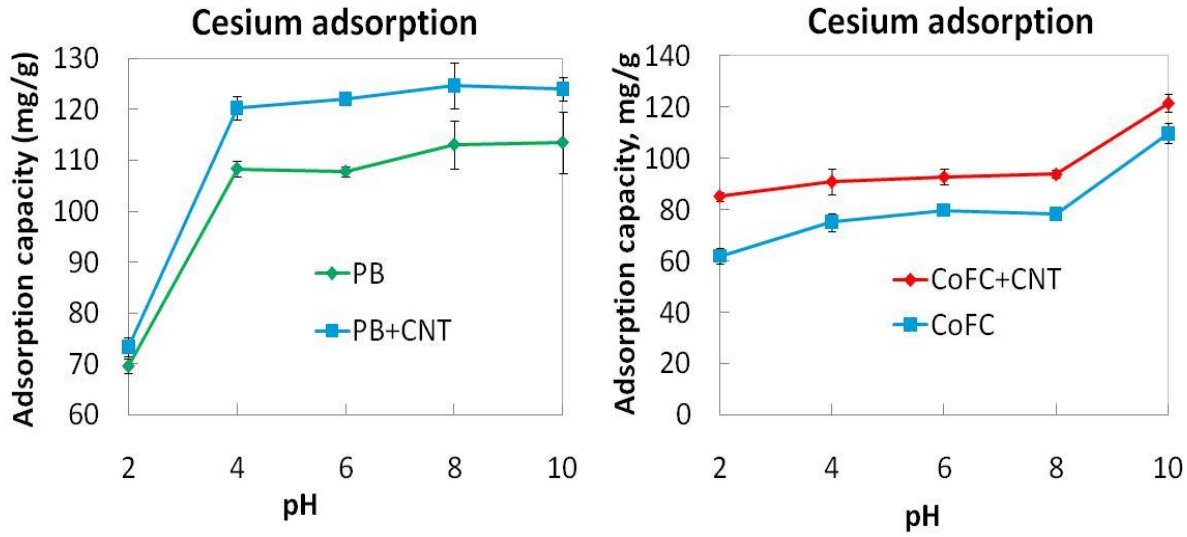

Figure 3-24 Effect of pH on adsorption of cesium ions by PB and CoFC beads

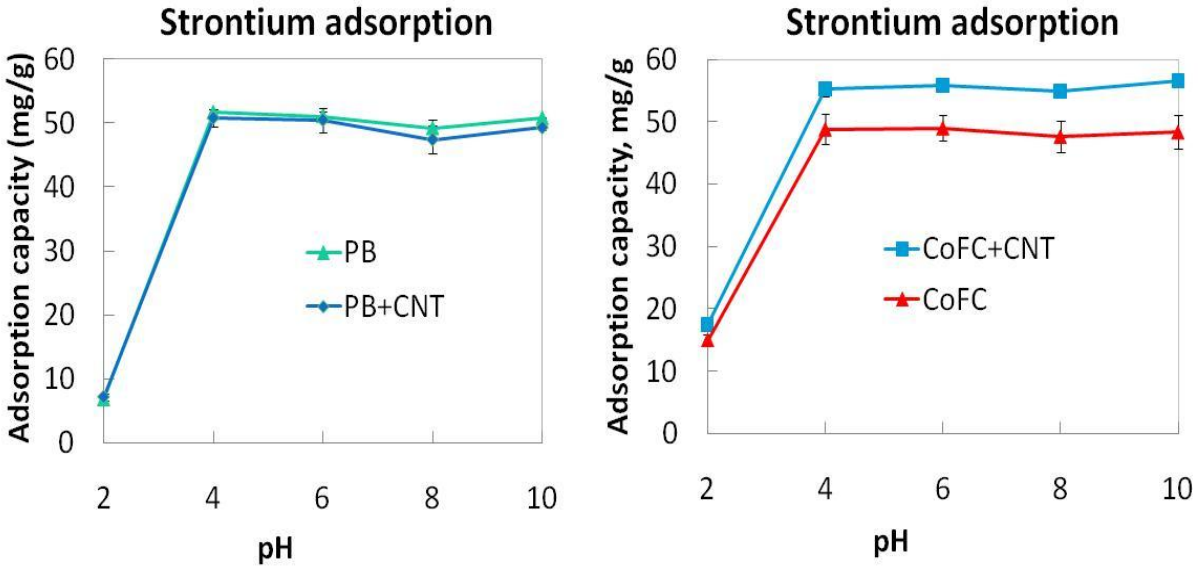

Figure 3-25. Effect of pH on adsorption of strontium ions by PB and CoFC beads

3.11. Effect of ionic competition on adsorption

The adsorption of a metal ion generally depends on the competition with other ions, which are present in solution. This research considered the competition of sodium, potassium, calcium and magnesium ions on the adsorption of cesium and strontium ions. In the control groups, concentrations of cesium and strontium ions were 0.75 mM and 1.1 mM respectively. Effects of competitive ions of various concentrations on adsorption are shown in Figure 3-26. In the case of cesium adsorption, most of the divalent ions showed little effect, sodium ions offered a negligible competition and potassium ions showed a modest effect at higher concentrations. From the results showed that the adsorbent was highly selective towards cesium adsorption.

The competition of monovalent ions on strontium adsorption was nil, but magnesium ions showed competition only at higher concentration. Even though, the adsorbent showed a high affinity towards strontium ions than other divalent ions in all concentrations, calcium ions showed an average effect on strontium adsorption compared to magnesium ions. The selectivity of an ion is mainly depends on its ionic size (Taj et al., 2011). Cesium and strontium are comparatively bigger than other elements in the same group of periodic table. Increasing the size of the ions with similar charge would reduce the charge to size ratio, the charge density would be low. This means that soft acid behavior getting higher and higher while moving down in the group. The ion exchange can be explained based on hard and soft acid concept. Compare with hard acid

soft acid are more favorable for ion exchange. More over each adsorptive crystal should possess effective window with specific radius (Lehto et al., 1992). The ion that has suitable ionic size will penetrate the window more easily compare with competing ions. The cesium and strontium have suitable ionic radii to penetrate the effective window than other elements in the same group, the main reason for the better selectivity (Maciejewski and Walkowiak, 2004).

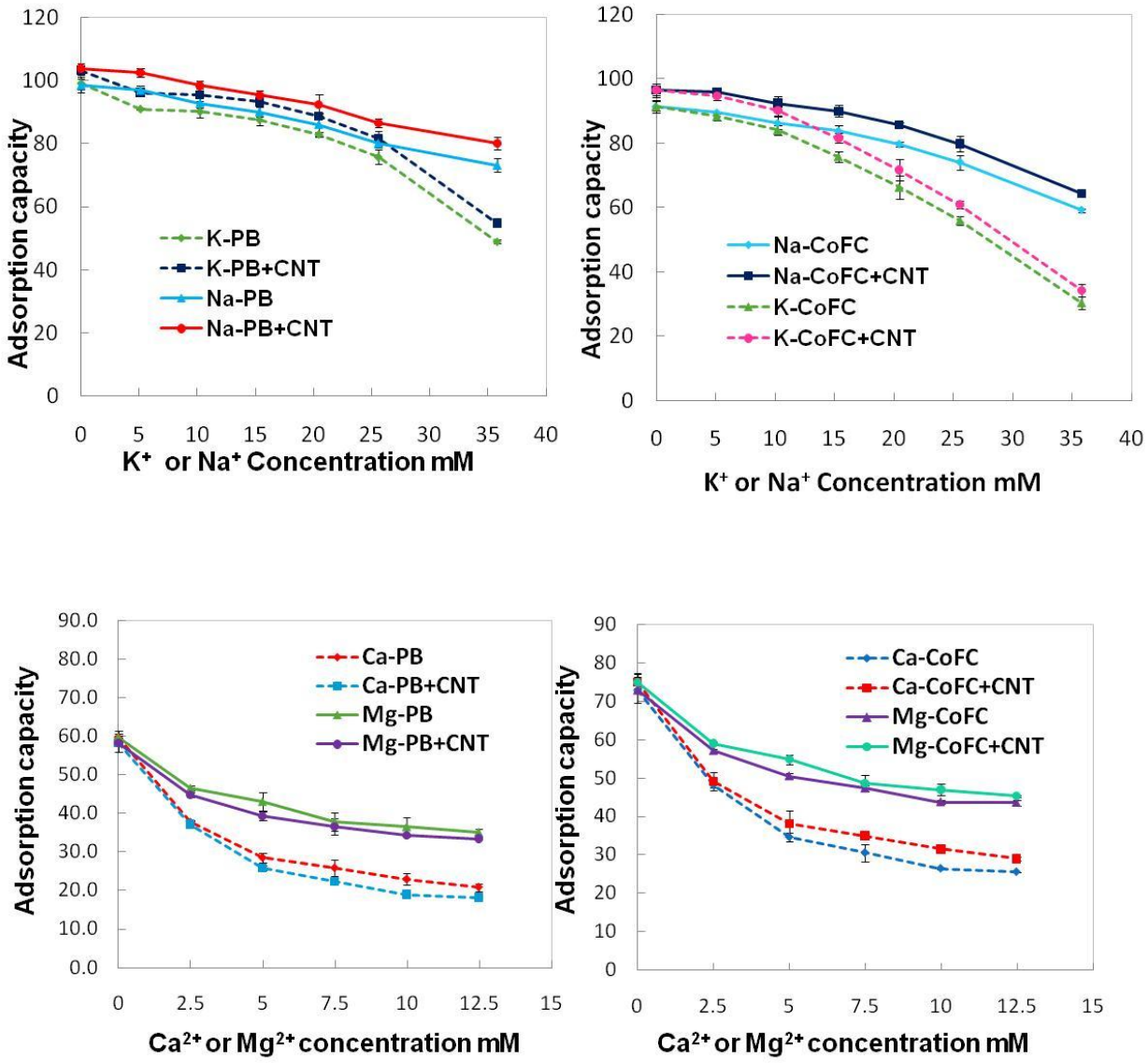

Figure 3-26 Effect of competitive ions on adsorption of cesium and strontium ions

3.12. Column breakthrough study

For both types of CoFC encapsulated beads, the breakthrough curves were obtained by plotting the ratio of effluent concentration to the influent concentration versus time (Figure 3-27). The breakthrough is defined as the point when the effluent concentration from the column is about to 5-10% of the influent concentration

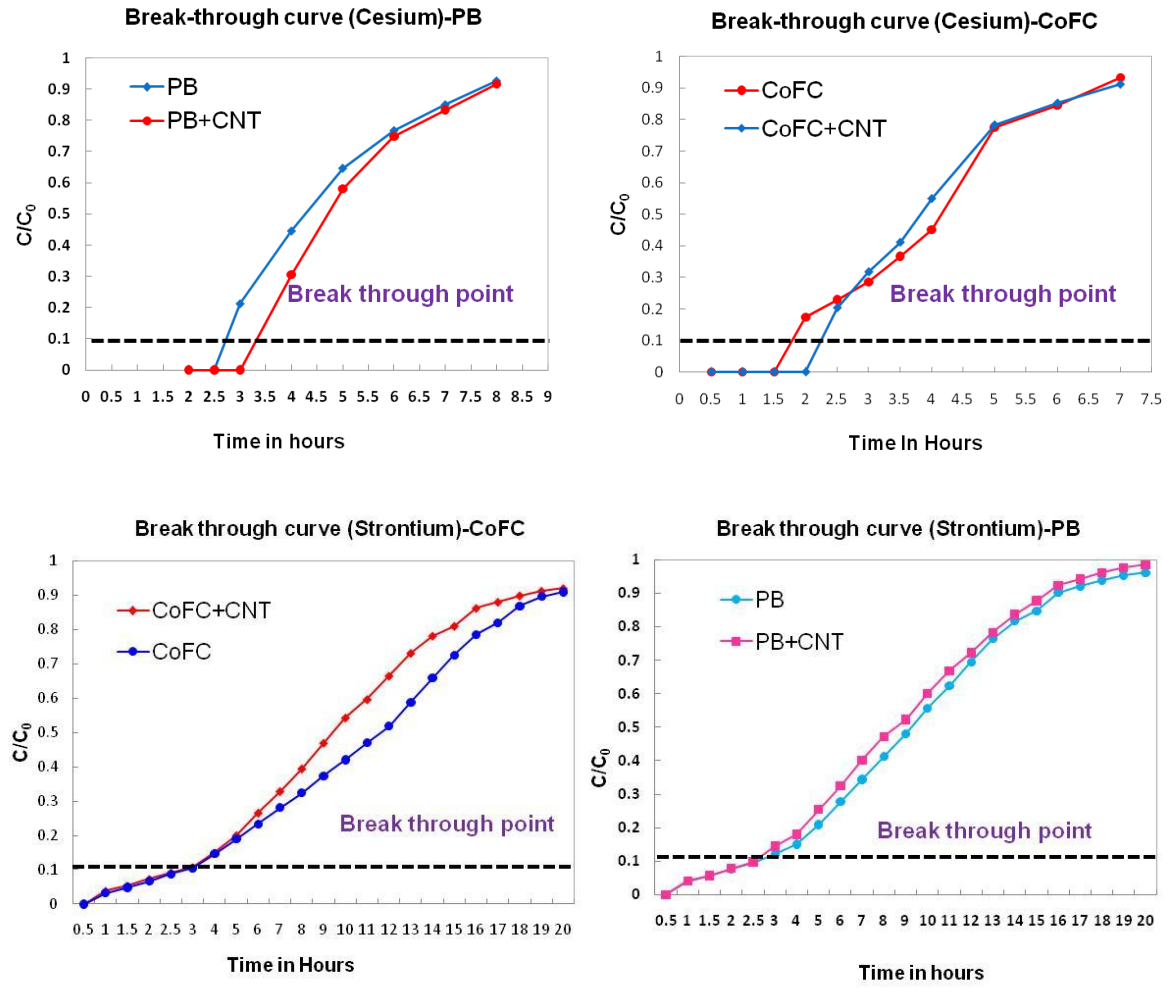

Figure 3-27 Column breakthrough curve for the adsorption of cesium and strontium

The breakthrough adsorption capacity can be determined by using the following formula,

$$q_b = \left[\frac{C_i - C_b}{m}\right] bv \qquad (12)$$

Where C_i and C_e are the initial and breakthrough concentrations (ppm) respectively. b_v is the breakthrough volume in litres and m is the mass of the adsorbent used (g).

The other important parameters for column studies are total percentage removal, the empty bed residence time, and the adsorbent exhaustion rate.

Total percentage removal is defined as:

$$S = \frac{q_t}{m_t} * 100 \qquad (13)$$

Where q_t is the adsorption capacity and m_t is amount of ions flowing through the column at time t.

$$m_t = \frac{C_0 Q t_t}{1000} \qquad (14)$$

where Q is the flow rate mL/min and t_t is the time in minutes.

$$\text{The adsorbent exhaustion rate (Ra)} = \frac{\text{Mass of adsorbent in column}}{\text{Volume treated at breakthrough}}. \qquad (15)$$

The various parameters such as breakthrough capacity (q_b), influent concentration (C_i) and effluent concentration at breakthrough (C_e), breakthrough volume (b_v), amount of contaminant ions flowing through column at breakthrough (m_t) , total percentage removal of pollutant ions (S) and adsorbent exhaustion rate (Ra) (Ghomshe et al., 2011; Gupta Suresh, 2010; Soni et al.,

2012) are given in Table 2. The values gave us a conclusion that beads could perform well in continuous treatment condition. Application in industrial scale removal of cesium and strontium ions can be easily achievable. The removal capability of both cesium and strontium was relative huge that we required for solving the current problem.

Table 2. Various parameters for the removal of cesium and strontium ions using fixed bed adsorption column.

Beads	C_i (ppm)	C_e (ppm)	b_v (mL)	m_t (mg)	q_b (mg/g)	S %	Ra (g/L)
Cesium							
PB	400	40	660	264	110.5	42	3.25
PB+CNT	400	40	804	321.6	144.7	45	2.5
CoFC	400	40	432	172.8	86.4	50	4.1
CoFC +CNT	400	40	552	220.8	116.9	53	3
Strontium							
PB	100	10	468	42.12	21.2	49.5	4.3
PB+CNT	100	10	459	41.31	20.25	48.8	4.5
CoFC	100	10	672	58.9	29.7	50.4	2.9
CoFC +CNT	100	10	696	61	31.3	51.3	2.84

Chapter 4

GENERAL CONCLUSIONS

Radio active cesium and strontium are the inevitable medium lived fission products have half-lives of 30.17 and 28.8 years respectively. Till now, simultaneous removal of these extremely hazardous elements was an unsolved problem. For decades scientists are familiar with various transition metal cyano ferrates as well as zeolites to decontaminate water from radionuclides. However, it is unfeasible to use them directly into water because of their small particle size, moreover low permeability made their application in fixed-bed columns impractical.

The caging of those adsorptive materials in nontoxic and inexpensive alginate vesicle will be a promising method for the safe and effective use. In order to enhance further stability and efficiency highly dispersed MWCNTs are the versatile material, because of their intense networking ability and high surface area.

Ferric hexacyanoferrate (Prussian blue), sodium cobalt hexacyanoferrate and zeolite-A were successfully synthesized and promisingly encapsulated in calcium alginate beads with dispersed MWCNTs. The newly developed adsorbent beads could withstand in extreme pH, temperature and ionic strength without any break and leak. Usually immobilization decrease the availability of adsorbent towards adsorbate, but MWCNTs increased the encapsulation efficiency along with making them fully available for adsorption.

The adsorption behavior and adsorption rate were carefully examined by means of different isothermal and kinetic models. Mathematical fitting of experimental data on the adsorption isotherm model showed Langmuir isotherm greater than Freundlich isotherm. MWCNT modified Prussian blue, sodium cobalt hexacyanoferrate and zeolite-A bead´s Cs^{+}/Sr^{2+} maximum adsorption capacity were 143/55 mg/g, 133/72 mg/g and 113/107 mg/g, and that of without MWCNT were 131/53 mg/g, 121/70 mg/g and 102/96 mg/g respectively. Similarly, in kinetic models pseudo second order gave better fitting than pseudo first order. The adsorption was monolayer site-to-site attachment and immediate.

The investigation to understand the effect of pH and ionic competition on adsorption brought into a conclusion that the performance of beads was consistent with a broad range of pH values as well as ionic competition. The research was further extended to fixed bed column adsorption analysis showed that beads can be used for large scale treatment. In short the performance of beads is innovative among currently using adsorbent. Their relevance ranges from low to high level of contamination as well as household to industrial design. Consequently, this newly developed adsorbent will be a potential solution for the existing radiation problem.

GENERAL APPLICATIONS

Novel beads were successfully developed for the elimination of both cesium and strontium ions from water. Performance evaluation of developed beads showed that beads have numerous applications in the demanding water treatment process. Newly developed adsorbent will be a potential solution for the existing radiation problems. Their relevance ranges from the treatment of low to high level of radioactive contamination. Also, they can be used for both households to industrial purposes depending on the conditions of polluted water. The most common types of application method are shown in figure A0.

Figure A0 Simple schematic representation of application methods using developed beads.

REFERENCES

Abd El-Latif, M.M., Elkady, M.F., 2010. Equilibrium isotherms for harmful ions sorption using nano zirconium vanadate ion exchanger. Desalination 255, 21–43.

Al-Degs, Y.S., Khraisheh, M. a M., Allen, S.J., Ahmad, M.N., 2009. Adsorption characteristics of reactive dyes in columns of activated carbon. J. Hazard. Mater. 165, 944–9.

Aparicio, C., Machala, L., Marusak, Z., 2011. Thermal decomposition of Prussian blue under inert atmosphere. J. Therm. Anal. Calorim. 110, 661–669.

Application of Ion Exchange Processes for the Treatment of Radioactive Waste and Management of Spent Ion Exchangers, 2002.

Augustine, A.A., Orike, B.D., Edidiong, A.D., 2007. Adsorption kinetics and modeling of Cu(II) ion sorption from aqueous solution by Mercapoacetic acid modified cassava (Manihot sculenta cranz) wastes. Electron. J. Environ. Agric. Food Chem. 6, 2221–2234.

Avery, S. V., 1995. Caesium accumulation by microorganisms: uptake mechanisms, cation competition, compartmentalization and toxicity. J. Ind. Microbiol. 14, 76–84.

Avery, S. V., 1996. Fate of caesium in the environment: Distribution between the abiotic and biotic components of aquatic and terrestrial ecosystems. J. Environ. Radioact. 30, 139–171.

Azizian, S., 2004. Kinetic models of sorption: a theoretical analysis. J. Colloid Interface Sci. 276, 47–52.

Blandino, A.N.A., Macias, M., Cantero, D., 1999. Formation of calcium alginate gel capsules: influence of sodium alginate and $CaC1_2$ concentration on gelation kinetics. J. Biosci. BIOENCINEERING 88, 686–689.

Buser, H.J., Schwarzenbach, D., Petter, W., Ludi, A., 1977. The crystal structure of prussian blue. Inorg. Chem. 16, 2704–2710.

Chen, S., 1998. Characterization and electrocatalytic properties of cobalt hexacyanoferrate films. Electrochim. Acta 43, 3359–3369.

Crumbliss, A.L., Lugg, P.S., Morosoff, N., 1984. Alkali metal cation effects in a prussian blue surface-modified electrode. Inorg. Chem. 23, 4701–4708.

Denton, M.S., Manos, M.J., Kanatzidis, M.G., 2009. Highly selective removal of cesium and strontium a new class of inorganic ion specific media, in: WM2009 Conference. pp. 1–8.

El-Kamash, A.M., 2008. Evaluation of zeolite A for the sorptive removal of Cs+ and Sr2+ ions from aqueous solutions using batch and fixed bed column operations. J. Hazard. Mater. 151, 432–45.

Farah, A.M., Shooto, N.D., Thema, F.T., Modise, J.S., 2012. Fabrication of prussian blue / multi-walled carbon nanotubes modified glassy carbon electrode for electrochemical detection of hydrogen peroxide . Int. J. Electrochem. Sci. 7, 4302–4313.

Faustino, P.J., Yang, Y., Progar, J.J., Brownell, C.R., Sadrieh, N., May, J.C., Leutzinger, E., Place, D. a, Duffy, E.P., Houn, F., Loewke, S. a, Mecozzi, V.J., Ellison, C.D., Khan, M. a, Hussain, A.S., Lyon, R.C., 2008. Quantitative determination of cesium binding to ferric hexacyanoferrate: Prussian blue. J. Pharm. Biomed. Anal. 47, 114–25.

Foo, K.Y., Hameed, B.H., 2010. Insights into the modeling of adsorption isotherm systems. Chem. Eng. J. 156, 2–10.

Foo, K.Y., Hameed, B.H., 2011. The environmental applications of activated carbon/zeolite composite materials. Adv. Colloid Interface Sci. 162, 22–28.

Fundueanu, G., Nastruzzi, C., Carpov, a, Desbrieres, J., Rinaudo, M., 1999. Physico-chemical characterization of Ca-alginate microparticles produced with different methods. Biomaterials 20, 1427–35.

Gao, Z., Wang, G., Li, P., Zhao, Z., 1991. Electrochemical and spectroscopic studies of cobalt-hexacyanoferrate film modified electrodes. Electrochim. Acta 36, 147–152.

Ghomshe, S.M.T., Mousavi, S.M., Soltanieh, M., Kordi, A.K.S., 2011. Batch and column study of haloacetic acids adsorption onto granular activated carbon. Sci. Res. Essays 6, 3553–3560.

Günay, A., Arslankaya, E., Tosun, İ., 2007. Lead removal from aqueous solution by natural and pretreated clinoptilolite: Adsorption equilibrium and kinetics. J. Hazard. Mater. 146, 362–371.

Gupta, R.K., Dubey, S.S., 2005. Removal of cesium ions from aqueous solution by polyaniline: A radiotracer study. J. Polym. Res. 12, 31–35.

Gupta Suresh, B.B.V., 2010. Experimental investigations and theoretical modeling aspects in column studies for removal of Cr(VI) from aqueous solutions using activated tamarind seeds. J. Water Resour. Prot. 02, 706–716.

Ho, Y.S., Mckay, G., 2002. Application of kinetic models to the sorption of copper (II) on to peat. Adsorpt. Sci. Technol. 20, 797–815.

Ho, Y.S., Porter, J.F., Mckay, G., 2002. Equilibrium isotherm studies for the sorption of divalent metal ions onto peat: copper, Nickel and lead single component systems. Water. Air. Soil Pollut. 141, 1–33.

Hu, B., Fugetsu, B., Yu, H., Abe, Y., 2012. Prussian blue caged in spongiform adsorbents using diatomite and carbon nanotubes for elimination of cesium. J. Hazard. Mater. 217-218, 85–91.

Ishihara, R., Fujiwara, K., Harayama, T., Okamura, Y., Uchiyama, S., Sugiyama, M., Someya, T., Amakai, W., Umino, S., Ono, T., Nide, A., Hirayama, Y., Baba, T., Kojima, T., Umeno, D., Saito, K., Asai, S., Sugo, T., 2011. Removal of cesium using cobalt-ferrocyanide- impregnated polymer-chain-grafted fibers. J. Nucl. Sci. Technol. 48, 1281–1284.

Ismail, A. a., Mohamed, R.M., Ibrahim, I. a., Kini, G., Koopman, B., 2010. Synthesis, optimization and characterization of zeolite A and its ion-exchange properties. Colloids Surfaces A Physicochem. Eng. Asp. 366, 80–87.

Ismail, I.M., El-Sourougy, M.R., Moneim, N.A., Aly, H.F., 1998. Preparation, characterization, and utilization of potassium nickel hexacyanoferrate for the separation of cesium and cobalt from contaminated waste water. J. Radioanal. Nucl. Chem. 237, 97–103.

Jukka, L., Mika, P., Juha, H., Markku, R., Matti, E., 1995. Gases evolved in the thermal decomposition of potassium cobalt hexacyanoferrate(II). Thermochim. Acta 265, 25–30.

Karyakin, A. a., 2001. Prussian Blue and Its Analogues: Electrochemistry and analytical applications. Electroanalysis 13, 813–819.

Keggin, J.F., Miles, F.D., 1936. Structures and formulæ of the prussian Bblue and related compounds. Nature 137, 577–578.

Kulesza, P.J., Malik, M. a., Denca, A., Strojek, J., 1996. In situ FT-IR/ATR spectroelectrochemistry of prussian blue in the solid state. Anal. Chem. 68, 2442–2446.

Kumar, K.V., 2006. Linear and non-linear regression analysis for the sorption kinetics of methylene blue onto activated carbon. J. Hazard. Mater. 137, 1538–44.

Kunrath, J.I., Muller, C.S., Frank, E., 1978. Thermal decomposition of potassium hexacyanoferrate(ii) trihydrate. J. Therm. Anal. 14, 253–264.

Lehto, J., Harjula, R., Wallace, J., 1987. Absorption of cesium on potassium cobalt hexacyanoferrate(II). J. Radioanal. Nucl. Chem. 111, 297–304.

Lehto, J., Haukka, S., Koskinen, P., Blomberg, M., 1990. Thermal decomposition of potassium cobalt hexacyanoferrate(II). Thermochim. Acta 160, 343–347.

Lehto, J., Paajanen, A., Harjula, R., 1992. Selectivity of potassium cobalt hexacyanoferrate(II) for alkali and alkaline earth metal ions. J. Radioanal. Nucl. Chem. 164, 39–46.

Li, Z., Zhang, J., Mu, T., Du, J., Liu, Z., Han, B., Chen, J., 2004. Preparation of polyvinylpyrrolidone-protected prussian blue nanocomposites in microemulsion. Colloids Surfaces A Physicochem. Eng. Asp. 243, 63–66.

Lin, Y.-B., Fugetsu, B., Terui, N., Tanaka, S., 2005. Removal of organic compounds by alginate gel beads with entrapped activated carbon. J. Hazard. Mater. 120, 237–41.

Liu, S.-Q., Li, H., Sun, W.-H., Wang, X.-M., Chen, Z.-G., Xu, J.-J., Ju, H.-X., Chen, H.-Y., 2011. Photoinducedly electrochemical preparation of prussian blue film and electrochemical modification of the film with cetyltrimethylammonium cation. Electrochim. Acta 56, 4007–4014.

Maciejewski, P., Walkowiak, W., 2004. Selective removal of cesium (I), strontium (II) and barium (II) cations with proton process. Physicochem. probelms Miner. Process. 38, 139–146.

Maliyekkal, S.M., Philip, L., Pradeep, T., 2009. As(III) removal from drinking water using manganese oxide-coated-alumina: Performance evaluation and mechanistic details of surface binding. Chem. Eng. J. 153, 101–107.

Mardan, A., Ajaz, R., Mehmood, A., Raza, S.., Ghaffar, A., 1999. Preparation of silica potassium cobalt hexacyanoferrate composite ion exchanger and its uptake behavior for cesium. Sep. Purif. Technol. 16, 147–158.

Mimura, H., Lehto, J., Harjula, R., 1997. Chemical and thermal stability of potassium nickel hexacyanoferrate (11). J. Nucl. Sci. Technol. 34, 582–587.

Moon, J.-K., Lee, E.-H., Kim, H.-T., 2004. Ion exchange of Cs ion in acid solution with potassium cobalt hexacyanoferrate. Korean J. Chem. Eng. 21, 1026–1031.

Naushad, M., 2009. Inorganic and composite ion exchange materials and their applications. Ion Exch. Lett. 2, 1–14.

Nilchi, A., Malek, B., Maragheh, M.G., Khanchi, A., 2003. Exchange properties of cyanide complexes Part I . Ion exchange of cesium on ferrocyanides. J. Radioanal. Nucl. Chem. 258, 457–462.

Osmanlioglu, A.E., 2006. Treatment of radioactive liquid waste by sorption on natural zeolite in Turkey. J. Hazard. Mater. 137, 332–335.

Papageorgiou, S.K., Katsaros, F.K., Kouvelos, E.P., Nolan, J.W., Le Deit, H., Kanellopoulos, N.K., 2006. Heavy metal sorption by calcium alginate beads from Laminaria digitata. J. Hazard. Mater. 137, 1765–72.

Papageorgiou, S.K., Kouvelos, E.P., Katsaros, F.K., 2008. Calcium alginate beads from Laminaria digitata for the removal of Cu+2 and Cd+2 from dilute aqueous metal solutions. Desalination 224, 293–306.

Properties of Selected Radioisotopes, 1968.

Qiu, H., Lv, L., Pan, B., Zhang, Qing-jian, Zhang, W., Zhang, Quan-xing, 2009. Critical review in adsorption kinetic models. J. Zhejiang Univ. Sci. A 10, 716–724.

Radiation Protection [WWW Document], n.d. URL http://www.epa.gov/radiation/radionuclides/cesium.html

Round, C.I., Hill, S.J., Latham, K., Williams, C.D., 1997. The crystal morphology of zeolite A . The e ff ects of the source of the reagents. Microporous Mater. 11, 213–225.

Rousseau, I., Le Cerf, D., Picton, L., Argillier, J.F., Muller, G., 2004. Entrapment and release of sodium polystyrene sulfonate (SPS) from calcium alginate gel beads. Eur. Polym. J. 40, 2709–2715.

Rudzinski, W., Plazinski, W., 2006. Kinetics of solute adsorption at solid/solution interfaces: a theoretical development of the empirical pseudo-first and pseudo-second order kinetic rate equations, based on applying the statistical rate theory of interfacial transport. J. Phys. Chem. B 110, 16514–25.

Ruiz-Bermejo, M., Rogero, C., Menor-Salván, C., Osuna-Esteban, S., Martín-Gago, J.A., Veintemillas-Verdaguer, S., 2009. Thermal wet decomposition of Prussian Blue: implications for prebiotic chemistry. Chem. Biodivers. 6, 1309–22.

Shokouhimehr, M., Soehnlen, E.S., Khitrin, A., Basu, S., Huang, S.D., 2010. Biocompatible Prussian blue nanoparticles: Preparation, stability, cytotoxicity, and potential use as an MRI contrast agent. Inorg. Chem. Commun. 13, 58–61.

Smidsrød, O., Skjåk-Braek, G., 1990. Alginate as immobilization matrix for cells. Trends Biotechnol. 8, 71–8.

Soni, A., Tiwari, A., Bajpai, A.K., 2012. Adsorption of o-nitrophenol onto nano iron oxide and alginate microspheres: Batch and column studies. African J. Pure Appl. Chem. 6, 161–173.

Sun, L., Yu, H., Fugetsu, B., 2012. Graphene oxide adsorption enhanced by in situ reduction with sodium hydrosulfite to remove acridine orange from aqueous solution. J. Hazard. Mater. 203-204, 101–10.

Taj, S., Muhammad, D., Chaudhry, M.A., Mazhar, M., 2011. Lithium, rubidium and cesium ion removal using potassium iron(III) hexacyanoferrate(II) supported on polymethylmethacrylate. J. Radioanal. Nucl. Chem. 288, 79–88.

Thompson, R.W., Franklin, K.C., 2001. Verified synthesis of zeolitic materials 179–180.

Todd, T.A., Batcheller, T.A., Law, J.D., Herbst, R.S., 2004. Cesium and strontium separation technologies literature review.

Veglio', F., Esposito, a, Reverberi, a. ., 2002. Copper adsorption on calcium alginate beads: equilibrium pH-related models. Hydrometallurgy 65, 43–57.

Vijaya, Y., Krishnaiah, A., 2010. Column adsorption and desorption studies of fluoride on perchloric acid cross-linked calcium alginate beads. E-Journal Chem. 7, 265–270.

Yakout, S.M., Elsherif, E., 2010. Batch kinetics, isotherm and thermodynamic studies of adsorption of strontium from aqueous solutions onto low cost rice-straw based carbons. Carbon – Sci. Technol. 1, 144–153.

Yang, Y., Faustino, P.J., Progar, J.J., Brownell, C.R., Sadrieh, N., May, J.C., Leutzinger, E., Place, D. a, Duffy, E.P., Yu, L.X., Khan, M. a, Lyon, R.C., 2008. Quantitative determination of thallium binding to ferric hexacyanoferrate: Prussian blue. Int. J. Pharm. 353, 187–94.

APPENDIX I

Table AI-1. Various adsorption isotherm model parameters for PB and PB+CNT beads.

	Cesium		**Strontium**	
	PB	**PB+CNT**	**PB**	**PB+CNT**
Langmuir				
q_m (mg/g)	131.57	142.85	55.2	53.2
K (L/mg)	0.0724	0.058	0.169	0.122
R_L	0.058	0.71	0.09	0.11
R^2	0.9948	0.9983	0.9857	0.9739
Freundlich				
Kf	61.06	57.84	33.36	21.22
nf	7.28	6.22	6.394	4.165
R^2	0.8495	0.9128	0.7822	0.8058

Table AI-2. Various adsorption isotherm model parameters for CoFC and CoFC+CNT beads.

	Cesium		**Strontium**	
	CoFCN	**CoFCN+CNT**	**CoFCN**	**CoFCN+CNT**
Langmuir				
q_m (mg/g)	121.95	133.33	72.9927	71.9424
K (L/mg)	0.048	0.023	0.06	0.197
R_L	0.095	0.18	0.20496	0.076
R^2	0.9911	0.983	0.9814	0.9842
Freundlich				
Kf	54.15	31.817	36.6	18.7
nf	7.386	4.274	6.7659	3.643
R^2	0.8125	0.8884	0.7443	0.953

Table AI-3. Various adsorption isotherm model parameters for Zeolite and Zeolite+CNT beads.

	Cesium		**Strontium**	
	Zeolite	**Zeolite+CNT**	**Zeolite**	**Zeolite+CNT**
Langmuir				
q_m (mg/g)	102	113.6	96.15	107.5
K (L/mg)	0.02	0.022	0.044	0.065
R_L	0.165	0.155	0.145	0.104
R^2	0.9955	0.9962	0.9856	0.989
Freundlich				
Kf	23.32	29.01	21.54	31.73
nf	3.86	3.69	3.34	3.9
R^2	0.9897	0.9377	0.9658	0.9785

Table AI-4. Various kinetic model parameters for PB and PB+CNT beads.

	Cesium		**Strontium**	
	PB	**PB+CNT**	**PB**	**PB+CNT**
Pseudo-first order				
K_1 (L/min)	0.038	0.0386	0.1588	0.0169
q_e (mg/g)	117.216	124.799	55.721	50.21
R^2	0.9785	0.9479	0.9649	0.9757
Pseudo-second order				
k_2 (g/mg min)	0.00050	0.00048	0.00033	0.00039
q_e (mg/g)	125.51	134.81	63.023	56.13
h (mg/g.min)	7.8764	8.7961	1.2988	1.2161
R^2	0.9939	0.9964	0.9964	0.995

Table AI-5. Various kinetic model parameters for CoFC and CoFC+CNT beads.

	Cesium		**Strontium**	
	CoFCN	**CoFCN+CNT**	**CoFCN**	**CoFCN+CNT**
Pseudo-first order				
K_1 (L/min)	0.0486	0.0368	0.011	0.0106
q_e (mg/g)	96.43	102.56	63.35	60.66
R^2	0.7158	0.901	0.9698	0.9661
Pseudo-second order				
k_2 (g/mg min)	0.0008	0.00054	0.000185	0.000185
q_e (mg/g)	103	111.30	73.011	70.15
h (mg/g.min)	8.4872	6.689353	0.986162	0.910389
R^2	0.9326	0.9962	0.9918	0.9966

Table AI-6. Various kinetic model parameters for Zeolite and Zeolite+CNT beads.

	Cesium		**Strontium**	
	Zeolite	**Zeolite+CNT**	**Zeolite**	**Zeolite+CNT**
Pseudo-first order				
K_1 (L/min)	0.0091	0.011	0.0148	0.0103
q_e (mg/g)	104.66	115.49	84.96	93.45
R^2	0.8945	0.88	0.856	0.866
Pseudo-second order				
k_2 (g/mg min)	0.0001	0.00012	0.00015	0.00014
q_e (mg/g)	108.803	118.94	95.6478	104.62
h (mg/g.min)	1.65901	2.31652	1.372275	1.532348
R^2	0.9477	0.9364	0.9651	0.9568

APPENDIX II

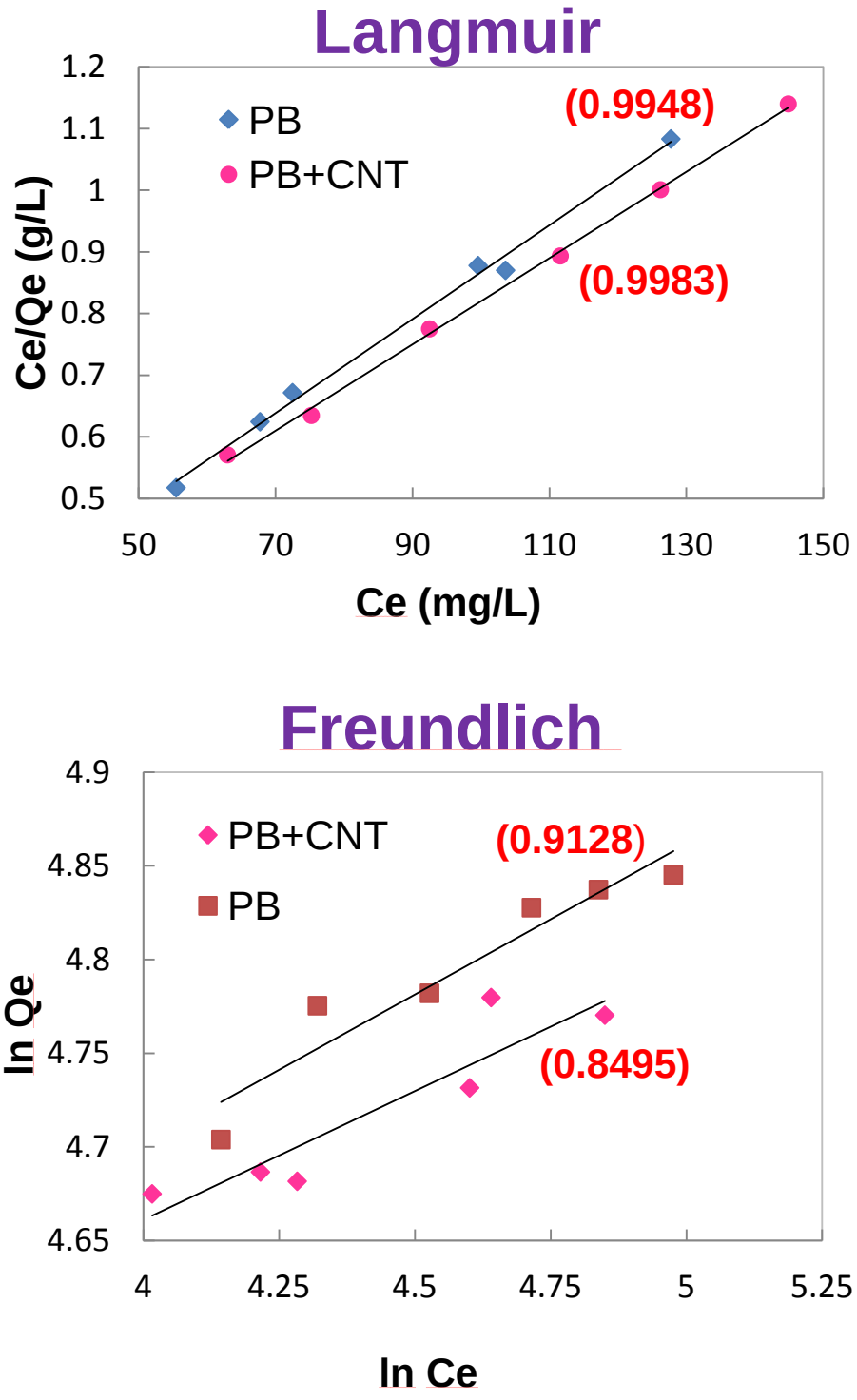

Figure AII-1. Linear plots of Langmuir and Freundlich isotherm model of cesium adsorption by PB and PB+CNT beads

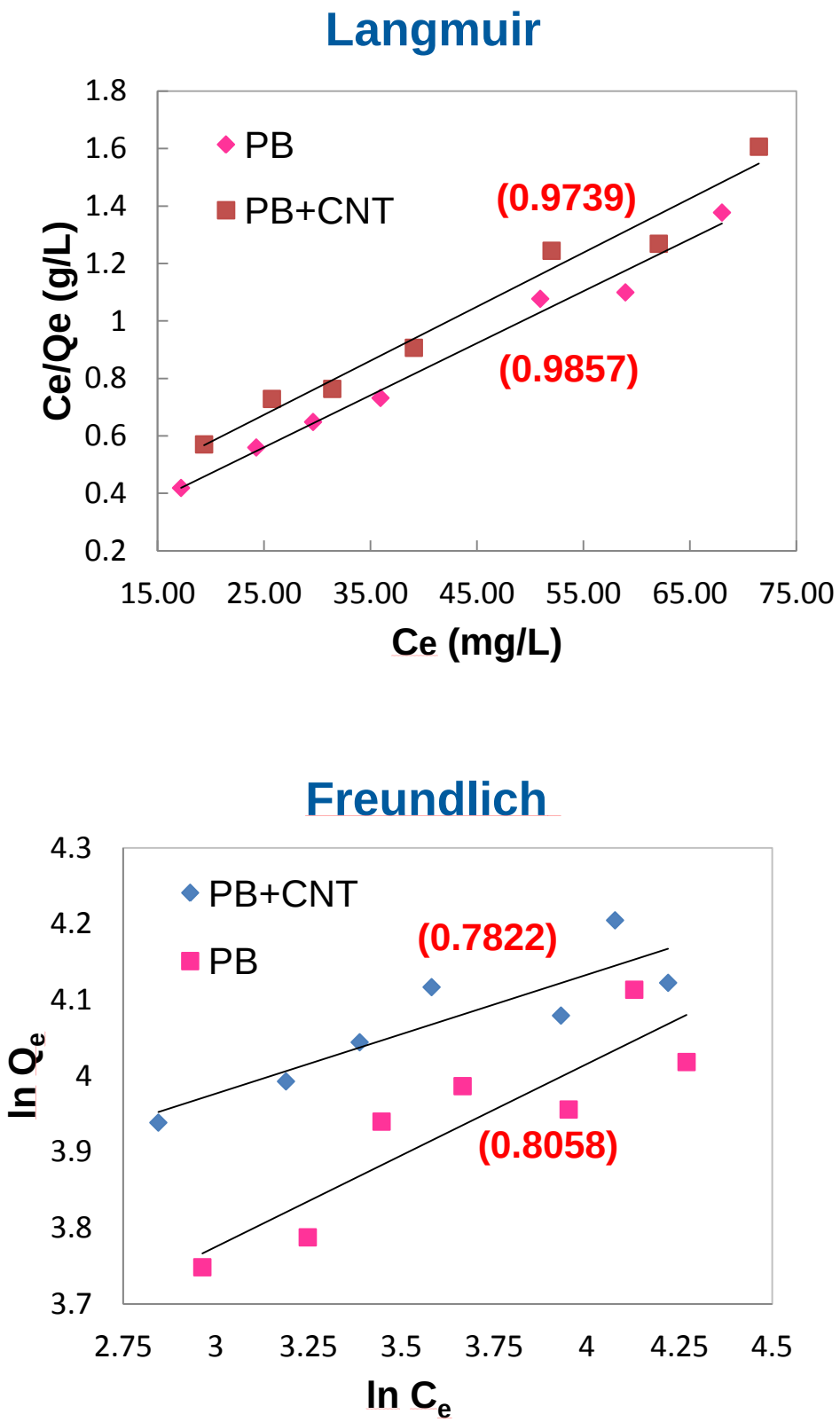

Figure AII-2. Linear plots of Langmuir and Freundlich isotherm model of strontium adsorption by PB and PB+CNT beads

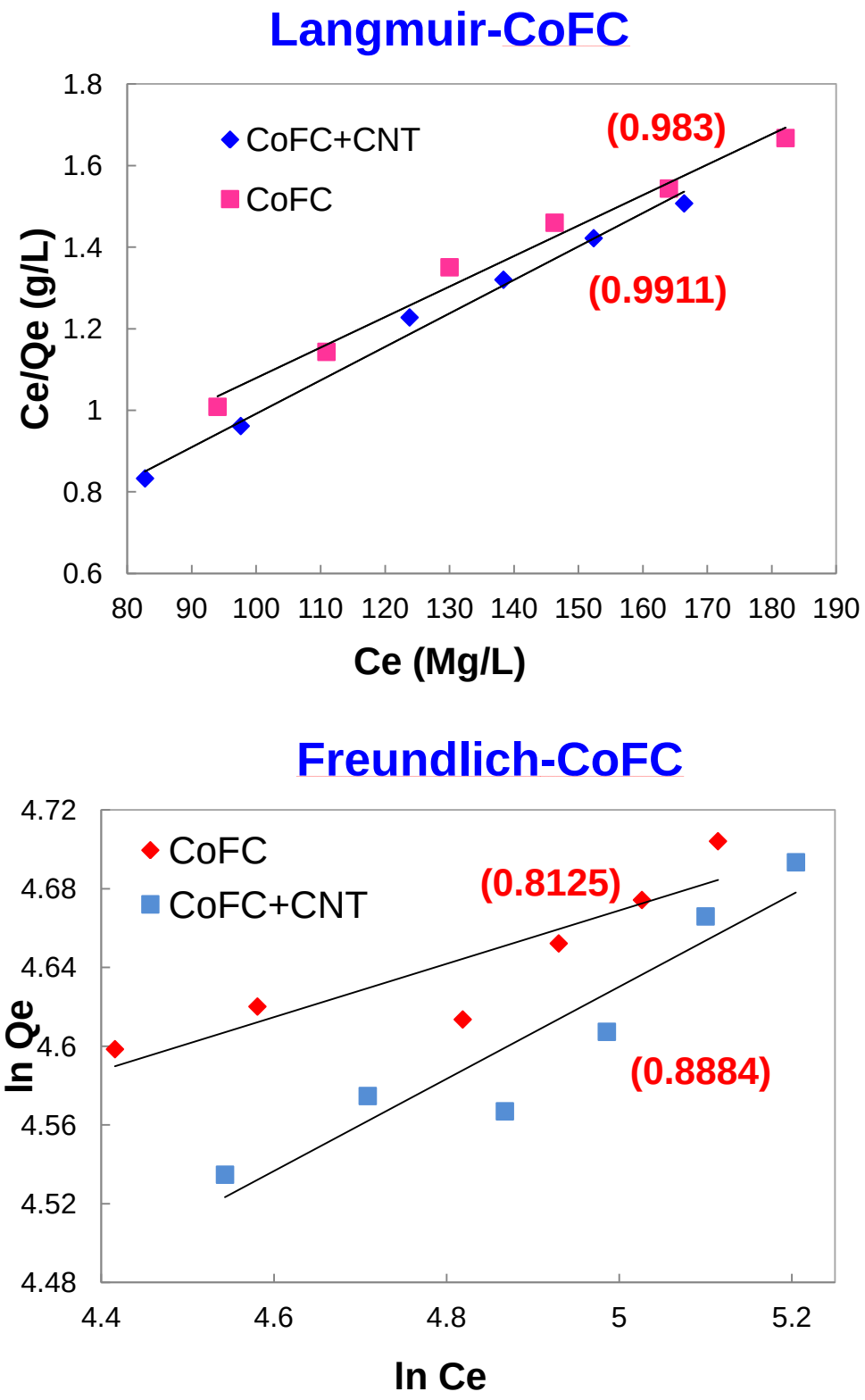

Figure AII-3. Linear plots of Langmuir and Freundlich isotherm model of cesium adsorption by CoFC and CoFC+CNT beads

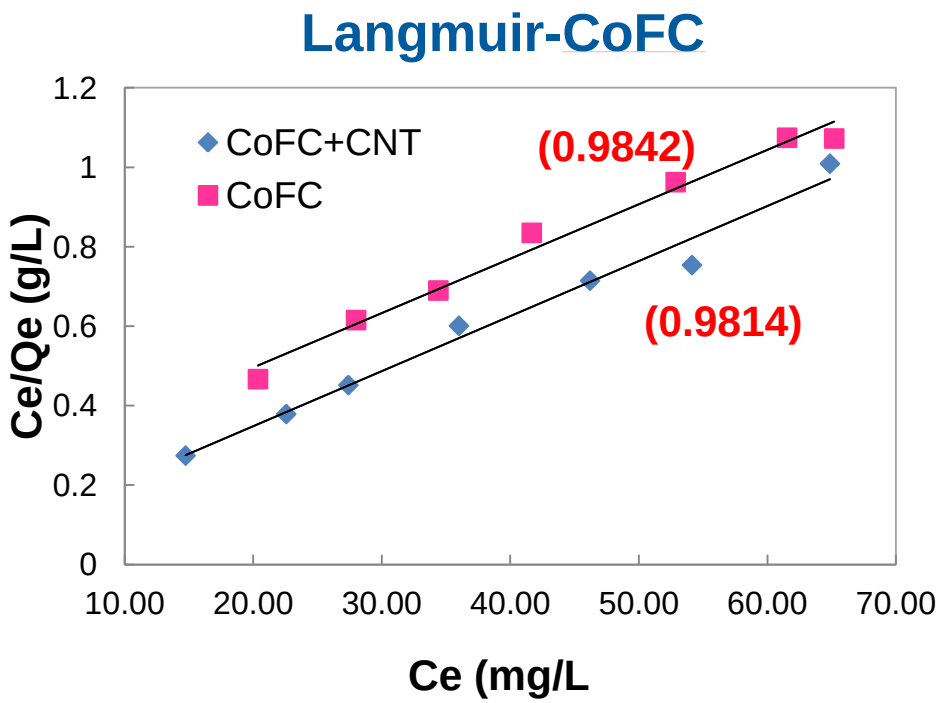

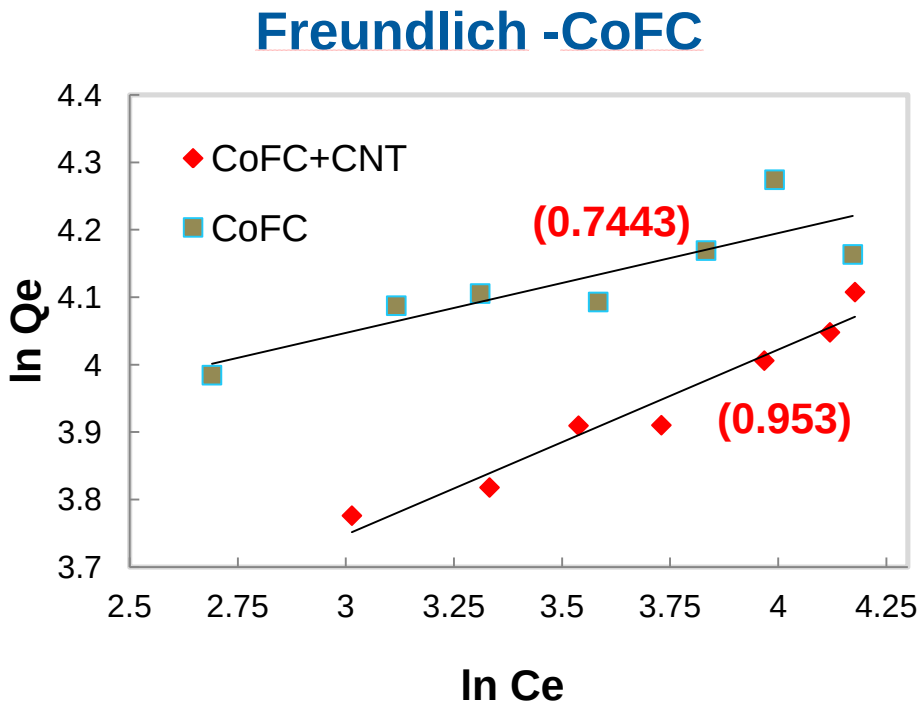

Figure AII-4. Linear plots of Langmuir and Freundlich isotherm model of strontium adsorption by CoFC and CoFC+CNT beads

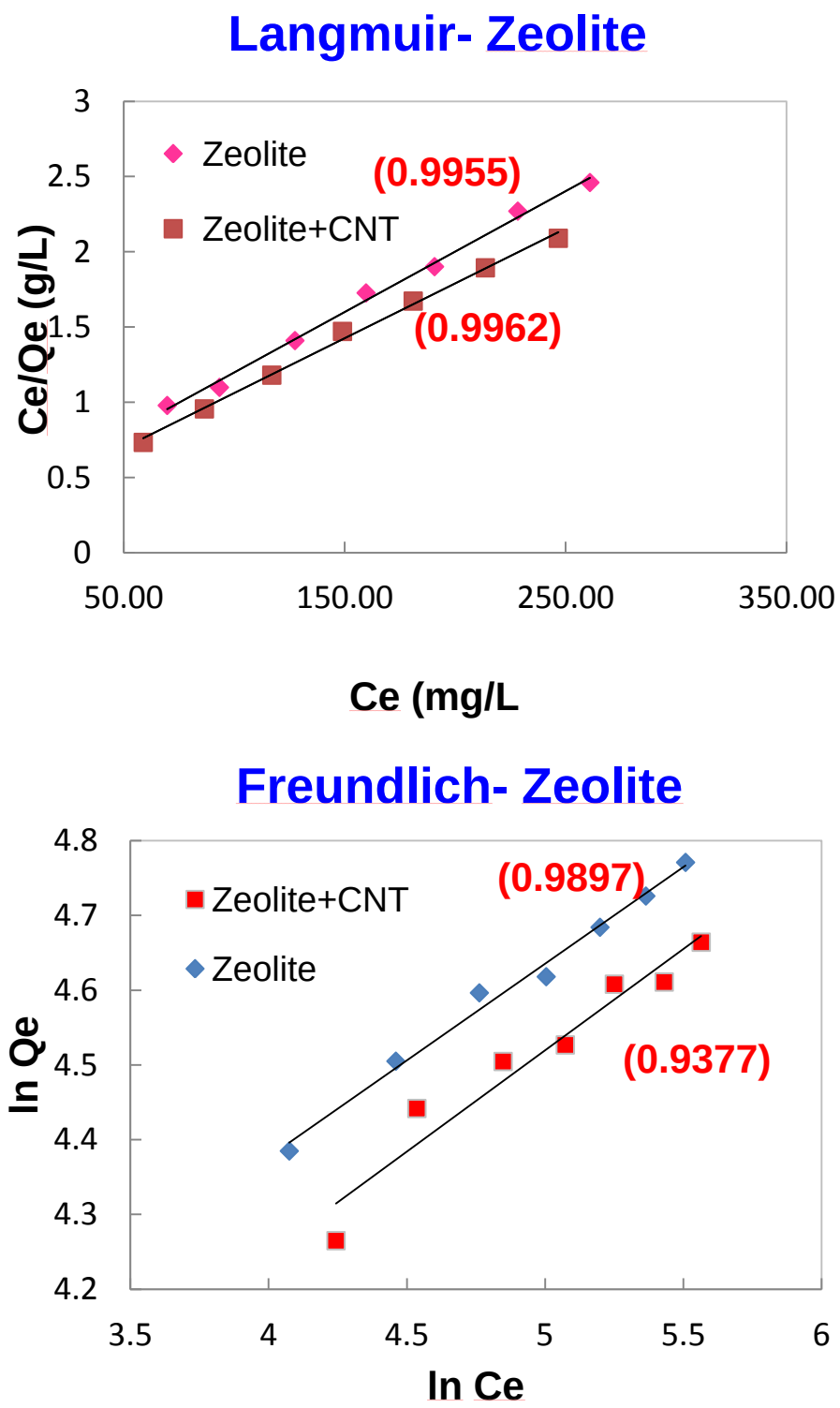

Figure AII-5. Linear plots of Langmuir and Freundlich isotherm model of cesium adsorption by Zeolite and zeolite+CNT beads

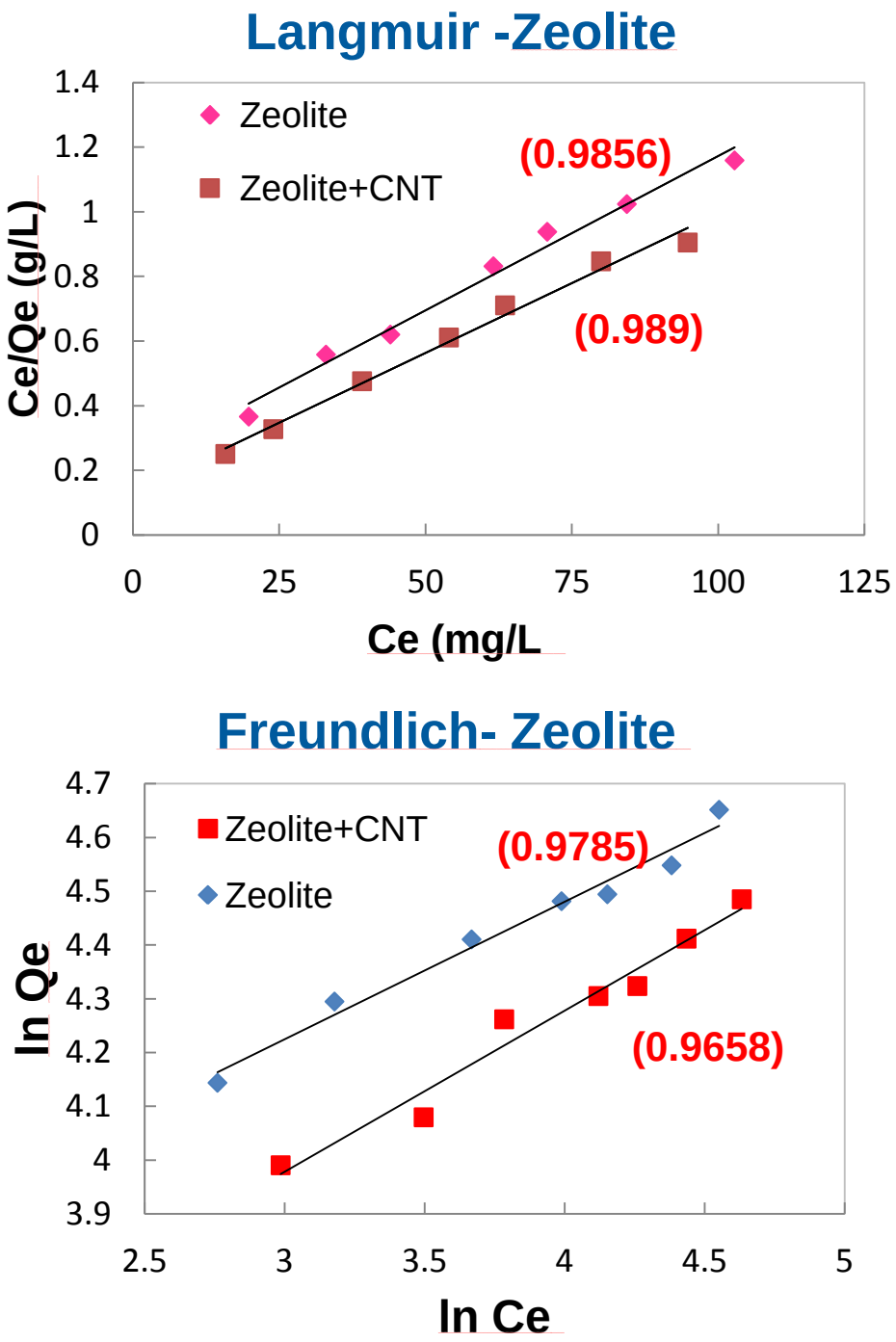

Figure AII-6. Linear plots of Langmuir and Freundlich isotherm model of strontium adsorption by Zeolite and zeolite+CNT beads

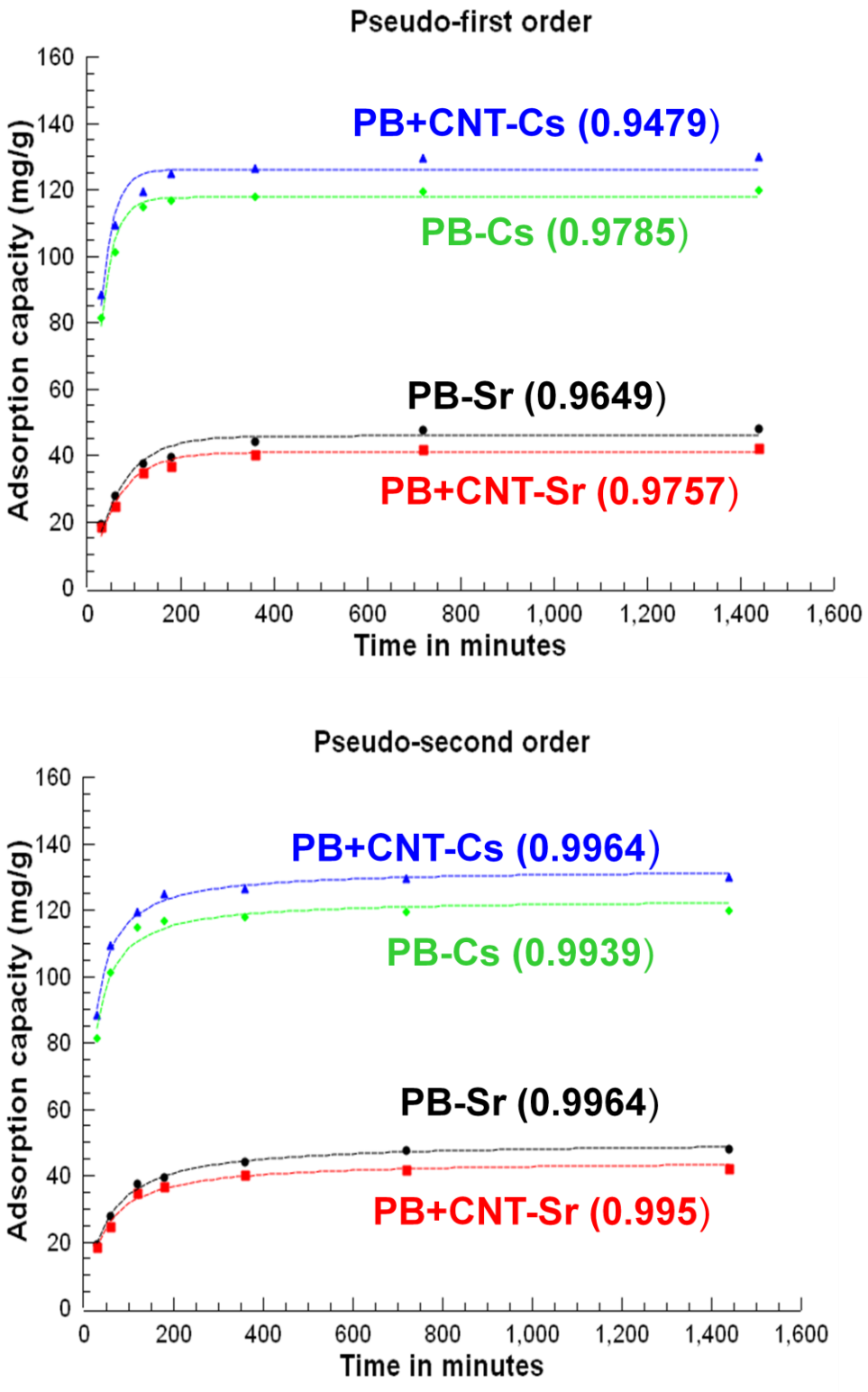

Figure AII-7. Non linear plots of kinetic model of cesium and strontium adsorption by PB and PB+CNT beads

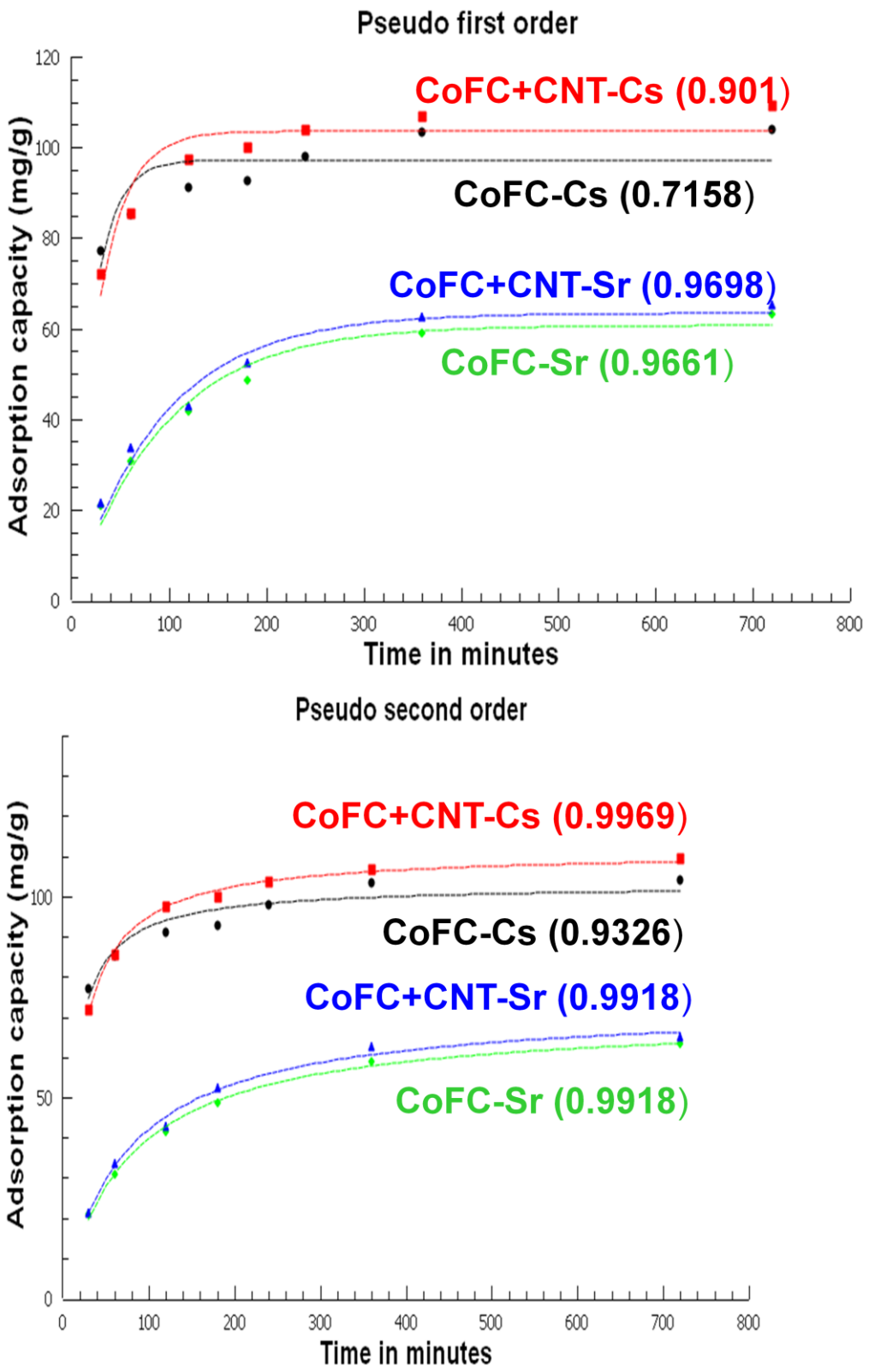

Figure AII-8. Non linear plots of kinetic model of cesium and strontium adsorption by CoFC and CoFC+CNT beads

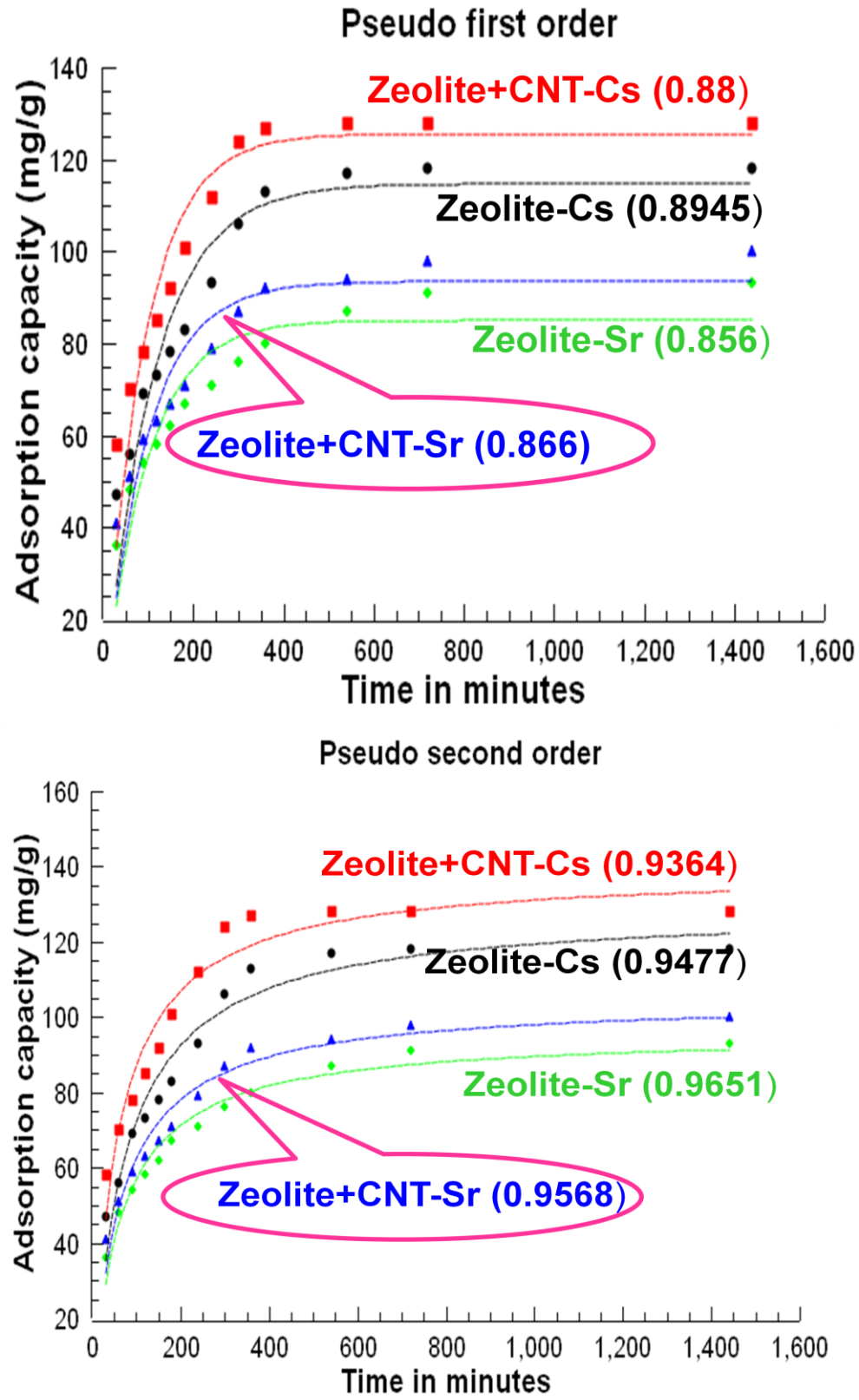

Figure AII-9. Non linear plots of kinetic model of cesium and strontium adsorption by zeolite and Zeolite+CNT beads

.

LIST OF ACHIEVEMENTS

In international journal

- **Adavan Kiliyankil Vipin**, Baiyang Hu, Bunshi Fugetsu*, Prussian blue caged in alginate/calcium beads as adsorbent for removal of cesium ions from contaminated water, ***Journal of Hazardous Materials***, *Volumes 258–259, 15 August 2013, Pages 93-101.*
- **Adavan Kiliyankil Vipin*,** Sun Ling, Bunshi Fugetsu, Encapsulation of sodium cobalt hexacyanoferrate into alginate based gels for the development of high-performance adsorbent for cesium and strontium elimination, ***Submitted***
- **Adavan Kiliyankil Vipin*,** Sun Ling, Bunshi Fugetsu, Enhanced encapsulation of zeolite A into alginate vesicle using MWCNT for the development of novel adsorbent for cesium and strontium elimination, ***to be submited.***

Awards

- ANF-Asia Nano Safe Prize-2013 (Runners Up), Funded by Asia Nano Forum.

International conference

- **Adavan Kiliyankil Vipin**, Baiyang Hu, Bunshi Fugetsu, Prussian blue caged in alginate/calcium beads for removal of cesium and strontiumions from water, *6th International Symposium on Nanotechnology, Occupational and Environmental Health*, October 28-31

Domestic conference

- Adavan Kiliyankil Vipin, Ferric ferrocyanide and cobalt ferrocyanide encapsulated in cross-linked Alginate vesicle for treating cesium contaminated water, The 4th Hokkaido University Sustainability Research Poster Contest, 2012.10.
- Adavan Kiliyankil Vipin, Removal of cesium ions from the water using Prussian blue encapsulated Ca- alginate beads modified with carbon nano tubes, The 3rd Hokkaido University Sustainability Weeks Reserch Poster Contest, 2011.11.

ACKNOWLEDGMENTS

Three years ago, **Professor Dr. Bunshi Fugetsu**, *Division of Environmental development, Graduate school of Environmental science, Hokkaido University*, gave me the precious opportunity to pursue my research. Thus, I would like to express the greatest appreciation to my supervisor not only for academic advices but also for financial support throughout my doctoral course. I wish to express my thanks to **Professor Shunitz Tanaka**, who gave an opportunity to come Hokkaido University and introduced me to Prof. Dr. Bunshi Fugetsu.

I want to send my hearty thanks to my laboratory members; **Professor Fumio Watari, Professor Hideyuki Hisashi, Dr. Sun Ling, Dr. Parvin Begum, Mrs. Maki Sugawara, Mr. Baiyang Hu, Mr. Yanqing Wang, Mrs. Saki Hirota, Dr. Takeshima, Mr. Refi Ikhtiari, and Mrs. Mari Imai.**

I would like to express my thanks to all members of Environmental Adaption course, *Division of Environmental Development* for their kind help and encourages. Also, my sincere thanks to Hokkaido University for giving me an excellent facility to conduct research.

In addition, I wish to express my thanks to GCOE, HIECC for providing financial support to my research,

Furthermore, I would like to thank **my all friends** for their encouragement and support.

In the end, I would like to say ever-not-enough thanks to **my beloved family.**